


A new flow dynamic approach for Wasserstein gradient flows

Qing Cheng^{a, }, Qianqian Liu^{b, *}, Wenbin Chen^c, Jie Shen^d

^a Key Laboratory of Intelligent Computing and Application (Tongji University), Ministry of Education, Department of Mathematics, Tongji University, Shanghai, 200092, China

^b School of Mathematical Sciences, Fudan University, Shanghai, 200433, China

^c Shanghai Key Laboratory for Contemporary Applied Mathematics, School of Mathematical Sciences, Fudan University, Shanghai, 200433, China

^d Eastern Institute of Technology, Ningbo, Zhejiang, 315200, China

ARTICLE INFO

MSC:

65M06
65M12
35K65
35A15

Keywords:

Wasserstein gradient flow
Energetic variational approach
Lagrangian coordinates
Structure preservation

ABSTRACT

We develop in this paper a new regularized flow dynamic approach to construct efficient numerical schemes for Wasserstein gradient flows in Lagrangian coordinates. Instead of approximating the Wasserstein distance which needs to solve constrained minimization problems, we reformulate the problem using the Benamou-Brenier's flow dynamic approach, leading to algorithms which only need to solve unconstrained minimization problem in L^2 distance. Our schemes automatically inherit some essential properties of Wasserstein gradient systems such as positivity-preserving, mass conservative and energy dissipation. We present ample numerical simulations of Porous-Medium equations, Keller-Segel equations and Aggregation equations to validate the accuracy and stability of the proposed schemes. Compared to numerical schemes in Eulerian coordinates, our new schemes can capture sharp interfaces for various Wasserstein gradient flows using relatively smaller number of unknowns.

1. Introduction

Equations that are gradient flows in the Wasserstein metric arise in many physical and biological applications, including Porous-Medium equations [2,43], Poisson-Nernst-Planck equations [20,21] and Keller-Segel equations [24,26,47]. In this paper, we consider numerical approximation of Wasserstein gradient flows which take the following form [1]:

$$\partial_t \rho = -\nabla \cdot (\rho \mathbf{v}), \quad \mathbf{v} = -\nabla \frac{\delta E}{\delta \rho}, \quad (1.1)$$

with the initial value $\rho(\mathbf{x}, 0) = \rho_0(\mathbf{x}) \geq 0$, where $\rho(\mathbf{x}, t)$ is the particle density on the domain $\Omega \subset \mathbb{R}^d$ ($d \geq 1$), and \mathbf{v} is the velocity field of the transport equation, and the energy functional is given by [14]

$$E(\rho) = \int_{\Omega} F(\rho) d\mathbf{x} = \int_{\Omega} U(\rho(\mathbf{x})) + V(\mathbf{x})\rho(\mathbf{x}) d\mathbf{x} + \frac{1}{2} \int_{\Omega \times \Omega} W(\mathbf{x} - \mathbf{y})\rho(\mathbf{x})\rho(\mathbf{y}) d\mathbf{x} d\mathbf{y}, \quad (1.2)$$

* Corresponding author.

E-mail addresses: qingcheng@tongji.edu.cn (Q. Cheng), qianqianliu21@m.fudan.edu.cn (Q. Liu), wbchen@fudan.edu.cn (W. Chen), jshen@eitech.edu.cn (J. Shen).

<https://doi.org/10.1016/j.jcp.2024.113696>

Received 26 June 2024; Received in revised form 17 December 2024; Accepted 18 December 2024

where $F(\rho)$ is the energy density, $U(\rho)$ is the internal energy which can be taken as $U_m(s) = s \log s$ for $m = 1$ and $U_m(s) = \frac{s^m}{m-1}$ for $m > 1$, $V(\mathbf{x})$ is a drift potential and $W(\mathbf{x}, \mathbf{y}) = W(\mathbf{y}, \mathbf{x})$ is an interaction potential, see also [5,13]. Solutions of the Wasserstein gradient flows possess three essential properties: positivity-preserving; mass conservation; and the energy dissipation in the sense that

$$\frac{d}{dt} E(\rho)(t) = - \int_{\Omega} \rho |\mathbf{v}|^2 dx. \tag{1.3}$$

In recent years, considerable attention has been devoted to constructing structure-preserving schemes of various Wasserstein gradient flows (1.1), e.g., Porous-Medium equation [19,29,36,37,48], Fokker-Planck equation [18,25,32,34,40], Keller-Segel equation [16,23,35,41,44], drift diffusion and aggregation equation [9]. Specially, numerical methods based on the approximation for the Wasserstein metric have attracted much more attention, see [5,8–10,28]. For example, the celebrated Jordan-Kinderlehrer-Otto (JKO) scheme [25] is proposed to solve Fokker-Planck equation in [25]. The scheme preserves essential properties of the Wasserstein gradient flows, but a key difficulty of its numerical implementation is to approximate the Wasserstein metric efficiently. Benamou and Brenier discovered [4] that the Wasserstein metric can be rewritten into the Brenier formulae [4].

In the present work, we will adopt Benamou-Brenier’s dynamic formulation for the Wasserstein metric [4]. In particular, given two measures ρ_0 and ρ_1 , their Wasserstein distance can be obtained by solving

$$\begin{cases} W_2(\rho_0, \rho_1) = \inf_{\rho, \mathbf{v}} \left\{ \int_0^1 \int_{\Omega} |\mathbf{v}(\mathbf{x}, t)|^2 \rho(\mathbf{x}, t) dx dt \right\}^{\frac{1}{2}}, \\ s.t. \quad \partial_t \rho + \nabla \cdot (\rho \mathbf{v}) = 0, \\ (\rho \mathbf{v}) \cdot \mathbf{n} = 0 \quad \text{on} \quad \partial\Omega \times [0, 1], \quad \rho(0, \mathbf{x}) = \rho_0, \quad \rho(1, \mathbf{x}) = \rho_1, \end{cases} \tag{1.4}$$

where \mathbf{n} is the outer unit normal on the boundary of the domain Ω . Denote $\mathbf{m} = \rho \mathbf{v}$, then the original JKO scheme, proposed by Jordan, Kinderlehrer and Otto [25], can be reformulated into the following equivalent form [9,28]: given ρ^k , solve $\rho^{k+1} = \rho(1, \mathbf{x})$ as

$$\begin{cases} (\rho, \mathbf{m}) = \arg \inf_{\rho, \mathbf{v}} \frac{1}{2\delta t} \int_0^1 \int_{\Omega} G(\rho, \mathbf{m}) dx dt + E(\rho(1, \mathbf{x})), \\ s.t. \quad \partial_t \rho + \nabla \cdot (\rho \mathbf{v}) = 0, \\ (\rho \mathbf{v}) \cdot \mathbf{n} = 0 \quad \text{on} \quad \partial\Omega \times [0, 1], \quad \rho(0, \mathbf{x}) = \rho^k, \end{cases} \tag{1.5}$$

where $G(\rho, \mathbf{m})$ is defined by

$$G(\rho, \mathbf{m}) = \begin{cases} \frac{m^2}{\rho}, & \text{if } \rho > 0, \\ 0, & \text{if } (\rho, \mathbf{m}) = (0, \mathbf{0}), \\ +\infty, & \text{otherwise.} \end{cases}$$

Various numerical methods [6,7,9,10,27,33] are proposed based on the dynamic formulation (1.5). But they usually require solving, at each time step, a constrained minimization problem which can be difficult and costly. We adopt in this paper the flow dynamic approach to develop a new class of numerical schemes in Lagrangian coordinates which only need to solve an unconstrained minimization problem at each time step. The relationship between the strong formula and variational formula is shown in Fig. 1. The strong formula is obtained directly by discretizing the flow map equation, while the variational formula is derived by combining the JKO scheme and the flow map. It is noteworthy that the two forms are equivalent. This flow dynamic approach also enjoys the following advantages:

- It allows us to construct positivity-preserving schemes for Wasserstein gradient systems with positive solutions, and the schemes can also conserve mass in both semi-discrete and fully-discrete cases.
- Since the schemes are derived from an energetic variational approach, they are energy dissipative for Wasserstein gradient flows.
- The flow dynamic approach, behaving like a moving mesh method, can automatically capture the trajectory of movement in Lagrangian coordinates, and as a consequence, requires fewer spatial points than an Eulerian approach to capture the interface movements or solutions with large gradients.

We present several numerical results to validate the proposed approach. In particular, for Porous-Medium equations, our numerical schemes can accurately capture the sharp interface, and obtain the correct finite propagation speed and waiting time; and for the Keller-Segel equations, they allow us to simulate the phenomenon of blow-up.

The rest of the paper is organized as follows. In Section 2, the semi-discrete numerical scheme is proposed for the Wasserstein gradient flow (1.1). In Section 3, fully discrete numerical schemes for the Wasserstein gradient flow (1.1) in 1D and 2D are constructed and analyzed, respectively. Numerical experiments in 1D and 2D are carried out in Section 4 to validate the theoretical results.

2. Regularized flow dynamic approach

As our objective is to develop numerical methods for Wasserstein gradient flows based on flow dynamic approach, we will first introduce this approach [17,29,45] and then apply it to Wasserstein gradient flows in the semi-discrete case.

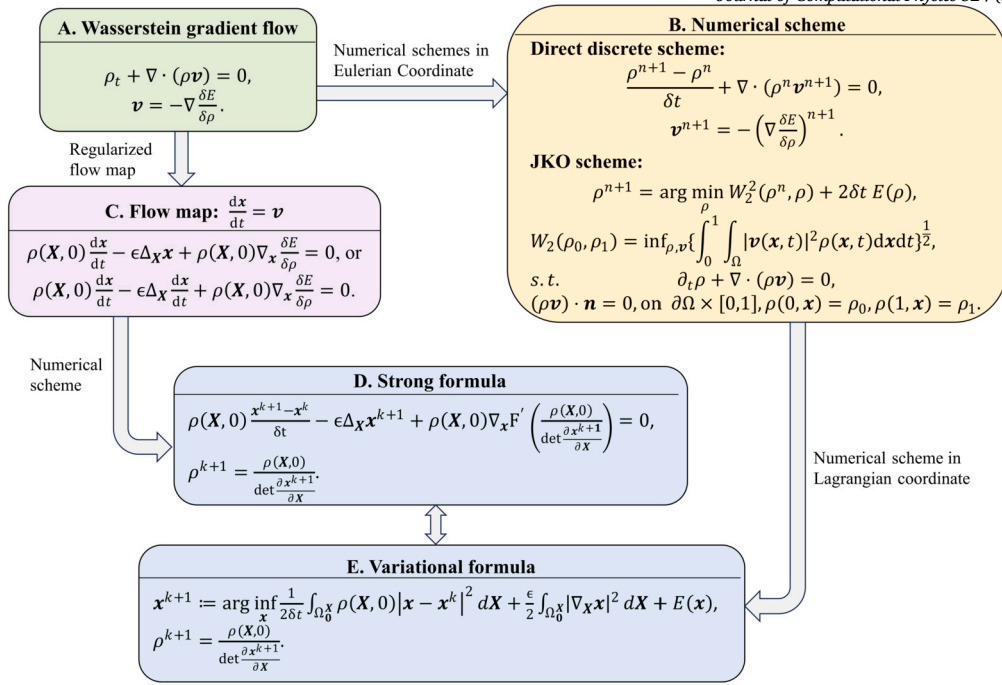


Fig. 1. Relationship between the strong formula and the variational formula for Wasserstein gradient flows. (For interpretation of the colors in the figure(s), the reader is referred to the web version of this article.)

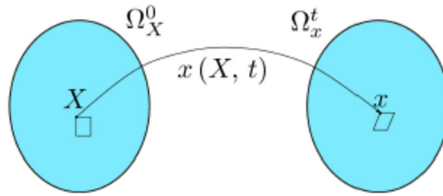


Fig. 2. A schematic illustration of a flow map $\mathbf{x}(X, t)$ at a fixed time t : $\mathbf{x}(X, t)$ maps Ω_0^X to Ω_t^x . X is the Lagrangian coordinate while \mathbf{x} is the Eulerian coordinate, and $F(X, t) = \frac{\partial \mathbf{x}(X, t)}{\partial X}$ represents the deformation associated with the flow map.

Given an initial position or a reference configuration X , and a velocity field \mathbf{v} , define the flow map $\mathbf{x}(X, t)$ [17,18] as follows:

$$\frac{d\mathbf{x}(X, t)}{dt} = \mathbf{v}(\mathbf{x}(X, t), t), \tag{2.1}$$

$$\mathbf{x}(X, 0) = X, \tag{2.2}$$

where \mathbf{x} is the Eulerian coordinate and X is the Lagrangian coordinate, $\frac{\partial \mathbf{x}}{\partial X}$ represents the deformation associated with the flow map, see Fig. 2. We assume that \mathbf{v} is the velocity such that

$$\partial_t \rho + \nabla \cdot (\rho \mathbf{v}) = 0. \tag{2.3}$$

Then the transport equation (2.3) and the flow map (2.1)-(2.2) determine the following kinematic relationship between the Eulerian and Lagrangian coordinates:

$$\frac{\rho(X, 0)}{\det \frac{\partial \mathbf{x}}{\partial X}} = \rho(\mathbf{x}, t). \tag{2.4}$$

According to the Energetic Variational Approach [21,30,31,38,39,42], from the energy dissipative law (1.3) of Wasserstein gradient flows, we can use the least action principle and the maximum dissipation law to derive the conservative and dissipative forces, respectively [17–19,29–31,45,46]:

$$F_{\text{conservative}} = -\frac{\delta E}{\delta \mathbf{x}} = -\rho \nabla_{\mathbf{x}} \frac{\delta E}{\delta \rho}, \quad F_{\text{dissipative}} = \frac{\delta \frac{1}{2} \int_{\Omega} \rho |\mathbf{v}|^2 d\mathbf{x}}{\delta \mathbf{v}} = \rho \mathbf{v},$$

and then apply the force balance law to obtain the following constitutive relation:

$$F_{\text{conservative}} = -\frac{\delta E}{\delta \mathbf{x}} = \rho \mathbf{v} = F_{\text{dissipative}}. \tag{2.5}$$

Combining (2.5) with Wasserstein gradient system (1.1), we derive the following equivalent formulation:

$$\rho \mathbf{v} = \rho \frac{d\mathbf{x}}{dt} = -\frac{\delta E}{\delta \mathbf{x}} = -\rho \nabla_{\mathbf{x}} \frac{\delta E}{\delta \rho}, \tag{2.6}$$

which can be written in Lagrangian coordinates as

$$\rho(\mathbf{X}, 0) \frac{d\mathbf{x}}{dt} + \rho(\mathbf{X}, 0) \nabla_{\mathbf{x}} \frac{\delta E}{\delta \rho} = 0. \tag{2.7}$$

Notice that equation (2.7) is a fully nonlinear equation with respect to \mathbf{x} in Lagrangian coordinate. By adding an extra regularizing term into (2.7), we obtain

$$\rho(\mathbf{X}, 0) \frac{d\mathbf{x}}{dt} - \epsilon \Delta_{\mathbf{X}} \mathbf{x} + \rho(\mathbf{X}, 0) \nabla_{\mathbf{x}} \frac{\delta E}{\delta \rho} = 0, \tag{2.8}$$

where $\epsilon \ll 1$ is a non-negative regularization parameter.

Notice that $F(\mathbf{X}, t) = \frac{\partial \mathbf{x}(\mathbf{X}, t)}{\partial \mathbf{X}}$ represents the deformation associated with the flow map, the term $\epsilon \Delta_{\mathbf{X}} \mathbf{x}$ can be interpreted as a viscous term to smooth the computational meshes from a geometric perspective. Taking the inner product of (2.8) with \mathbf{x} , we obtain the following energy dissipative law:

$$\frac{d}{dt} \tilde{E}(t) = - \int_{\Omega_0^{\mathbf{x}}} \rho(\mathbf{X}, 0) \left| \frac{d\mathbf{x}}{dt} \right|^2 d\mathbf{X}, \tag{2.9}$$

where \tilde{E} is defined by $\tilde{E}(t) = E(t) + \frac{\epsilon}{2} \int_{\Omega_0^{\mathbf{x}}} |\nabla_{\mathbf{X}} \mathbf{x}|^2 d\mathbf{X}$.

Another regularized approach is

$$\rho(\mathbf{X}, 0) \frac{d\mathbf{x}}{dt} - \epsilon \Delta_{\mathbf{X}} \frac{d\mathbf{x}}{dt} + \rho(\mathbf{X}, 0) \nabla_{\mathbf{x}} \frac{\delta E}{\delta \rho} = 0, \tag{2.10}$$

which satisfies the following energy dissipative law:

$$\frac{d}{dt} E(t) = - \int_{\Omega_0^{\mathbf{x}}} \rho(\mathbf{X}, 0) \left| \frac{d\mathbf{x}}{dt} \right|^2 d\mathbf{X} - \int_{\Omega_0^{\mathbf{x}}} \epsilon \left| \nabla_{\mathbf{X}} \frac{d\mathbf{x}}{dt} \right|^2 d\mathbf{X} \leq 0. \tag{2.11}$$

This regularized approach can be used to construct second-order Lagrangian schemes for Wasserstein gradient flow (1.1) where the regularization term is $\epsilon \Delta_{\mathbf{X}} \frac{d\mathbf{x}}{dt}$ in (2.10) with $0 \leq \epsilon \ll 1$.

Remark 2.1. For both regularized approaches proposed above, the regularized terms in the force balance equations (2.8) and (2.10) can be regarded as adding a small extra force into the original force balance equations

$$F_{\text{conservative}} - F_{\text{dissipative}} = \epsilon F_{\text{extra force}}, \tag{2.12}$$

where the extra force can be frictional force or viscous force. Actually, the extra energy dissipative term in (2.11) $\int_{\Omega_0^{\mathbf{x}}} \epsilon \left| \nabla_{\mathbf{X}} \frac{d\mathbf{x}}{dt} \right|^2 d\mathbf{X}$ will be converted into heat due to the work done by frictional force.

2.1. Numerical schemes based on the FDM approach

We observed from (2.9) that the flow map \mathbf{x} also satisfies a gradient flow structure in Lagrangian coordinate. A benefit of the gradient flow structure is that one can construct numerical schemes to inherit the energy dissipation of the gradient flows. In contrast to the classic JKO scheme [25], we shall construct numerical schemes based on FDM approach which do not involve the calculation of the Wasserstein metric, but only of a L^2 distance which is much easier to obtain.

2.1.1. First-order scheme

Given $\delta t > 0$, $t^k = k \delta t$ for $k = 0, 1, \dots, \frac{T}{\delta t}$, let \mathbf{x}^k denote the numerical approximation to $\mathbf{x}(\cdot, t^k)$. Then, a first-order scheme in a variational form to the solution of (2.8) at t^{k+1} can be obtained by

$$\begin{cases} \mathbf{x}^{k+1} := \arg \inf_{\mathbf{x}} \frac{1}{2\delta t} \int_{\Omega_0^{\mathbf{x}}} \rho(\mathbf{X}, 0) |\mathbf{x} - \mathbf{x}^k|^2 d\mathbf{X} + \frac{\epsilon}{2} \int_{\Omega_0^{\mathbf{x}}} |\nabla_{\mathbf{X}} \mathbf{x}|^2 d\mathbf{X} + E(\mathbf{x}), \\ \rho^{k+1} = \frac{\rho(\mathbf{X}, 0)}{\det \frac{\partial \mathbf{x}^{k+1}}{\partial \mathbf{X}}}. \end{cases} \tag{2.13}$$

Motivated from the minimization problem (2.13), a first-order semi-discrete scheme for (1.1) based on (2.8) with $\epsilon = \delta t$ and (2.13) is:

$$\rho(\mathbf{X}, 0) \frac{\mathbf{x}^{k+1} - \mathbf{x}^k}{\delta t} - \delta t \Delta_{\mathbf{X}} \mathbf{x}^{k+1} + \rho(\mathbf{X}, 0) \nabla_{\mathbf{x}} F' \left(\frac{\rho(\mathbf{X}, 0)}{\det \frac{\partial \mathbf{x}^{k+1}}{\partial \mathbf{X}}} \right) = 0, \tag{2.14}$$

$$\rho^{k+1} = \frac{\rho(\mathbf{X}, 0)}{\det \frac{\partial \mathbf{x}^{k+1}}{\partial \mathbf{X}}}, \tag{2.15}$$

with the Dirichlet boundary condition $\mathbf{x}^{k+1}|_{\partial\Omega} = \mathbf{X}|_{\partial\Omega}$, and $\Omega_0^{\mathbf{x}} = \Omega_0^{\mathbf{X}}$.

We will show that the numerical scheme (2.14)-(2.15) in Lagrangian coordinate achieves a first-order accuracy to (1.1) in Eulerian coordinate:

Proposition 2.1. *The solution ρ^{k+1} to numerical scheme (2.14)-(2.15) is a first-order approximation to the exact solution of Wasserstein gradient flow (1.1) at t^{k+1} .*

Proof. Firstly, we shall calculate the variational derivative of the energy E :

$$\begin{aligned} \delta E &= \int_{\Omega_0^{\mathbf{x}}} -F' \left(\frac{\rho(\mathbf{X}, 0)}{\det \frac{\partial \mathbf{x}}{\partial \mathbf{X}}} \right) \frac{\rho(\mathbf{X}, 0)}{\left(\det \frac{\partial \mathbf{x}}{\partial \mathbf{X}}\right)^2} \det \frac{\partial \mathbf{x}}{\partial \mathbf{X}} \frac{\partial \delta \mathbf{x}}{\partial \mathbf{X}} + F \left(\frac{\rho(\mathbf{X}, 0)}{\det \frac{\partial \mathbf{x}}{\partial \mathbf{X}}} \right) \frac{\partial \delta \mathbf{x}}{\partial \mathbf{X}} d\mathbf{X} \\ &= \int_{\Omega_0^{\mathbf{x}}} \partial_{\mathbf{X}} \left(F' \left(\frac{\rho(\mathbf{X}, 0)}{\det \frac{\partial \mathbf{x}}{\partial \mathbf{X}}} \right) \frac{\rho(\mathbf{X}, 0)}{\left(\det \frac{\partial \mathbf{x}}{\partial \mathbf{X}}\right)^2} \det \frac{\partial \mathbf{x}}{\partial \mathbf{X}} - F \left(\frac{\rho(\mathbf{X}, 0)}{\det \frac{\partial \mathbf{x}}{\partial \mathbf{X}}} \right) \right) \delta \mathbf{x} d\mathbf{X} \\ &= \int_{\Omega_0^{\mathbf{x}}} \partial_{\mathbf{X}} \left(F' \left(\frac{\rho(\mathbf{X}, 0)}{\det \frac{\partial \mathbf{x}}{\partial \mathbf{X}}} \right) \frac{\rho(\mathbf{X}, 0)}{\det \frac{\partial \mathbf{x}}{\partial \mathbf{X}}} - F \left(\frac{\rho(\mathbf{X}, 0)}{\det \frac{\partial \mathbf{x}}{\partial \mathbf{X}}} \right) \right) \delta \mathbf{x} d\mathbf{X} \\ &= \int_{\Omega_0^{\mathbf{x}}} \partial_{\mathbf{x}} (F'(\rho) \rho - F(\rho)) \delta \mathbf{x} d\mathbf{x} = \int_{\Omega_0^{\mathbf{x}}} \rho \partial_{\mathbf{x}} F'(\rho) \delta \mathbf{x} d\mathbf{x}. \end{aligned} \tag{2.16}$$

We can then derive from (2.16) the variational derivatives of E in Eulerian coordinates and Lagrangian coordinates, respectively:

$$\frac{\delta E}{\delta \mathbf{x}} = \rho \partial_{\mathbf{x}} F'(\rho), \tag{2.17}$$

$$\frac{\delta E}{\delta \mathbf{X}} = \partial_{\mathbf{X}} \left(F' \left(\frac{\rho(\mathbf{X}, 0)}{\det \frac{\partial \mathbf{x}}{\partial \mathbf{X}}} \right) \frac{\rho(\mathbf{X}, 0)}{\det \frac{\partial \mathbf{x}}{\partial \mathbf{X}}} - F \left(\frac{\rho(\mathbf{X}, 0)}{\det \frac{\partial \mathbf{x}}{\partial \mathbf{X}}} \right) \right) = \rho(\mathbf{X}, 0) \frac{\partial_{\mathbf{X}} F' \left(\frac{\rho(\mathbf{X}, 0)}{\det \frac{\partial \mathbf{x}}{\partial \mathbf{X}}} \right)}{\det \frac{\partial \mathbf{x}}{\partial \mathbf{X}}}. \tag{2.18}$$

From (2.18), we observe that the last term in (2.14) is exactly the variational derivative of $E(\frac{\rho(\mathbf{X}, 0)}{\det \frac{\partial \mathbf{x}}{\partial \mathbf{X}}})$ with respect to \mathbf{x} in Lagrangian coordinates. Then the equation (2.14) can be obtained by taking the variational derivative of (2.13) with respect to \mathbf{x} , which also show that the minimizer $(\mathbf{x}^{k+1}, \rho^{k+1})$ of the variational problem (2.13) is the solution of (2.14)-(2.15). Assuming that $\rho(\mathbf{X}, 0) \neq 0$ and rewriting the equation (2.14) into the following equivalent form:

$$\frac{\mathbf{x}^{k+1} - \mathbf{x}^k}{\delta t} = \frac{\delta t}{\rho(\mathbf{X}, 0)} \Delta_{\mathbf{X}} \mathbf{x}^{k+1} - \nabla_{\mathbf{x}} F' \left(\frac{\rho(\mathbf{X}, 0)}{\det \frac{\partial \mathbf{x}^{k+1}}{\partial \mathbf{X}}} \right). \tag{2.19}$$

Notice the definition of flow map $\mathbf{v}(\mathbf{X}, t^{k+1}) = \frac{d\mathbf{x}(\mathbf{X}, t^{k+1})}{dt}$, we can easily derive from (2.19) that

$$\mathbf{v}^{k+1} = -\nabla_{\mathbf{x}} F'(\rho(\mathbf{x}^{k+1})) + O(\delta t) = -\nabla_{\mathbf{x}} \left(\frac{\delta E}{\delta \rho} \right)^{k+1} + O(\delta t).$$

Then we conclude that the numerical scheme (2.14) achieves a first-order accuracy in time for the Wasserstein gradient flow (1.1). \square

Remark 2.2. It is worth mentioning that there are several choices to add the regularization term in scheme (2.13), such as $\int_{\Omega_0^{\mathbf{x}}} \delta t \rho(\mathbf{X}, 0) |\nabla_{\mathbf{X}} \mathbf{x}|^2 d\mathbf{X}$ and $\int_{\Omega_0^{\mathbf{x}}} |\nabla_{\mathbf{X}} (\mathbf{x} - \mathbf{x}^k)|^2 d\mathbf{X}$, which can also be proved to be a first-order approximation to the Wasserstein gradient flow (1.1).

Remark 2.3. We can solve the nonlinear scheme (2.14)–(2.15) by using the damped Newton’s iteration. Denote the linear and nonlinear operators by

$$\mathcal{L}(\mathbf{x}^{k+1}) := \frac{\rho(\mathbf{X}, 0)}{\delta t} \mathbf{x}^{k+1} - \delta t \Delta_{\mathbf{X}} \mathbf{x}^{k+1}, \quad \mathcal{N}(\mathbf{x}^{k+1}) := \rho(\mathbf{X}, 0) \nabla_{\mathbf{x}} F' \left(\frac{\rho(\mathbf{X}, 0)}{\det \frac{\partial \mathbf{x}^{k+1}}{\partial \mathbf{X}}} \right),$$

and $b(\mathbf{x}^k) := \frac{\rho(\mathbf{X}, 0)}{\delta t} \mathbf{x}^k$, then the scheme (2.14) can be reformulated as a nonlinear system

$$\mathcal{L}(\mathbf{x}^{k+1}) + \mathcal{N}(\mathbf{x}^{k+1}) = b(\mathbf{x}^k),$$

which can be solved iteratively by finding $\mathbf{x}^{k+1, n+1}$, such that

$$\mathbf{x}^{k+1, n+1} = \mathbf{x}^{k+1, n} + \alpha \delta \mathbf{x}, \quad \text{with} \quad \delta \mathbf{x} = \frac{b(\mathbf{x}^k) - \mathcal{L}(\mathbf{x}^{k+1, n}) - \mathcal{N}(\mathbf{x}^{k+1, n})}{\mathcal{L}'(\mathbf{x}^{k+1, n}) + \mathcal{N}'(\mathbf{x}^{k+1, n})},$$

where $0 < \alpha \leq 1$ is a damping coefficient. For Keller-Segel equations, Porous medium equations and Aggregation diffusion equations, we can obtain good accuracy and convergence rates by using the standard Newton’s iteration with $\alpha = 1$. Then, we just set the damped coefficient $\alpha = 1$ to compute numerical solutions in the numerical experiments presented in Section 4.

2.1.2. Second-order scheme

In analogy to the first-order scheme (2.14)-(2.15), we can construct a second-order scheme for (1.1) based on a Crank-Nicolson discretization of (2.10) with $\epsilon = \delta t^2$:

$$\begin{cases} \mathbf{x}^{k+1} = \arg \inf_{\mathbf{x}} \frac{1}{2\delta t} \int_{\Omega_0} \rho(\mathbf{X}, 0) |\mathbf{x} - \mathbf{x}^k|^2 + \delta t^2 (|\nabla_{\mathbf{X}}(\mathbf{x} - \mathbf{x}^k)|^2) d\mathbf{X} \\ \quad + \frac{1}{2} E \left(\frac{\rho(\mathbf{X}, 0)}{\det \frac{\partial \mathbf{x}}{\partial \mathbf{X}}} \right) + \frac{1}{2} \int_{\Omega_0} \mathbf{x} \left(\frac{\delta E}{\delta \mathbf{x}} \right)^k d\mathbf{X}, \\ \rho^{k+1} = \frac{\rho(\mathbf{X}, 0)}{\det \frac{\partial \mathbf{x}^{k+1}}{\partial \mathbf{X}}}. \end{cases} \tag{2.20}$$

Next, we show that the above unconstrained minimization problem is equivalent to a Crank-Nicolson discretization.

Theorem 2.4. For any $k > 0$, the minimizer of the variational problem (2.20) is the solution of the following second-order Crank-Nicolson scheme: given $(\mathbf{x}^k, \rho(\mathbf{X}, 0))$, solve $(\mathbf{x}^{k+1}, \rho^{k+1})$ from

$$\begin{aligned} \rho(\mathbf{X}, 0) \frac{\mathbf{x}^{k+1} - \mathbf{x}^k}{\delta t} - \delta t (\Delta_{\mathbf{X}} \mathbf{x}^{k+1} - \Delta_{\mathbf{X}} \mathbf{x}^k) + \frac{1}{2} \rho(\mathbf{X}, 0) \nabla_{\mathbf{x}} F' \left(\frac{\rho(\mathbf{X}, 0)}{\det \frac{\partial \mathbf{x}^{k+1}}{\partial \mathbf{X}}} \right) \\ + \frac{1}{2} \rho(\mathbf{X}, 0) \nabla_{\mathbf{x}} F' \left(\frac{\rho(\mathbf{X}, 0)}{\det \frac{\partial \mathbf{x}^k}{\partial \mathbf{X}}} \right) = 0, \end{aligned} \tag{2.21}$$

$$\rho^{k+1} = \frac{\rho(\mathbf{X}, 0)}{\det \frac{\partial \mathbf{x}^{k+1}}{\partial \mathbf{X}}}, \tag{2.22}$$

with the Dirichlet boundary condition $\mathbf{x}^{k+1}|_{\partial\Omega} = \mathbf{X}|_{\partial\Omega}$.

Proof. The equation (2.21) can be obtained by taking the variational derivative of (2.20) with respect to \mathbf{x} , then the minimizer $(\mathbf{x}^{k+1}, \rho^{k+1})$ of the minimization problem (2.20) is the solution of (2.21) with (2.15). The equation (2.21) can be rewritten into

$$\frac{\mathbf{x}^{k+1} - \mathbf{x}^k}{\delta t} - \frac{\delta t}{\rho(\mathbf{X}, 0)} (\Delta_{\mathbf{X}} \mathbf{x}^{k+1} - \Delta_{\mathbf{X}} \mathbf{x}^k) + \frac{1}{2} \nabla_{\mathbf{x}} F' \left(\frac{\rho(\mathbf{X}, 0)}{\det \frac{\partial \mathbf{x}^{k+1}}{\partial \mathbf{X}}} \right) + \frac{1}{2} \nabla_{\mathbf{x}} F' \left(\frac{\rho(\mathbf{X}, 0)}{\det \frac{\partial \mathbf{x}^k}{\partial \mathbf{X}}} \right) = 0,$$

which is equivalent to

$$\mathbf{v}^{k+\frac{1}{2}} = -\nabla_{\mathbf{x}} F'(\rho(\mathbf{x}^{k+\frac{1}{2}})) + O(\delta t^2) = -\nabla_{\mathbf{x}} \left(\frac{\delta E}{\delta \rho} \right)^{k+\frac{1}{2}} + O(\delta t^2),$$

where the fact that the term $\frac{1}{2} \nabla_{\mathbf{x}} F'(\rho(\mathbf{x}^k)) + \frac{1}{2} \nabla_{\mathbf{x}} F'(\rho(\mathbf{x}^{k+1}))$ is a second-order approximation to $\nabla_{\mathbf{x}} F'(\rho(\mathbf{x}^{k+\frac{1}{2}}))$ has been utilized. Then the numerical scheme (2.21) is a second-order time discretization for the Wasserstein gradient flow (1.1). \square

Similarly as in the last subsection, we can also show that ρ^{k+1} obtained from (2.20) is a second-order approximation to the solution $\rho(\mathbf{x}, t)$ at $t = t^{k+1}$.

Proposition 2.2. The solution ρ^{k+1} to numerical scheme (2.21)-(2.22) is a second-order approximation to the exact solution of Wasserstein gradient flow (1.1) at t^{k+1} .

The proof is analogous to that of Proposition 2.1 so we omit it for the sake of brevity.

Remark 2.5. Similarly as (2.14), the nonlinear scheme (2.21) can also be reformulated as a nonlinear system

$$\mathcal{L}(\mathbf{x}^{k+1}) + \frac{1}{2}\mathcal{N}(\mathbf{x}^{k+1}) = \mathcal{L}(\mathbf{x}^k) - \frac{1}{2}\mathcal{N}(\mathbf{x}^k),$$

which can be solved by finding $\mathbf{x}^{k+1,n+1}$, such that

$$\mathbf{x}^{k+1,n+1} = \mathbf{x}^{k+1,n} + \alpha\delta\mathbf{x}, \quad \text{with} \quad \delta\mathbf{x} = \frac{\mathcal{L}(\mathbf{x}^k - \mathbf{x}^{k+1,n}) - \frac{1}{2}\mathcal{N}(\mathbf{x}^k) - \frac{1}{2}\mathcal{N}(\mathbf{x}^{k+1,n})}{\mathcal{L}'(\mathbf{x}^{k+1,n}) + \frac{1}{2}\mathcal{N}'(\mathbf{x}^{k+1,n})},$$

where $0 < \alpha \leq 1$ is a damping coefficient.

Remark 2.6. From energy stability we can only derive that the norm $\|\nabla_{\mathbf{X}} \mathbf{x}^{k+1}\|$ is bounded. For both first-order and second-order Lagrangian schemes proposed above based on the regularized flow dynamic approach, we shall make very refined error analysis to clarify that the regularized terms should be $\delta t \Delta_{\mathbf{X}} \mathbf{x}^{k+1} = O(\delta t)$ and $\delta t(\Delta_{\mathbf{X}} \mathbf{x}^{k+1} - \Delta_{\mathbf{X}} \mathbf{x}^k) = O(\delta t^2)$ in which the bound of $\|\Delta_{\mathbf{X}} \mathbf{x}^{k+1}\|_{\infty}$ is needed.

2.2. Properties of numerical schemes based on FDM approach

Now we show that our numerical schemes based on the FDM approach inherit essential properties of the Wasserstein gradient flows. More precisely, we have

Theorem 2.7. For any $0 \leq k \leq \frac{T}{\delta t}$, assume initial value $\rho(\mathbf{X}, 0) > 0$ and consider the internal energy to be the form of $U(s) = s \log s$ in (2.13), then the solution $\rho^{k+1}(\mathbf{x})$ of numerical scheme (2.14)-(2.15) satisfies the following properties:

- The numerical solution $\rho^{k+1} > 0$ is also positive.
- The scheme (2.14)-(2.15) is mass conservative in the sense that

$$\int_{\Omega_t^x} \rho^{k+1}(\mathbf{x}) d\mathbf{x} = \int_{\Omega_0^x} \rho(\mathbf{X}, 0) d\mathbf{X}. \tag{2.23}$$

- It is unconditionally energy stable in the sense that

$$E(\mathbf{x}^{k+1}) + \frac{\delta t}{2} \int_{\Omega_0^x} |\nabla_{\mathbf{X}} \mathbf{x}^{k+1}|^2 d\mathbf{X} \leq E(\mathbf{x}^k) + \frac{\delta t}{2} \int_{\Omega_0^x} |\nabla_{\mathbf{X}} \mathbf{x}^k|^2 d\mathbf{X}. \tag{2.24}$$

Proof. Since we choose the internal energy $U(s)$ to be the form of $s \log s$ and \mathbf{x}^{k+1} is the minimizer of variational problem (2.13), then $\frac{\rho(\mathbf{X}, 0)}{\det \frac{\partial \mathbf{x}^{k+1}}{\partial \mathbf{X}}}$ should stay in the domain of the logarithmic function which implies $\rho^{k+1} > 0$.

Using the equality (2.15), we derive

$$\int_{\Omega_t^x} \frac{\rho(\mathbf{X}, 0)}{\det \frac{\partial \mathbf{x}^{k+1}}{\partial \mathbf{X}}} d\mathbf{x} = \int_{\Omega_0^x} \frac{\rho(\mathbf{X}, 0)}{\det \frac{\partial \mathbf{x}^{k+1}}{\partial \mathbf{X}}} \det \frac{\partial \mathbf{x}^{k+1}}{\partial \mathbf{X}} d\mathbf{X} = \int_{\Omega_0^x} \rho(\mathbf{X}, 0) d\mathbf{X},$$

where the equality $\det \frac{\partial \mathbf{x}^{k+1}}{\partial \mathbf{X}} d\mathbf{X} = d\mathbf{x}$ has been used. Then the scheme (2.14)-(2.15) is mass conservative.

From the minimization problem (2.13), we obtain that

$$E(\mathbf{x}^{k+1}) + \frac{\delta t}{2} \int_{\Omega_0^x} |\nabla_{\mathbf{X}} \mathbf{x}^{k+1}|^2 d\mathbf{X} \leq E(\mathbf{x}^k) + \frac{\delta t}{2} \int_{\Omega_0^x} |\nabla_{\mathbf{X}} \mathbf{x}^k|^2 d\mathbf{X},$$

the energy stability property is arrived. \square

Remark 2.8. If the regularization term in (2.13) is taken as $\int_{\Omega_0^x} |\nabla_{\mathbf{X}}(\mathbf{x} - \mathbf{x}^k)|^2 d\mathbf{X}$, the energy dissipation $E(\mathbf{x}^{k+1}) \leq E(\mathbf{x}^k)$ for any $0 \leq k \leq \frac{T}{\delta t}$ can also be derived.

Remark 2.9. Similarly to the first-order scheme (2.14)-(2.15), we can show that the second-order Crank-Nicolson scheme (2.21) is mass conservative and its numerical solution ρ^{k+1} is also positivity-preserving if the internal energy is chosen as a logarithm type function. But we are unable to prove that the Crank-Nicolson scheme (2.21) is energy dissipative.

3. Fully discretizations based on FDM approach

In this section, we provide more details about the spatial discretizations and propose full discrete schemes for the Wasserstein gradient flows (1.1) based on the FDM approach. To better explain our approach, we first consider the discretization in one dimension, then we generalize our FDM approach to two-dimensional case. More specifically, we show that our fully discrete schemes are also positivity-preserving, mass conservative and energy dissipative.

3.1. Numerical scheme in 1D

In this subsection, we develop an implicit finite difference scheme for the Wasserstein gradient flows (1.1). For convenience, we define some notations, let $\Omega_0^X = [-L, L]$ and $\Omega_0^x = [-L, L]$ be the computational domain in Lagrangian and Eulerian coordinate and choose the spatial grids: $-L = X_0 < X_1 < \dots < X_N = L$. We define

$$\begin{aligned} x_j(t_k) &= x(X_j, t_k), & 0 \leq j \leq N, & 0 \leq k \leq \frac{T}{\delta t}, \\ \rho_j(t_k) &= \rho(x_j, t_k), & 0 \leq j \leq N, & 0 \leq k \leq \frac{T}{\delta t}, \end{aligned}$$

where $X_j = X_0 + j\delta X$, $\delta X = X_{j+1} - X_j$.

For the following finite dimensional minimization problem, we define the admissible set $S_{ad} := \{\mathbf{x} : x_{j+1} > x_j \text{ for } j = 0, 1, \dots, N-1, \text{ and } x_0 = X_0, x_N = X_N\}$:

$$\left\{ \begin{aligned} \mathbf{x}^{k+1} &:= \arg \inf_{\mathbf{x} \in S_{ad}} \frac{1}{2\delta t} \sum_{j=0}^{N-1} \rho(X_{j+\frac{1}{2}}, 0) |x_{j+\frac{1}{2}} - x_{j+\frac{1}{2}}^k|^2 \delta X + \frac{\epsilon}{2} \sum_{j=0}^{N-1} \left| \frac{x_{j+1} - x_j}{\delta X} \right|^2 \delta X \\ &\quad + E_h(\mathbf{x}), \\ \rho_{j+\frac{1}{2}}^{k+1} &:= \frac{\rho(X_{j+\frac{1}{2}}, 0)}{\frac{x_{j+1}^{k+1} - x_j^{k+1}}{\delta X}}, \end{aligned} \right. \quad (3.1)$$

where $\mathbf{x} = (x_0, x_1, \dots, x_{N-1}, x_N)$, $x_{j+\frac{1}{2}} := \frac{1}{2}(x_{j+1} + x_j)$, and the discrete energy is defined by

$$E_h(\mathbf{x}) := \sum_{j=0}^{N-1} F \left(\frac{\rho(X_{j+\frac{1}{2}}, 0)}{\frac{x_{j+1} - x_j}{\delta X}} \right) \frac{x_{j+1} - x_j}{\delta X} \delta X. \quad (3.2)$$

Lemma 3.1. *The minimizer of the variational problem (3.1) is the solution of the following numerical scheme with $\epsilon = \delta t$: given $(\mathbf{x}^k, \rho(X, 0))$, we solve $(\mathbf{x}^{k+1}, \rho^{k+1})$ from*

$$\begin{aligned} \frac{1}{2\delta t} \rho(X_{j+\frac{1}{2}}, 0) (x_{j+\frac{1}{2}}^{k+1} - x_{j+\frac{1}{2}}^k) \delta X + \frac{1}{2\delta t} \rho(X_{j-\frac{1}{2}}, 0) (x_{j-\frac{1}{2}}^{k+1} - x_{j-\frac{1}{2}}^k) \delta X \\ - \delta t \frac{x_{j+1}^{k+1} - 2x_j^{k+1} + x_{j-1}^{k+1}}{(\delta X)^2} \delta X + \frac{\delta E_h}{\delta x_j}(\mathbf{x}^{k+1}) = 0, \end{aligned} \quad (3.3)$$

$$\rho_{j+\frac{1}{2}}^{k+1} := \frac{\rho(X_{j+\frac{1}{2}}, 0)}{\frac{x_{j+1}^{k+1} - x_j^{k+1}}{\delta X}}, \quad j = 0, 1, \dots, N-1, \quad (3.4)$$

with the initial and boundary conditions

$$\mathbf{x}^0 = (X_0, X_1, \dots, X_N) \quad \text{and} \quad x_0^{k+1} = X_0, \quad x_N^{k+1} = X_N. \quad (3.5)$$

The last term $\frac{\delta E_h}{\delta x_j}(\mathbf{x}^{k+1})$ in (3.3) is defined as follows:

$$\begin{aligned} \frac{\delta E_h}{\delta x_j}(\mathbf{x}^{k+1}) &= F' \left(\frac{\rho(X_{j+\frac{1}{2}}, 0)}{\frac{x_{j+1}^{k+1} - x_j^{k+1}}{\delta X}} \right) \frac{\rho(X_{j+\frac{1}{2}}, 0) \delta X}{(x_{j+1}^{k+1} - x_j^{k+1})^2} \frac{x_{j+1}^{k+1} - x_j^{k+1}}{\delta X} \delta X - F \left(\frac{\rho(X_{j-\frac{1}{2}}, 0)}{\frac{x_{j+1}^{k+1} - x_j^{k+1}}{\delta X}} \right) \\ &\quad - F' \left(\frac{\rho(X_{j-\frac{1}{2}}, 0)}{\frac{x_j^{k+1} - x_{j-1}^{k+1}}{\delta X}} \right) \frac{\rho(X_{j-\frac{1}{2}}, 0) \delta X}{(x_j^{k+1} - x_{j-1}^{k+1})^2} \frac{x_j^{k+1} - x_{j-1}^{k+1}}{\delta X} \delta X + F \left(\frac{\rho(X_{j-\frac{1}{2}}, 0)}{\frac{x_j^{k+1} - x_{j-1}^{k+1}}{\delta X}} \right) \end{aligned}$$

The discrete energy is strictly convex if the Hessian matrix $\nabla^2 E_h$ is positive definite. For instance, when choosing $W(x) = \frac{|x|^2}{2} - \ln|x|$, we can find that the discrete energy $E_h(\mathbf{x}^{k+1})$ is convex since $W''(x) = 1 + \frac{1}{x^2} > 0$. However, for the Keller-Segel equation with $U(\rho) = \rho \log \rho$ and $W(x) = \frac{1}{2\pi} \ln|x|$, we consider the discrete energy

$$E_h(\mathbf{x}^{k+1}) = \sum_{i=0}^{N-1} \delta X \rho(X_{i+\frac{1}{2}}, 0) \log \left(\frac{\rho(X_{i+\frac{1}{2}}, 0)}{\frac{x_{i+\frac{1}{2}}^{k+1} - x_j^k}{\delta X}} \right) - \frac{\delta X}{2\pi} \sum_{i=0}^{N-1} \rho(X_{i+\frac{1}{2}}, 0) \times \sum_{j=0}^{N-1} \rho_{j+\frac{1}{2}}^k \left((x_{i+\frac{1}{2}}^{k+1} - x_{j+\frac{1}{2}}^k) \ln(|x_{i+\frac{1}{2}}^{k+1} - x_{j+\frac{1}{2}}^k|) - (x_{i+\frac{1}{2}}^{k+1} - x_j^k) \ln(|x_{i+\frac{1}{2}}^{k+1} - x_j^k|) \right), \tag{3.12}$$

it is uncertain whether the discrete energy is convex. The details are shown in Appendix.

The fully discretized numerical scheme (3.3)-(3.4) in one dimensional case holds the following structure-preserving properties.

Theorem 3.2. Assume the initial value $\rho(X, 0) > 0$ for $X \in \Omega_X^X$, the energy density $F(s)$ satisfies $F(s) \geq 0$ for $s \geq 0$, and $\lim_{s \rightarrow 0} F(\frac{1}{s})s = \infty$, then the scheme (3.3)-(3.4) has a unique solution $\mathbf{x}^{k+1} \in S_{ad}$ when $\frac{\delta^2 E_h}{\delta \mathbf{x}^2} > 0$, and the following properties hold:

- the solution to numerical scheme (3.3)-(3.4) is positive, $\rho_{j+\frac{1}{2}}^{k+1} > 0$,
- the numerical scheme (3.3)-(3.4) satisfies the property of mass conserving for the density ρ^{k+1} in the sense that

$$\sum_{j=0}^{N-1} \rho_{j+\frac{1}{2}}^{k+1} (x_{j+\frac{1}{2}}^{k+1} - x_j^{k+1}) = \sum_{j=0}^{N-1} \rho_{j+\frac{1}{2}}^k (x_{j+\frac{1}{2}}^k - x_j^k) = \sum_{j=0}^{N-1} \rho(X_{j+\frac{1}{2}}, 0) \delta X, \tag{3.13}$$

- the discrete energy in scheme (3.3)-(3.4) is dissipative in the sense that

$$\tilde{E}_h(\mathbf{x}^{k+1}) \leq \tilde{E}_h(\mathbf{x}^k), \tag{3.14}$$

where the energy $\tilde{E}_h(\mathbf{x}^{k+1})$ is defined by

$$\tilde{E}_h(\mathbf{x}^{k+1}) = E_h(\mathbf{x}^{k+1}) + \sum_{i=0}^{N-1} \frac{\delta t}{2} \left| \frac{x_{i+\frac{1}{2}}^{k+1} - x_j^{k+1}}{\delta X} \right|^2 \delta X. \tag{3.15}$$

Proof. Step 1 (energy law):

We can easily check that \mathbf{x}^{k+1} is the minimizer of the following Lagrangian function which is defined by

$$L(\mathbf{x}^{k+1}) = \frac{1}{2\delta t} \sum_{j=0}^{N-1} \left(\rho(X_{j+\frac{1}{2}}, 0) |x_{j+\frac{1}{2}}^{k+1} - x_{j+\frac{1}{2}}^k|^2 \delta X + \delta t^2 \left| \frac{x_{j+\frac{1}{2}}^{k+1} - x_j^{k+1}}{\delta X} \right|^2 \delta X \right) + E_h(\mathbf{x}^{k+1}). \tag{3.16}$$

Since \mathbf{x}_j^{k+1} is the minimizer of (3.1), it is easy to show that the discrete energy is dissipative in the sense that

$$E_h(\mathbf{x}^{k+1}) + \sum_{i=0}^{N-1} \frac{\delta t}{2} \left| \frac{x_{i+\frac{1}{2}}^{k+1} - x_j^{k+1}}{\delta X} \right|^2 \delta X \leq E_h(\mathbf{x}^k) + \sum_{i=0}^{N-1} \frac{\delta t}{2} \left| \frac{x_{i+\frac{1}{2}}^k - x_j^k}{\delta X} \right|^2 \delta X \leq E_h(\mathbf{x}^0) + \sum_{i=0}^{N-1} \frac{\delta t}{2} \left| \frac{x_{i+\frac{1}{2}}^0 - x_j^0}{\delta X} \right|^2 \delta X.$$

Step 2 (positivity-preserving):

Taking variational derivative with respect to the Lagrangian $\frac{\partial L}{\partial x_j^{k+1}} = 0$ for $j = 1, \dots, N - 1$, we derive the numerical scheme

(3.3). Obviously, the first two terms of (3.16) are strictly convex with respect to \mathbf{x}^{k+1} . Combining the assumption that $\frac{\delta^2 E_h}{\delta \mathbf{x}^2} > 0$, we find there exists a unique minimizer \mathbf{x}^{k+1} belonging to the closed convex set $\overline{S_{ad}} = \{\mathbf{x} : x_{j+1} \geq x_j \text{ for } j = 0, 1, \dots, N - 1, x_{j_0+1} = x_{j_0} \text{ for some } 0 \leq j_0 \leq N - 1, \text{ and } x_0 = X_0, x_N = X_N\}$.

Next, we prove that the minimizer does not lie on the boundary of $\overline{S_{ad}}$ by contradiction. We assume there exists a minimizer \mathbf{x}^{k+1} satisfies $x_{j_0+1}^{k+1} = x_{j_0}^{k+1}$ for some $0 \leq j_0 \leq N - 1$, then we obtain $E(\mathbf{x}^{k+1}) = \infty$ since we have

$$F \left(\frac{\rho(X_{j_0+\frac{1}{2}}, 0)}{\frac{x_{j_0+\frac{1}{2}}^{k+1} - x_{j_0}^{k+1}}{\delta X}} \right) \frac{x_{j_0+\frac{1}{2}}^{k+1} - x_{j_0}^{k+1}}{\delta X} = \infty,$$

under the assumption $\lim_{s \rightarrow 0} F(\frac{1}{s})s = \infty$. The above result implies

$$L(\mathbf{x}^{k+1}) = \infty,$$

which leads to a contradiction. Then the minimizer \mathbf{x}^{k+1} must lie in the interior of the admissible set S_{ad} satisfying $x_{j+1}^{k+1} > x_j^{k+1}$ for all $j = 0, 1, \dots, N - 1$. Combining the $x_{j+1} \geq x_j$ and using the equality (3.4), the positivity of the numerical solution $\rho_{j+\frac{1}{2}}^{k+1}$ can easily be obtained.

Step 3 (mass conserving):

From the equality (3.4), we derive the following result:

$$\sum_{j=0}^{N-1} \rho_{j+\frac{1}{2}}^{k+1} (x_{j+1}^{k+1} - x_j^{k+1}) = \sum_{j=0}^{N-1} \frac{\rho(X_{j+\frac{1}{2}}, 0)}{\frac{x_{j+1}^{k+1} - x_j^{k+1}}{\delta X}} (x_{j+1}^{k+1} - x_j^{k+1}) = \sum_{j=0}^{N-1} \rho(X_{j+\frac{1}{2}}, 0) \delta X,$$

which implies that the proposed scheme is mass conserving. Finally, the proof is completed. \square

Remark 3.3. Specifically, for the porous medium equation and the Fokker-Planck equation, we have $\frac{\delta^2 E_h}{\delta x^2} > 0$ since the convexity of the energy, then Theorem 3.2 will also hold without the regularization term. Actually, numerical experiments for both models are implemented without the regularization term in Section 4.

Remark 3.4. To be specific, for the Fokker-Planck equation with energy (3.6) and porous medium equation with energy (3.8), from the energy dissipation law $E_h(\mathbf{x}^{k+1}) \leq E_h(\mathbf{x}^0) + \frac{T\delta X}{2}$, we have

$$F \left(\frac{\rho(X_{j+\frac{1}{2}}, 0)}{\frac{x_{j+1}^{k+1} - x_j^{k+1}}{\delta X}} \right) \frac{x_{j+1}^{k+1} - x_j^{k+1}}{\delta X} \leq E_h(\mathbf{x}^0) + \frac{T\delta X}{2}, \quad 0 \leq j \leq N - 1.$$

Using the fact that energy density in both cases satisfies $F(\frac{1}{s})s \rightarrow \infty$ as $s \rightarrow 0$, we derive that $\frac{x_{j+1}^{k+1} - x_j^{k+1}}{\delta X} > 0, 0 \leq j \leq N - 1$ is uniformly away from zero.

Remark 3.5. If the regularization term is taken as $\sum_j |\frac{(x_{j+1}^{k+1} - x_{j+1}^k) - (x_j^{k+1} - x_j^k)}{\delta X}|^2 \delta X$, properties in Theorem 3.2 will also be derived, and the unconditionally discrete energy dissipation law $E_h(\mathbf{x}^{k+1}) \leq E_h(\mathbf{x}^k)$ holds.

Remark 3.6. In fact, the first term of the optimization problem (3.1) can also be substituted by

$$\frac{1}{2} \sum_{j=0}^{N-1} \rho(X_j, 0) |x_j^{k+1} - x_j^k|^2 \delta X + \rho(X_{j+1}, 0) |x_{j+1}^{k+1} - x_{j+1}^k|^2 \delta X,$$

which is also an approximation to $\int_{\Omega^X} \rho(X, 0) |x^{k+1} - x^k|^2 dX$. Then the corresponding numerical scheme follows

$$\rho(X_j, 0) \frac{x_j^{k+1} - x_j^k}{\delta t} \delta X - \delta t \frac{x_{j+1}^{k+1} - 2x_j^{k+1} + x_{j-1}^{k+1}}{(\delta X)^2} \delta X + \frac{\delta E_h}{\delta x_j}(\mathbf{x}^{k+1}) = 0, \tag{3.17}$$

with the initial and boundary conditions (3.5), and ρ^{k+1} defined by (3.4). The solution to scheme (3.17) also preserves properties proved in Theorem 3.2.

3.2. Two dimensional case

We extend our numerical approach to multidimensional case, for simplicity, we only consider two-dimensions. Denote $\mathbf{x} = (x, y)$, $\mathbf{X} = (X, Y)$, and the Jacobian matrix $\frac{\partial \mathbf{x}}{\partial \mathbf{X}} = \frac{\partial(x,y)}{\partial(X,Y)}$. Set $\Omega_0^{\mathbf{X}} = [-L_x, L_x] \times [-L_y, L_y]$ with $L_x, L_y > 0$, and $\Omega_0^{\mathbf{x}} = \Omega_0^{\mathbf{X}}$. Let $M_x, M_y \in \mathbb{N}$ be given, and define the grid spacing $h_x = \frac{2L_x}{M_x}, h_y = \frac{2L_y}{M_y}$. Let $X_{ij} = X_0 + jh_x, Y_{ij} = Y_0 + ih_y$ for $0 \leq j \leq M_x, 0 \leq i \leq M_y$. We define

$$\mathbf{x}_{ij}(t_k) = \mathbf{x}(X_{ij}, Y_{ij}, t_k), \quad 0 \leq j \leq M_x, 0 \leq i \leq M_y, 1 \leq k \leq \frac{T}{\delta t},$$

$$\rho_{ij}^0 = \rho(X_{ij}, Y_{ij}, 0) \geq 0.$$

The explicit and implicit numerical schemes will be proposed in the following.

3.2.1. Implicit numerical scheme

The following fully implicit numerical scheme with the regularization term $\epsilon \Delta_{\mathbf{X}} \mathbf{x}$, $\epsilon = \delta t$ can be proposed: given (x^k, y^k) , solving (x^{k+1}, y^{k+1}) from

$$\rho_{ij}^0 \frac{x_{ij}^{k+1} - x_{ij}^k}{\delta t} - \delta t \left(\frac{x_{i,j+1}^{k+1} + x_{i,j-1}^{k+1} - 2x_{ij}^{k+1}}{h_x^2} + \frac{x_{i+1,j}^{k+1} + x_{i-1,j}^{k+1} - 2x_{ij}^{k+1}}{h_y^2} \right) + \frac{\delta \bar{E}_h}{\delta x}(\mathbf{x}^{k+1}) = 0, \tag{3.18}$$

$$\rho_{ij}^0 \frac{y_{ij}^{k+1} - y_{ij}^k}{\delta t} - \delta t \left(\frac{y_{i,j+1}^{k+1} + y_{i,j-1}^{k+1} - 2y_{ij}^{k+1}}{h_x^2} + \frac{y_{i+1,j}^{k+1} + y_{i-1,j}^{k+1} - 2y_{ij}^{k+1}}{h_y^2} \right) + \frac{\delta \bar{E}_h}{\delta y}(\mathbf{x}^{k+1}) = 0, \tag{3.19}$$

with the following initial and boundary conditions:

$$\mathbf{x}^0 = \mathbf{X}, \quad \mathbf{x}^{k+1}|_{\partial\Omega} = \mathbf{X}|_{\partial\Omega}. \tag{3.20}$$

Then the density ρ_{ij}^{k+1} can be obtained by

$$\rho_{ij}^{k+1} = \frac{\rho_{ij}^0}{\mathcal{F}_{ij}^{k+1}} \quad \text{with} \quad \mathcal{F}_{ij}^{k+1} = \left| \begin{array}{cc} \frac{\partial x_{ij}^{k+1}}{\partial Y} & \frac{\partial y_{ij}^{k+1}}{\partial Y} \\ \frac{\partial x_{ij}^{k+1}}{\partial X} & \frac{\partial y_{ij}^{k+1}}{\partial X} \end{array} \right| = \left| \begin{array}{cc} \frac{x_{i,j+1}^{k+1} - x_{i,j-1}^{k+1}}{2h_x} & \frac{y_{i,j+1}^{k+1} - y_{i,j-1}^{k+1}}{2h_x} \\ \frac{x_{i+1,j}^{k+1} - x_{i-1,j}^{k+1}}{2h_y} & \frac{y_{i+1,j}^{k+1} - y_{i-1,j}^{k+1}}{2h_y} \end{array} \right|. \tag{3.21}$$

The proposed fully implicit scheme (3.18)-(3.19) is highly nonlinear and should be solved in the admissible set $E_{ad} = \{\mathbf{x} : \det \frac{\partial \mathbf{x}}{\partial \mathbf{X}}|_{ij} > 0 \text{ for all } i, j \in \mathbb{N}, \mathbf{x}|_{\partial\Omega} = \mathbf{X}|_{\partial\Omega}\}$. The solution of the implicit scheme (3.18)-(3.19) is the minimizer of the minimization problem:

$$\mathbf{x}^{k+1} := \arg \inf_{\mathbf{x} \in E_{ad}} J_k(\mathbf{x}), \tag{3.22}$$

where $J_k(\mathbf{x})$ is defined by

$$J_k(\mathbf{x}) = \frac{1}{2\delta t} \sum_{i,j} \rho_{ij}^0 |\mathbf{x}_{ij} - \mathbf{x}_{ij}^k|^2 h_x h_y + \delta t^2 \left(\left| \frac{\mathbf{x}_{i,j+1} - \mathbf{x}_{i,j}}{h_x} \right|^2 + \left| \frac{\mathbf{x}_{i+1,j} - \mathbf{x}_{i,j}}{h_y} \right|^2 \right) h_x h_y + \bar{E}_h(\mathbf{x}),$$

with $\bar{E}_h(\mathbf{x}) = \sum_{i,j} F \left(\frac{\rho_{ij}^0}{\det \frac{\partial \mathbf{x}}{\partial \mathbf{X}}|_{ij}} \right) \det \frac{\partial \mathbf{x}}{\partial \mathbf{X}}|_{ij} h_x h_y$. Following the analysis in [10,29], we obtain the following result for the implicit numerical scheme (3.18)-(3.19).

Theorem 3.7. Assume the density of energy $F(s)$ satisfies $\lim_{s \rightarrow 0} F(\frac{1}{s}) = \infty$, and $F(s) \geq 0$ for $s \geq 0$. Then there exists a solution $\mathbf{x}^{k+1} \in E_{ad}$ to the nonlinear numerical scheme (3.18)-(3.19), and the following energy dissipation law holds:

$$\begin{aligned} & \bar{E}_h(\mathbf{x}^{k+1}) + \frac{h_x h_y}{2} \sum_{i,j} \delta t \left(\left| \frac{\mathbf{x}_{i,j+1}^{k+1} - \mathbf{x}_{i,j}^{k+1}}{h_x} \right|^2 + \left| \frac{\mathbf{x}_{i+1,j}^{k+1} - \mathbf{x}_{i,j}^{k+1}}{h_y} \right|^2 \right) \\ & \leq \bar{E}_h(\mathbf{x}^k) + \frac{h_x h_y}{2} \sum_{i,j} \delta t \left(\left| \frac{\mathbf{x}_{i,j+1}^k - \mathbf{x}_{i,j}^k}{h_x} \right|^2 + \left| \frac{\mathbf{x}_{i+1,j}^k - \mathbf{x}_{i,j}^k}{h_y} \right|^2 \right). \end{aligned} \tag{3.23}$$

Proof. The existence of the solution to the nonlinear numerical scheme (3.18)-(3.19) is equivalent to obtaining the minimizer of $J_k(\mathbf{x})$ in the admissible set E_{ad} . Then we turn to prove the existence of the minimizer of the minimization problem (3.22). If the minimizer lies on the boundary of the admissible set, i.e. $\mathbf{x} \in \partial E_{ad}$, we have $J_k(\mathbf{x}) = \infty$, which is a contradiction. Following the proof in [10,29], the claim of the theorem will be derived once we show that the sub-level set

$$S := \left\{ \mathbf{x} \in E_{ad} : J_k(\mathbf{x}) \leq \bar{E}_h(\mathbf{x}^k) + \frac{h_x h_y}{2} \sum_{i,j} \delta t \left(\left| \frac{\mathbf{x}_{i,j+1}^k - \mathbf{x}_{i,j}^k}{h_x} \right|^2 + \left| \frac{\mathbf{x}_{i+1,j}^k - \mathbf{x}_{i,j}^k}{h_y} \right|^2 \right) := \gamma \right\}$$

is a non-empty compact subset of \mathbb{R}^2 . Clearly, $\mathbf{x}^k \in S$, so it is non-empty.

S is bounded. Assume the initial value $\rho_{ij}^0 > 0$, there exists $\lambda > 0$ such that

$$\frac{\lambda}{2\delta t} \sum_{i,j} |\mathbf{x}_{ij} - \mathbf{x}_{ij}^k|^2 h_x h_y \leq \frac{1}{2\delta t} \sum_{i,j} \rho_{ij}^0 |\mathbf{x}_{ij} - \mathbf{x}_{ij}^k|^2 h_x h_y \leq \gamma. \tag{3.24}$$

Then S is bounded.

S is a closed subset of \mathbb{R}^2 . It suffices to show that the limit $\tilde{\mathbf{x}}$ of any sequence $\{\mathbf{x}^{(k)}\}_{k=1}^\infty \subset E_{ad}$ belongs to E_{ad} . For all k , we have

$$\gamma \geq \bar{E}_h(\mathbf{x}^{(k)}) \geq h_x h_y F \left(\frac{\rho_{ij}^0}{\det \frac{\partial \mathbf{x}^{(k)}}{\partial \mathbf{X}} |_{ij}} \right) \det \frac{\partial \mathbf{x}^{(k)}}{\partial \mathbf{X}} |_{ij}. \tag{3.25}$$

Since $F \left(\frac{\rho_{ij}^0}{\det \frac{\partial \mathbf{x}^{(k)}}{\partial \mathbf{X}} |_{ij}} \right) \det \frac{\partial \mathbf{x}^{(k)}}{\partial \mathbf{X}} |_{ij} \rightarrow \infty$ as $\det \frac{\partial \mathbf{x}^{(k)}}{\partial \mathbf{X}} |_{ij} \rightarrow 0$, it follows that $\det \frac{\partial \mathbf{x}^{(k)}}{\partial \mathbf{X}} |_{ij} > 0$ is bounded away from zero, uniformly in k .

Then we obtain $\det \frac{\partial \tilde{\mathbf{x}}}{\partial \mathbf{X}} |_{ij} > 0$, and $\tilde{\mathbf{x}} \in E_{ad}$.

If $\mathbf{x}^{k+1} \in S$ is a minimizer of the minimization problem (3.22), we have

$$\begin{aligned} & \bar{E}_h(\mathbf{x}^{k+1}) + \frac{h_x h_y}{2} \sum_{i,j} \delta t \left(\left| \frac{\mathbf{x}_{i,j+1}^{k+1} - \mathbf{x}_{i,j}^{k+1}}{h_x} \right|^2 + \left| \frac{\mathbf{x}_{i+1,j}^{k+1} - \mathbf{x}_{i,j}^{k+1}}{h_y} \right|^2 \right) \\ & \leq \bar{E}_h(\mathbf{x}^k) + \frac{h_x h_y}{2} \sum_{i,j} \delta t \left(\left| \frac{\mathbf{x}_{i,j+1}^k - \mathbf{x}_{i,j}^k}{h_x} \right|^2 + \left| \frac{\mathbf{x}_{i+1,j}^k - \mathbf{x}_{i,j}^k}{h_y} \right|^2 \right), \end{aligned}$$

which completes the proof. \square

Remark 3.8. As stated in [10,29], we do not claim the uniqueness of the solution to the nonlinear numerical scheme (3.18)-(3.19) due to the lack of convexity of $J_k(\mathbf{x})$ and $\bar{E}_h(\mathbf{x})$ in d -dimension ($d \geq 2$).

Remark 3.9. The regularization term can also be taken as $\epsilon \sum_{i,j} \left(\left| \frac{\mathbf{x}_{i,j+1} - \mathbf{x}_{i,j} - (\mathbf{x}_{i,j+1}^k - \mathbf{x}_{i,j}^k)}{h_x} \right|^2 + \left| \frac{\mathbf{x}_{i+1,j} - \mathbf{x}_{i,j} - (\mathbf{x}_{i+1,j}^k - \mathbf{x}_{i,j}^k)}{h_y} \right|^2 \right)$, then the energy dissipation law still holds $\bar{E}_h(\mathbf{x}^{k+1}) \leq \bar{E}_h(\mathbf{x}^k)$.

3.2.2. Explicit numerical scheme

The trajectories $(\mathbf{x}^{k+1}, \mathbf{y}^{k+1})$ can also be solved by the following linear scheme with the regularization term $\epsilon \Delta_X \mathbf{x}^{k+1}$, $\epsilon = \delta t$, for given $(\mathbf{x}^k, \mathbf{y}^k)$:

$$\rho_{ij}^0 \frac{\mathbf{x}_{ij}^{k+1} - \mathbf{x}_{ij}^k}{\delta t} - \delta t \left(\frac{\mathbf{x}_{i,j+1}^{k+1} + \mathbf{x}_{i,j-1}^{k+1} - 2\mathbf{x}_{ij}^{k+1}}{h_x^2} + \frac{\mathbf{x}_{i+1,j}^{k+1} + \mathbf{x}_{i-1,j}^{k+1} - 2\mathbf{x}_{ij}^{k+1}}{h_y^2} \right) + \frac{\delta \bar{E}_h}{\delta \mathbf{x}}(\mathbf{x}_{ij}^k) = 0, \tag{3.26}$$

$$\rho_{ij}^0 \frac{\mathbf{y}_{ij}^{k+1} - \mathbf{y}_{ij}^k}{\delta t} - \delta t \left(\frac{\mathbf{y}_{i,j+1}^{k+1} + \mathbf{y}_{i,j-1}^{k+1} - 2\mathbf{y}_{ij}^{k+1}}{h_x^2} + \frac{\mathbf{y}_{i+1,j}^{k+1} + \mathbf{y}_{i-1,j}^{k+1} - 2\mathbf{y}_{ij}^{k+1}}{h_y^2} \right) + \frac{\delta \bar{E}_h}{\delta \mathbf{y}}(\mathbf{x}_{ij}^k) = 0, \tag{3.27}$$

with the initial and boundary conditions (3.20), then density ρ^{k+1} will be derived by (3.21).

The last term $\frac{\delta \bar{E}_h}{\delta \mathbf{x}}(\mathbf{x}^k)$ of the proposed numerical scheme (3.26)-(3.27) is taken to be fully explicit in the following numerical experiments. Obviously, the proposed scheme (3.26)-(3.27) admits a unique solution from its linearity. To be specific, we give some explicit formulas of $\frac{\delta \bar{E}_h}{\delta \mathbf{x}}(\mathbf{x}^k)$ for various kinds of gradient flows.

For the porous medium equation, we have the following results for $m > 1$:

$$\frac{\delta \bar{E}_h}{\delta \mathbf{x}}(\mathbf{x}^n) = \frac{\partial}{\partial X} \left(\frac{\rho^0}{\mathcal{F}^n} \right)^m \frac{\partial \mathbf{y}^n}{\partial Y} - \frac{\partial}{\partial Y} \left(\frac{\rho^0}{\mathcal{F}^n} \right)^m \frac{\partial \mathbf{y}^n}{\partial X}, \tag{3.28}$$

$$\frac{\delta \bar{E}_h}{\delta \mathbf{y}}(\mathbf{x}^n) = \frac{\partial}{\partial Y} \left(\frac{\rho^0}{\mathcal{F}^n} \right)^m \frac{\partial \mathbf{x}^n}{\partial X} - \frac{\partial}{\partial X} \left(\frac{\rho^0}{\mathcal{F}^n} \right)^m \frac{\partial \mathbf{x}^n}{\partial Y}. \tag{3.29}$$

For the aggregation-diffusion models, we have

$$\frac{\delta \bar{E}_h}{\delta \mathbf{x}}(\mathbf{x}_{ij}^n) = \frac{\partial}{\partial X} \left(\frac{\rho^0}{\mathcal{F}^n} \right)^m \frac{\partial \mathbf{y}^n}{\partial Y} |_{ij} - \frac{\partial}{\partial Y} \left(\frac{\rho^0}{\mathcal{F}^n} \right)^m \frac{\partial \mathbf{y}^n}{\partial X} |_{ij} + \nu \rho_{ij}^0 \sum_{p,q} \rho_{p,q}^n W'_x(\mathbf{x}_{ij}^n - \mathbf{z}_{pq}^n) V_{pq}, \tag{3.30}$$

$$\frac{\delta \bar{E}_h}{\delta \mathbf{y}}(\mathbf{x}_{ij}^n) = \frac{\partial}{\partial Y} \left(\frac{\rho^0}{\mathcal{F}^n} \right)^m \frac{\partial \mathbf{x}^n}{\partial X} |_{ij} - \frac{\partial}{\partial X} \left(\frac{\rho^0}{\mathcal{F}^n} \right)^m \frac{\partial \mathbf{x}^n}{\partial Y} |_{ij} + \nu \rho_{ij}^0 \sum_{p,q} \rho_{p,q}^n W'_y(\mathbf{x}_{ij}^n - \mathbf{z}_{pq}^n) V_{pq}, \tag{3.31}$$

where V_{pq} represents the area of the control volume of \mathbf{x}_{pq}^n , $m = 1$ represents the linear diffusion case where $U(\rho) = \rho \log \rho$, and $m > 1$ denotes the nonlinear diffusion case where $U(\rho) = \frac{1}{m-1} \rho^m$.

Let us discuss the explicit numerical scheme (3.26)-(3.27) with a different regularization term $\epsilon_k \Delta_X (\mathbf{x}^{k+1} - \mathbf{x}^k)$, $\epsilon_k \geq 0$, which also has a unique solution. We assume the solution belongs to the set $E_{ad} := \{\mathbf{x} : \det \frac{\partial \mathbf{x}}{\partial \mathbf{X}} |_{ij} > 0 \text{ for all } i, j \in \mathbb{N}, \mathbf{x}|_{\partial \Omega} = \mathbf{X}|_{\partial \Omega}\}$, and introduce the following minimization problem in the admissible set E_{ad} :

$$\mathbf{x}^{k+1} := \arg \inf_{\mathbf{x} \in E_{ad}} L_k(\mathbf{x}), \tag{3.32}$$

where $L_k(\mathbf{x})$ is defined by

$$L_k(\mathbf{x}) = \frac{1}{2\delta t} \sum_{i,j} \rho_{ij}^0 |\mathbf{x}_{ij} - \mathbf{x}_{ij}^k|^2 h_x h_y + \frac{\epsilon_k}{2} \|\nabla_{\mathbf{X}}(\mathbf{x} - \mathbf{x}^k)\|^2 + \bar{E}_h(\mathbf{x}^k) + \left(\frac{\delta \bar{E}_h}{\delta \mathbf{x}}(\mathbf{x}^k), \mathbf{x} - \mathbf{x}^k\right),$$

with $\bar{E}_h(\mathbf{x}) = \sum_{i,j} F\left(\frac{\rho_{ij}^0}{\det \frac{\partial \mathbf{x}}{\partial X} |_{ij}}\right) \det \frac{\partial \mathbf{x}}{\partial X} |_{ij} h_x h_y$. Then the solution to the explicit numerical scheme (3.26)-(3.27) with regularization term $\epsilon \Delta_{\mathbf{X}}(\mathbf{x}^{k+1} - \mathbf{x}^k)$ is the minimizer of the minimization problem (3.32).

For the sake of simplicity, we consider the Porous-Medium equation in 2D, we have

$$\begin{aligned} \left(\frac{\delta \bar{E}_h}{\delta x}(\mathbf{x}^k), x - x^k\right) &= - \left(\frac{\rho^0}{\det \frac{\partial \mathbf{x}^k}{\partial X}}\right)^m \cdot \det \frac{\partial((x - x^k), y^k)}{\partial(X, Y)}, \\ \left(\frac{\delta \bar{E}_h}{\delta y}(\mathbf{x}^k), y - y^k\right) &= - \left(\frac{\rho^0}{\det \frac{\partial \mathbf{x}^k}{\partial X}}\right)^m \cdot \det \frac{\partial(x^k, (y - y^k))}{\partial(X, Y)}, \\ \left(\frac{\delta^2 \bar{E}_h}{\delta x^2}(\mathbf{x}^k), (x - x^k)^2\right) &= m \left(\frac{\rho^0}{\det \frac{\partial \mathbf{x}^k}{\partial X}}\right)^{m+1} \cdot \left(\det \frac{\partial((x - x^k), y^k)}{\partial(X, Y)}\right)^2, \\ \left(\frac{\delta^2 \bar{E}_h}{\delta y^2}(\mathbf{x}^k), (y - y^k)^2\right) &= m \left(\frac{\rho^0}{\det \frac{\partial \mathbf{x}^k}{\partial X}}\right)^{m+1} \cdot \left(\det \frac{\partial(x^k, (y - y^k))}{\partial(X, Y)}\right)^2. \end{aligned}$$

Assume that the initial value $\rho(\mathbf{X}, 0) \geq 0$ is bounded, and $\det \frac{\partial \mathbf{x}^k}{\partial X} > 0$ is uniformly bounded away from zero in k satisfying $\det \frac{\partial \mathbf{x}^k}{\partial X} \geq \delta_0$ for some $\delta_0 > 0$, we have $\left\| \frac{m(\rho^0)^m}{(\det \frac{\partial \mathbf{x}^k}{\partial X})^{m+1}} \right\|_{\infty} \leq \frac{C_0}{\delta_0^{m+1}}$, where C_0 is a positive constant depending on m and ρ^0 . Then the following estimates will be obtained:

$$\left| m \left(\frac{\rho^0}{\det \frac{\partial \mathbf{x}^k}{\partial X}}\right)^{m+1} \cdot \left(\det \frac{\partial((x - x^k), y^k)}{\partial(X, Y)}\right)^2 \right| \leq \frac{2C_0}{\delta_0^{m+1}} \|\nabla_{\mathbf{X}} y^k\|_{\infty}^2 \|\nabla_{\mathbf{X}}(x - x^k)\|^2, \tag{3.33}$$

$$\left| m \left(\frac{\rho^0}{\det \frac{\partial \mathbf{x}^k}{\partial X}}\right)^{m+1} \cdot \left(\det \frac{\partial(x^k, (y - y^k))}{\partial(X, Y)}\right)^2 \right| \leq \frac{2C_0}{\delta_0^{m+1}} \|\nabla_{\mathbf{X}} x^k\|_{\infty}^2 \|\nabla_{\mathbf{X}}(y - y^k)\|^2. \tag{3.34}$$

Under these assumptions, the following energy dissipation law can be obtained.

Theorem 3.10. *The solution to the explicit numerical scheme (3.26)-(3.27) with the regularization term $\epsilon_k \Delta_{\mathbf{X}}(\mathbf{x}^{k+1} - \mathbf{x}^k)$, $\epsilon_k \geq 0$ is the minimizer of the minimization problem (3.32). If either of the following conditions is true:*

- $\epsilon_k = 0$, choose suitable time step controlled by $\delta t \leq \tau_{\min} = \frac{\min_{i,j} \rho_{ij}^0 \delta_0^{m+1} h^2}{2C_1 C_0 \|\nabla_{\mathbf{X}} \mathbf{x}^k\|_{\infty}^2}$ with $h = h_x = h_y$,
- choose suitable regularization parameter $\epsilon_k \geq \frac{C_0 \|\nabla_{\mathbf{X}} \mathbf{x}^k\|_{\infty}^2}{\delta_0^{m+1}}$,

then we have the following energy dissipation law:

$$\bar{E}_h(\mathbf{x}^{k+1}) \leq \bar{E}_h(\mathbf{x}^k). \tag{3.35}$$

Proof. Notice that $L_k(\mathbf{x}^{k+1}) \leq L_k(\mathbf{x}^k) = \bar{E}_h(\mathbf{x}^k)$, and

$$\begin{aligned} \bar{E}_h(\mathbf{x}^{k+1}) &= \bar{E}_h(\mathbf{x}^k) + \left(\frac{\delta \bar{E}_h}{\delta \mathbf{x}}(\mathbf{x}^k), \mathbf{x}^{k+1} - \mathbf{x}^k\right) + \frac{1}{2} \left(\frac{\delta^2 \bar{E}_h}{\delta \mathbf{x}^2}((1-t)\mathbf{x}^k + t\mathbf{x}^{k+1}), (\mathbf{x}^{k+1} - \mathbf{x}^k)^2\right) \\ &\leq \bar{E}_h(\mathbf{x}^k) + \left(\frac{\delta \bar{E}_h}{\delta \mathbf{x}}(\mathbf{x}^k), \mathbf{x}^{k+1} - \mathbf{x}^k\right) + \frac{C_0}{\delta_0^{m+1}} \|\nabla_{\mathbf{X}} \mathbf{x}^k\|_{\infty}^2 \|\nabla_{\mathbf{X}}(\mathbf{x}^{k+1} - \mathbf{x}^k)\|^2, \end{aligned}$$

for $0 < t < 1$, then the energy dissipation law will be derived once we choose suitable ϵ_k and time step δt such that the following inequality holds:

$$\bar{E}_h(\mathbf{x}^k) + \left(\frac{\delta \bar{E}_h}{\delta \mathbf{x}}(\mathbf{x}^k), \mathbf{x}^{k+1} - \mathbf{x}^k\right) + \frac{C_0}{\delta_0^{m+1}} \|\nabla_{\mathbf{X}} \mathbf{x}^k\|_{\infty}^2 \|\nabla_{\mathbf{X}}(\mathbf{x}^{k+1} - \mathbf{x}^k)\|^2 \leq L_k(\mathbf{x}^{k+1}),$$

we only need to guarantee that

$$\frac{C_0}{\delta_0^{m+1}} \|\nabla_{\mathbf{X}} \mathbf{x}^k\|_{\infty}^2 \|\nabla_{\mathbf{X}}(\mathbf{x}^{k+1} - \mathbf{x}^k)\|^2 \leq \frac{1}{2\delta t} \sum_{i,j} \rho_{ij}^0 |\mathbf{x}_{ij}^{k+1} - \mathbf{x}_{ij}^k|^2 h^2 + \epsilon_k \|\nabla_{\mathbf{X}}(\mathbf{x}^{k+1} - \mathbf{x}^k)\|^2.$$

In the case where $\epsilon_k = 0$, using the inverse estimate, we have

$$\frac{C_0}{\delta_0^{m+1}} \|\nabla_{\mathbf{X}} \mathbf{x}^k\|_{\infty}^2 \|\nabla_{\mathbf{X}}(\mathbf{x}^{k+1} - \mathbf{x}^k)\|^2 \leq \frac{C_1 C_0 \|\nabla_{\mathbf{X}} \mathbf{x}^k\|_{\infty}^2}{h^2 \delta_0^{m+1}} \|\mathbf{x}^{k+1} - \mathbf{x}^k\|^2,$$

then the left hand side of above inequality will be controlled by $\frac{1}{2\delta t} \sum_{i,j} \rho_{ij}^0 |\mathbf{x}_{ij}^{k+1} - \mathbf{x}_{ij}^k|^2 h^2$ once we choose suitable time step $\delta t \leq \frac{\min \rho_{ij}^0 \delta_0^{m+1} h^2}{2C_1 C_0 \|\nabla_{\mathbf{X}} \mathbf{x}^k\|_{\infty}^2} := \tau_{\min}$ such that $\frac{C_1 C_0 \|\nabla_{\mathbf{X}} \mathbf{x}^k\|_{\infty}^2}{\delta_0^{m+1} h^2} \leq \frac{\min \rho_{ij}^0}{2\delta t}$. The energy dissipation law can be obtained.

In the other case where we choose suitable regularization parameter $\epsilon_k \geq \frac{C_0 \|\nabla_{\mathbf{X}} \mathbf{x}^k\|_{\infty}^2}{\delta_0^{m+1}}$ such that $\frac{C_0}{\delta_0^{m+1}} \|\nabla_{\mathbf{X}} \mathbf{x}^k\|_{\infty}^2 \|\nabla_{\mathbf{X}}(\mathbf{x}^{k+1} - \mathbf{x}^k)\|^2 \leq \epsilon_k \|\nabla_{\mathbf{X}}(\mathbf{x}^{k+1} - \mathbf{x}^k)\|^2$, the desired energy dissipation law is derived. \square

Remark 3.11. In the proof of Theorem 3.10, we assume that $\det \frac{\partial \mathbf{x}}{\partial \mathbf{X}} \geq \delta_0 > 0$ is away from zero. From determinant plots depicted by numerical experiments in Section 4.2, we observe that the determinant of the deformation gradient for the Porous-Medium equation with Barenblatt solution and Aggregation equation satisfies this assumption. However, for the Keller-Segel model, where the particles aggregate at the center or at the circumference under certain conditions, the positivity of the determinant will not be maintained with time, and eventually the trajectory will become distorted, and once this distortion occurs, the numerical experiment will be stopped. Such cases need to be further investigated.

Remark 3.12. Similarly, if we consider the minimization problem with the regularization term $\epsilon_k \delta t \|\nabla_{\mathbf{X}} \mathbf{x}^{k+1}\|^2$, the energy dissipation law $\bar{E}_h(\mathbf{x}^{k+1}) + \epsilon_k \delta t \|\nabla_{\mathbf{X}} \mathbf{x}^{k+1}\|^2 \leq \bar{E}_h(\mathbf{x}^k) + \epsilon_k \delta t \|\nabla_{\mathbf{X}} \mathbf{x}^k\|^2$ is derived if we choose suitable ϵ_k and δt such that the following inequality holds:

$$\frac{C_0}{\delta_0^{m+1}} \|\nabla_{\mathbf{X}} \mathbf{x}^k\|_{\infty}^2 \|\nabla_{\mathbf{X}}(\mathbf{x}^{k+1} - \mathbf{x}^k)\|^2 \leq \frac{1}{2\delta t} \sum_{i,j} \rho_{ij}^0 |\mathbf{x}_{ij} - \mathbf{x}_{ij}^k|^2 h^2 + \epsilon_k \delta t \|\nabla_{\mathbf{X}} \mathbf{x}^{k+1}\|^2.$$

In the case where we choose suitable regularization parameter ϵ_k to control the left hand side of above inequality by the regularization term, it can be roughly estimated that

$$\epsilon_k \geq \frac{1}{\delta t} \frac{C_0 \|\nabla_{\mathbf{X}} \mathbf{x}^k\|_{\infty}^2 \|\nabla_{\mathbf{X}}(\mathbf{x}^{k+1} - \mathbf{x}^k)\|^2}{\delta_0^{m+1} \|\nabla_{\mathbf{X}} \mathbf{x}^{k+1}\|^2} = \frac{C_0 \|\nabla_{\mathbf{X}} \mathbf{x}^k\|_{\infty}^2 \|\nabla_{\mathbf{X}} \frac{\mathbf{x}^{k+1} - \mathbf{x}^k}{\delta t}\|^2}{\delta_0^{m+1} \|\nabla_{\mathbf{X}} \mathbf{x}^{k+1}\|^2} \delta t \geq C_2 \delta t.$$

Remark 3.13. It is worth noting that when we simulate numerical experiments using the explicit numerical scheme without regularization term, the time step δt is supposed to be sufficient small to guarantee the stability of the numerical scheme. If we carry out numerical experiments with the regularization term $\epsilon_k \|\nabla_{\mathbf{X}}(\mathbf{x}^{k+1} - \mathbf{x}^k)\|^2$, the regularization parameter should be taken appropriately through $\epsilon_k \geq C_0 \|\nabla_{\mathbf{X}} \mathbf{x}^k\|_{\infty}^2 / \delta_0^{m+1}$ to ensure the stability of the numerical scheme. The regularization term can also be taken as $\epsilon_k \delta t \|\nabla_{\mathbf{X}} \mathbf{x}^{k+1}\|^2$ with $\epsilon_k \geq C_2 \delta t$, as displayed in the following numerical experiments.

4. Numerical simulations

In this section, numerical experiments for Porous-Medium equation, Fokker-Planck equation, Keller-Segel equation and Aggregation equation will be considered in one dimension and two dimension to validate the accuracy and stability of our proposed numerical schemes based on our flow dynamic approach.

4.1. One dimension

For simplicity, we shall first show numerical experiments for models in 1D, then we consider numerical simulations in 2D in next subsection.

4.1.1. Porous medium equation

The porous medium equation $\partial_t \rho = \Delta \rho^m$, $m > 1$, can be regarded as the Wasserstein gradient flow with energy defined by

$$E(\rho) = \int_{\Omega} \frac{1}{m-1} \rho^m dx.$$

Table 1
Convergence order of trajectory x and density ρ with $m = 2$ at $T = 0.5$.

M	δt	L_h^2 error (x)	order	L^∞ error (x)	order	L_h^2 error (ρ)	order
100	1/100	4.0522e-04		2.3834e-04		3.6068e-04	
200	1/400	9.6283e-05	2.0734	5.6442e-05	2.0782	8.8534e-05	2.0624
400	1/1600	2.3484e-05	2.0356	1.3746e-05	2.0377	2.2188e-05	1.9964
800	1/6400	5.5614e-06	2.0781	3.2461e-06	2.0822	5.4442e-06	2.0270

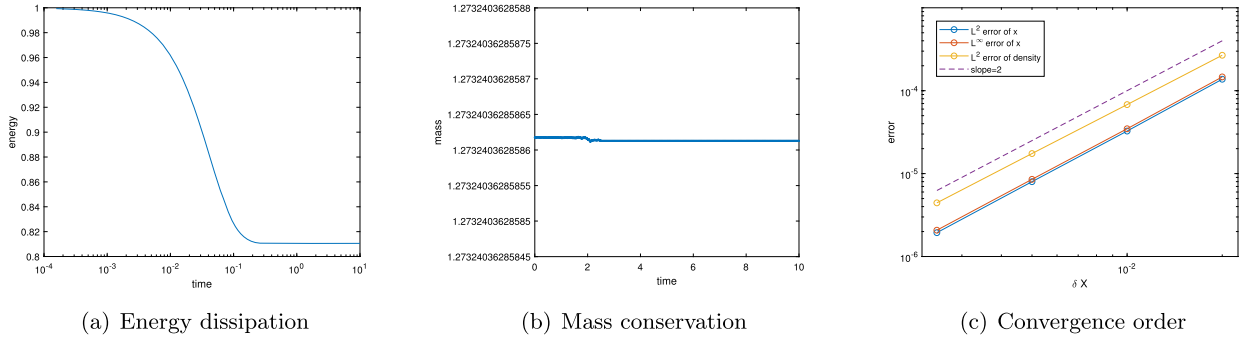


Fig. 3. The evolutions of energy and mass with respect to time under $m = 2$ with $M = 800$, $\delta t = 1/6400$.

Convergence test. Consider the following smooth initial value:

$$\rho_0(x) = \cos\left(\frac{\pi x}{2}\right), \quad x \in [-1, 1], \tag{4.1}$$

with Dirichlet boundary condition $x|_{\partial\Omega} = X|_{\partial\Omega}$. The numerical solution is solved by using scheme (3.3)-(3.4) without regularization term. The reference solution is computed under very fine meshes with $M = 8000$, $\delta t = 1/64000$. The convergence rates for density ρ and trajectories x in L^2 and L^∞ norms are shown in Table 1. We also depict the evolutions of energy and mass in Fig. 3 which show the property of energy dissipation and mass conserving with respect to time.

Free boundaries. Considering the Barenblatt solution for Porous medium equation with free boundaries [43]:

$$B_m(x, t) = (t + 1)^{-k} \left(1 - \frac{k(m-1)}{2m} \frac{|x|^2}{(t+1)^{2k}} \right)_+^{1/(m-1)}, \tag{4.2}$$

where $k = (m + 1)^{-1}$. The support set of the solution is $[l_m(t), r_m(t)]$ with the moving interface $r_m(t) = -l_m(t) := \sqrt{\frac{2m}{k(m-1)}}(t + 1)^k$.

Using scheme (3.3)-(3.4) without regularization term to calculate the interior points, and (A.2)-(A.3) to compute the boundaries. We choose the Barenblatt solution $B_m(x, 0)$ as the initial value to simulate the phenomenon of moving interface. The results are displayed in Fig. 4, it can be found that the free boundaries move with a finite speed, and the numerical propagation speed is consistent with the exact solution. The proposed scheme satisfies the property of energy dissipating, positivity-preserving and mass conserving for the density ρ .

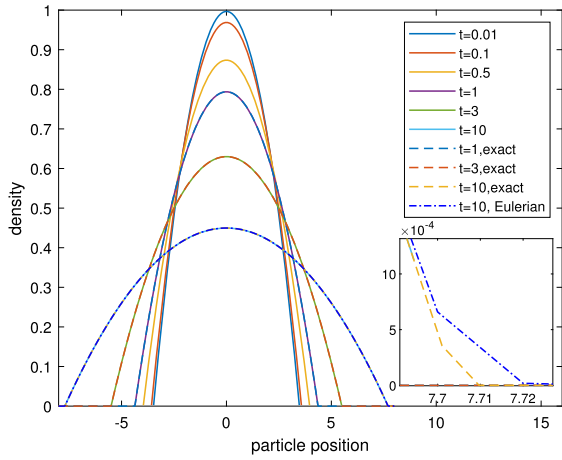
Comparison between Eulerian and Lagrangian schemes. We add one example in Fig. 4 to compare numerical solutions between Eulerian and Lagrangian coordinates. We compute the Porous Medium equations in 1D by using the following fully implicit scheme

$$\frac{\rho_i^{n+1} - \rho_i^n}{\delta t} = \frac{(\rho_{i+1}^{n+1})^m + (\rho_{i-1}^{n+1})^m - 2(\rho_i^{n+1})^m}{\delta X^2}. \tag{4.3}$$

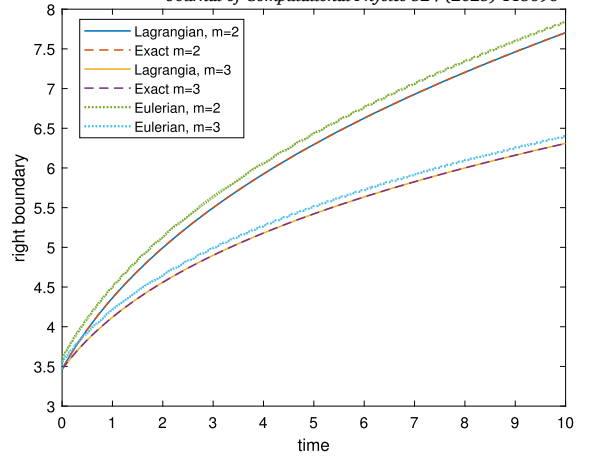
The computational domain is $X \in [-8, 8]$. For implementation, we use $M = 800$ mesh points and time step $\delta t = 1/800$. We compute the evolutions of density for Porous Medium equations in 1D in Fig. 4 (a-b), and the convergence results of scheme (4.3) are shown in Table 4.

From the following Fig. 4 (b), compared with numerical solutions in Eulerian coordinate, we observe that the right boundary of the moving interface can be computed more accurately for various times by using the Lagrangian scheme (3.3)-(3.4). In conclusion, for Porous Medium equations we find that the Lagrangian scheme (3.3)-(3.4) can capture the moving interface more accurately compared with the Eulerian scheme (4.3) from Fig. 4.

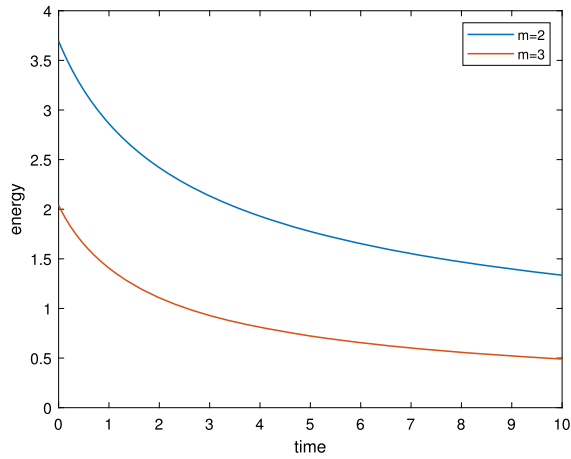
Convergence results of the trajectory and Barenblatt solution with $m = 2$ are shown in Table 2. The reference solution of trajectory is obtained on refine meshes, i.e. $M = 8000$, $\delta t = 1/64000$. The Barenblatt solution $B_m(x, 0.5)$ is taken as the exact solution to test the convergence rate for density ρ . It is observed in Table 2 and Table 3 that the convergence rates in time remain to be second order with $m = 2$, and we can not achieve optimal convergence rate when we take $m = 2.5$ due to limitation of regularity for density ρ . We also observe that the errors for density ρ at $x = 0$ away from the boundaries remains to be second order convergence rate when we take $m = 2.5$.



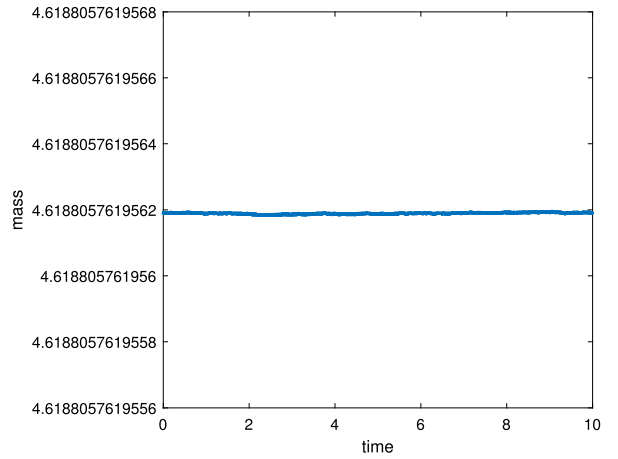
(a) Density ρ when $m = 2$



(b) Right boundary when $m = 2, 3$



(c) Energy when $m = 2, 3$



(d) Mass when $m = 2$

Fig. 4. The evolutions of density, energy and mass for the Barenblatt solution solved by the Lagrangian scheme (3.3)-(3.4) with $M = 800$, $\delta t = 1/6400$. The numerical solutions in Eulerian coordinate are solved by the fully implicit scheme: $\frac{\rho^{n+1} - \rho^n}{\delta t} = \frac{(\rho_{i+1}^{n+1})^m + (\rho_{i-1}^{n+1})^m - 2(\rho_i^{n+1})^m}{\delta x^2}$ with $M = 800$, $\delta t = 1/800$.

Table 2
Convergence order of trajectory x and density ρ with $B_m(x, T)$ at $T = 0.5$, $m = 2$.

M	δt	L_h^2 error (x)	order	L^∞ error (x)	order	L_h^2 error (ρ)	order	runtime (s)
100	1/100	0.0014		8.3240e-04		5.5360e-04		0.0340
200	1/400	3.4387e-04	2.0315	1.8335e-04	2.1827	1.3922e-04	1.9915	0.0681
400	1/1600	8.3217e-05	2.0496	4.4631e-05	2.0385	3.4935e-05	1.9946	0.4879
800	1/6400	1.8721e-05	2.1522	1.0040e-05	2.1523	8.7565e-06	1.9963	2.6089

Table 3
Convergence order of trajectory x and density ρ with $B_m(x, T)$ at $T = 0.5$, $m = 2.5$.

M	δt	L_h^2 error (x)	order	L_h^2 error (ρ)	order	error (0)	order
100	1/100	0.0011		8.0390e-04		2.2763e-04	
200	1/400	3.7503e-04	1.5509	3.6544e-04	1.1374	5.7061e-05	1.9961
400	1/1600	1.5814e-04	1.2458	1.8045e-04	1.0181	1.4262e-05	2.0003
800	1/6400	6.5878e-05	1.2634	8.7376e-05	1.0463	3.5611e-06	2.0017

Table 4
Convergence order of density ρ solved by scheme (4.3) with $B_m(x, T)$ at $T = 0.5, m = 2$.

M	δt	L^2_{Euler} error (ρ)	order	runtime (s)
100	1/100	0.0106		0.0193
200	1/400	0.0027	1.9893	0.0566
400	1/1600	6.6560e-04	1.9977	0.3178
800	1/6400	1.7630e-04	1.9166	2.0652
1600	1/25600	4.2717e-05	2.0451	16.9118

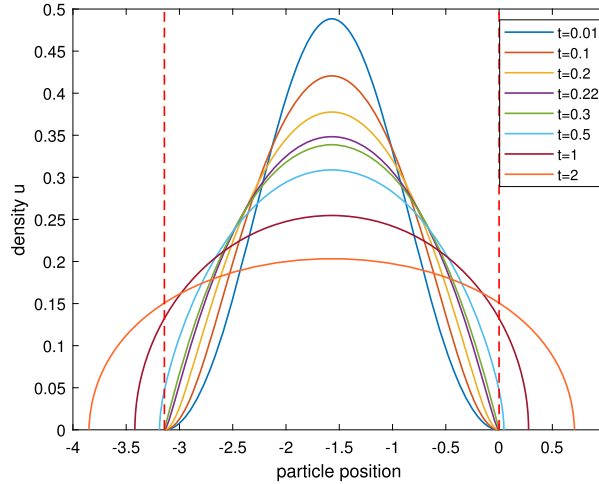


Fig. 5. Density plots for the initial value (4.4) with $m = 2, \theta = 0.25, M = 800, \delta t = 1/800$.

Notice that we use the same number of spatial points as the proposed Lagrangian scheme to solve the Eulerian scheme (4.3) in computational domain $X \in [-5, 5]$ with $m = 2$ and $T = 0.5$. We take the exact solution to be $B_2(x, 0.5)$. The convergence results and computational CPU times of the Eulerian scheme (4.3) are shown in Table 4. We also show the CPU time in Table 2 by using the proposed Lagrangian scheme. We run the Eulerian scheme (4.3) and Lagrangian scheme (3.3)-(3.4) in MATLAB on a laptop with 2.2 GHz Inter(R) Core(TM) i9-14900HX and 32 GB of RAM. We observe from Table 2 and Table 4 that to obtain the same accuracy in L^2 the Lagrangian method (3.3)-(3.4) requires fewer spatial points than the full-Implicit Eulerian method (4.3) from the CPU time. We can also observe that the Lagrangian scheme (3.3)-(3.4) achieves better accuracy than Eulerian scheme (4.3) with the same spatial points.

Waiting time. It is known that solutions to the porous medium equation may show the phenomenon of waiting time. This phenomenon indicates that the support set of solutions will not expand during a positive time t^* , after which, it will start moving at a finite speed. t^* is called the waiting time.

To be specific, the propagation speed at the boundary for the porous medium equation can be calculated by [18,19]

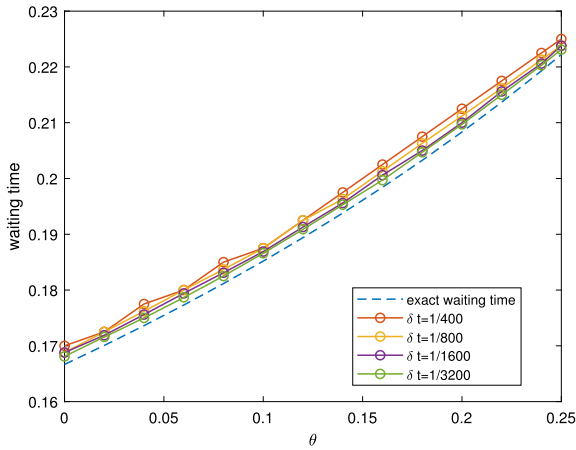
$$\partial_t x = -\frac{m}{m-1} \frac{\partial_X(\rho(X, 0))^{m-1}}{(\partial_X x)^m}.$$

The numerical waiting time can be calculated as the first instance such that $\partial_t x \neq 0$ as stated in [18,19]. Considering the following initial value:

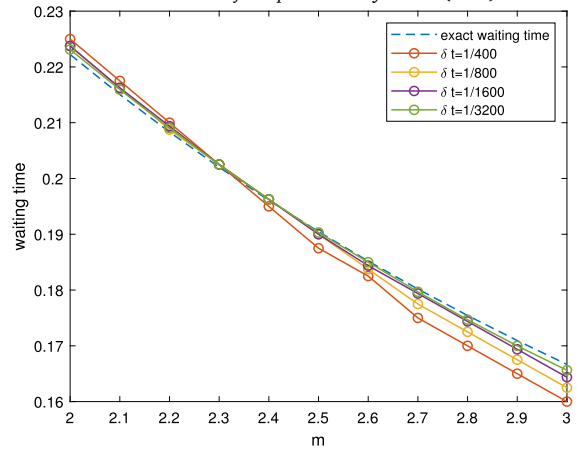
$$\rho_0(x) = \left(\frac{m-1}{m} ((1-\theta)\sin^2(x) + \theta\sin^4(x)) \right)^{1/(m-1)}, \quad x \in [-\pi, 0], \tag{4.4}$$

where $\theta \in [0, 0.25]$. For the initial value (4.4), $m = 2$ and $\theta = 0.25$, we use scheme (3.3)-(3.4) without regularization term to calculate the interior points, and use (A.2)-(A.3) to calculate the boundaries, the numerical results are displayed in Fig. 5, the free boundaries remain to be static during $0 < t \leq 0.22$. After the moment $t = 0.22$, the free boundaries begin to move at a finite speed.

The waiting time for the initial value (4.4) is given theoretically in [3] by $t_{w,e} := \frac{1}{2(m+1)(1-\theta)}$. Now, by using scheme (3.3)-(3.4) without regularization term to calculate the interior points and (A.2)-(A.3) to compute the boundaries, we calculate the waiting time numerically with different θ and m to compare the numerical waiting time with the exact formulation, the results are shown in Fig. 6, it can be observed that the tendency of the numerical waiting time is consistent with the theoretical result, and it will converge to the exact waiting time when we reduce time steps, as displayed in Table 5.



(a) Influence of θ with $m = 2$



(b) Influence of m with $\theta = 0.25$

Fig. 6. Influence of the parameter θ and m with different δt and $M = 1/\delta t$.

Table 5
Convergence order of the waiting time with the initial value (4.4), $m = 2$, $\theta = 0.25$, the exact waiting time is $t_{w,e} = \frac{1}{2(m+1)(1-\theta)} = \frac{2}{9}$.

M	δt	$t_{w,h}$	$ t_{w,h} - t_{w,e} $	order
1000	1/1000	0.2240	0.0018	
2000	1/2000	0.2235	0.0013	0.4695
4000	1/4000	0.2233	0.0011	0.2410
8000	1/8000	0.2229	0.0007	0.6521

4.1.2. Fokker-Planck equation

In this subsection, we will discuss the Fokker-Planck equation with different potentials by choosing various $U(\rho)$, $V(x)$ and taking $W(x) = 0$.

Nonlinear Fokker-Planck equation. For the nonlinear Fokker-Planck equation, $U(\rho)$ is taken to be $\frac{1}{m-1}\rho^m$, and $V(x)$ will be taken as one-well and double-well potential, respectively. If $V(x)$ is a confining drift potential, all solutions will approach to a unique steady state which is formulated as, see [9,12,15]

$$\rho_\infty(x) = \left(C_{fp} - \frac{m-1}{m} V(x) \right)_+^{\frac{1}{m-1}}, \tag{4.5}$$

where $C_{fp} > 0$ is determined by the mass of initial value such that $\int_\Omega \rho_0(x) dx = \int_\Omega \rho_\infty(x) dx$. In the following, one-well potential $V(x) = \frac{|x|^2}{2}$ and double-well potential $V(x) = \frac{|x|^4}{4} - \frac{|x|^2}{2}$ will be considered.

One well. Taking $V(x) = \frac{|x|^2}{2}$, we consider the following energy with one-well potential:

$$E(\rho) = \int_\Omega \frac{1}{m-1} \rho^m + \frac{|x|^2}{2} \rho \, dx.$$

Consider $m = 2$ and the initial value to be

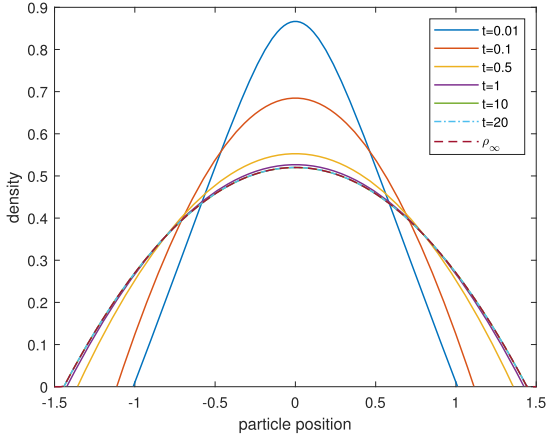
$$\rho_0(x) = \max\{1 - |x|, 0\}. \tag{4.6}$$

In this case, the stationary solution ρ_∞ is given in [18], formulated as

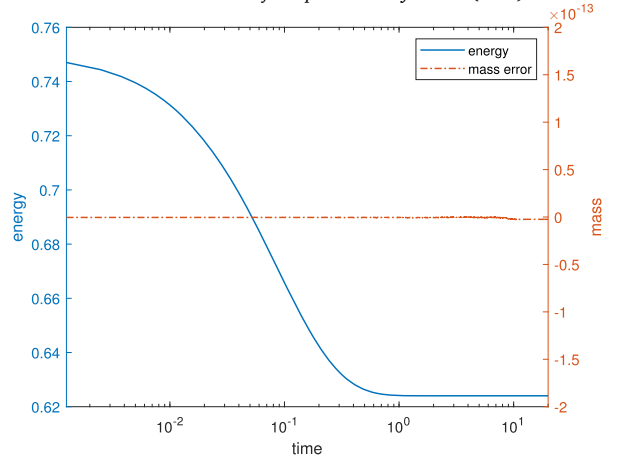
$$\rho_\infty = \max \left\{ \left(\frac{3}{8} \right)^{\frac{2}{3}} - \frac{x^2}{4}, 0 \right\}, \tag{4.7}$$

where $\left(\frac{3}{8}\right)^{\frac{2}{3}}$ is determined by the mass conservative property, such that $\int_\Omega \rho_\infty dx = \int_\Omega \rho_0 dx$. The relative energy is defined by $E(t) = E(t|\infty)/E(0|\infty)$ with $E(t|\infty) = E(t) - E(\infty)$.

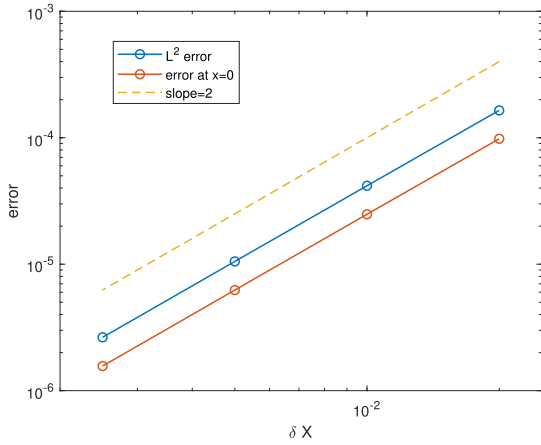
Using scheme (3.3)-(3.4) and enforcing the free boundary (A.4) without regularization term to solve the Fokker-Planck model, the numerical results are displayed in Fig. 7. As time increases, the profile of density converges to the steady state when time goes



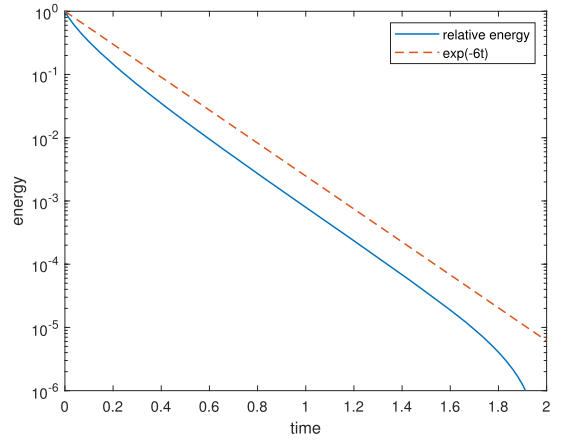
(a) Evolution of density



(b) Energy and mass



(c) Convergence rates of ρ at $T = 10$



(d) Scaling law

Fig. 7. Fokker-Planck equation with the one-well potential, $m = 2$, $M = 800$, $\delta t = 1/800$.

to $T = 10$. The convergence rate for the density is computed at the stationary time $T = 10$. It can be observed that the convergence rates of L^2 error and error at $x = 0$ are second-order. The proposed scheme is mass-conserving, and is also energy dissipative in time. As shown in diagram (d) in Fig. 7, the scaling law of the relative energy is about e^{-6t} .

Double well. Taking $V(x) = \frac{|x|^4}{4} - \frac{|x|^2}{2}$, we consider the following energy with double-well potential:

$$E(\rho) = \int_{\Omega} \frac{1}{m-1} \rho^m + \left(\frac{|x|^4}{4} - \frac{|x|^2}{2} \right) \rho \, dx.$$

Let $m = 2$, choosing the following initial value with $\sigma = 1$:

$$\rho_0(x) = (x^2 + 10^{-6} e^{-\frac{x^2}{2\sigma^2}})(1 - x^2), \quad x \in [-1, 1]. \tag{4.8}$$

Now, we implement numerical simulations with initial value (4.8) by using scheme (3.3)-(3.4) and (A.4) without regularization term, where the potential is taken as $V(x) = \frac{|x|^4}{4} - \frac{|x|^2}{2}$ and $V(x) = \frac{|x|^2}{2}$, respectively, the results are shown in Fig. 8. When the numerical solution is computed with double-well potential $V(x) = \frac{|x|^4}{4} - \frac{|x|^2}{2}$, the stationary state will also be double-well. If the potential is set to be one-well $V(x) = \frac{|x|^2}{2}$, the stationary state will also be one-well.

If we take the following one-well value as the initial condition:

$$\rho_0(x) = 1 - x^2, \quad x \in [-1, 1], \tag{4.9}$$

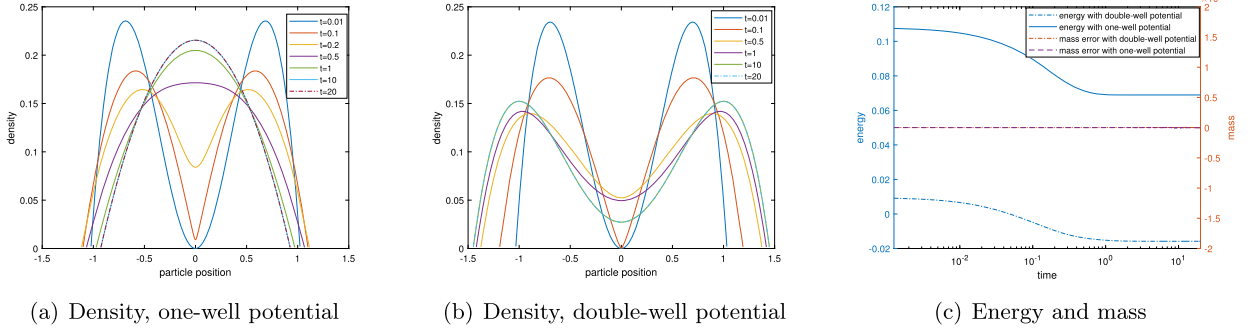


Fig. 8. Double-well initial problem for the Fokker-Planck equation with the one-well potential and the double-well potential, $m = 2$, $M = 800$, $\delta t = 1/800$.

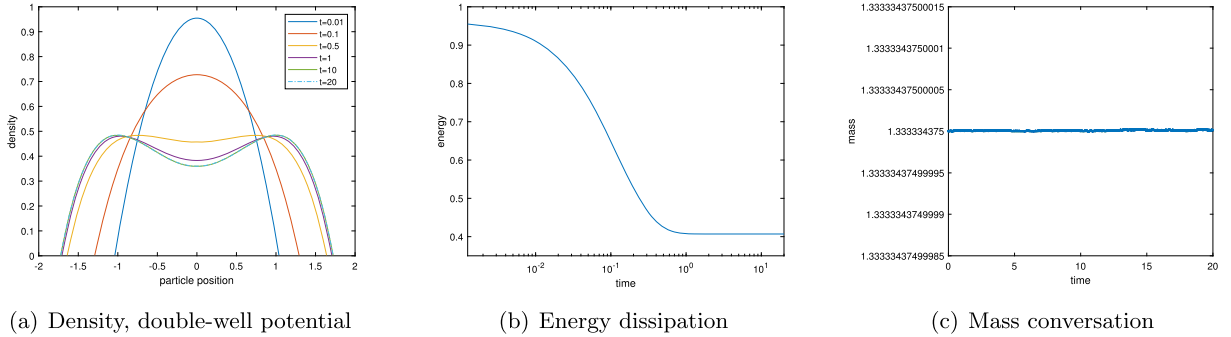


Fig. 9. One-well initial value for the Fokker-Planck equation with the double-well potential, $m = 2$, $M = 800$, $\delta t = 1/800$.

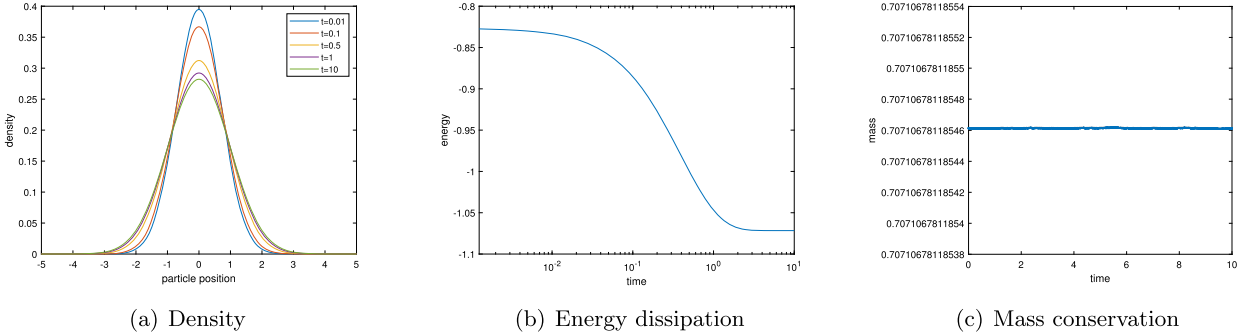


Fig. 10. One-well initial value for the Fokker-Planck equation with logarithmic potential, $M = 800$, $\delta t = 1/800$.

and calculate the numerical solution with the double-well potential, it will also converge to a double-well stationary state, as displayed in Fig. 9.

Linear Fokker-Planck equation with the logarithmic potential. Now, we consider the linear Fokker-Planck equation, i.e. taking $U(\rho) = \rho \log \rho$. Consider the following energy with one-well logarithmic potential:

$$E(\rho) = \int_{\Omega} \rho \log \rho + \frac{|x|^2}{2} \rho \, dx.$$

Numerical experiments are implemented by using scheme (3.3)-(3.4) without regularization term, and the following initial condition is considered:

$$\rho_0(x) = \frac{C_g}{\sqrt{2\pi}} e^{-x^2/\sigma}, \quad x \in [-5, 5], \tag{4.10}$$

with $C_g = \sigma = 1$. The results shown in Fig. 10 imply that numerical solution will converge to a one-well stationary state, and the curve of energy is dissipative with respect to time.

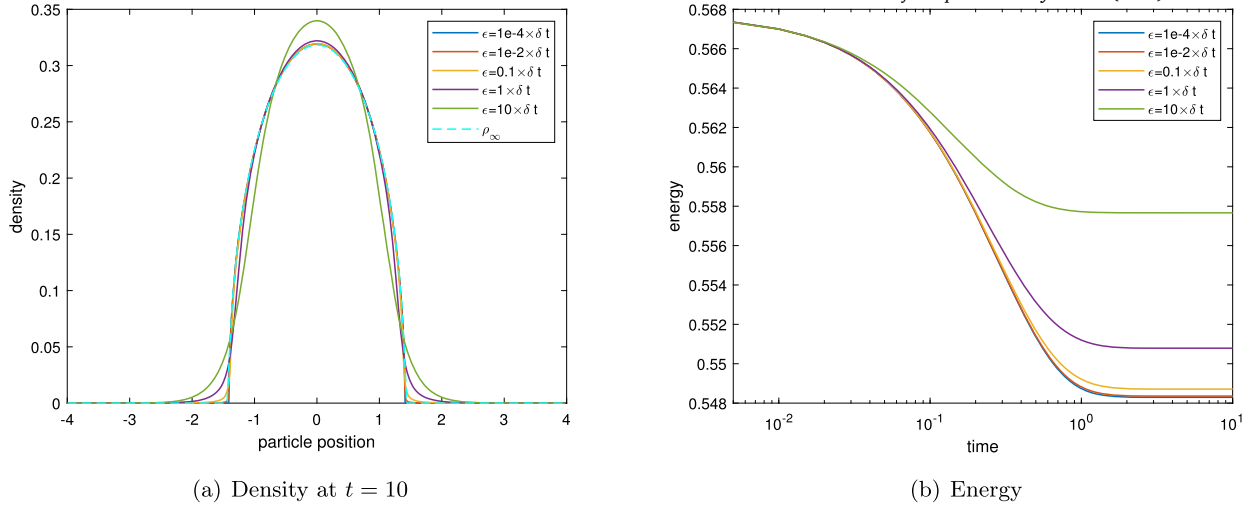


Fig. 11. Aggregation equation solved by (3.3)-(3.4) with the regularization term $\epsilon \Delta_X x^{k+1}$, the last term of (3.3) is defined by (A.6). The initial value (4.10), $C_g = \sigma = 1$, $N = 200$, $\delta t = 1/200$.

4.1.3. Aggregation equation

Considering the aggregation equation with the energy defined by

$$E(\rho) = \int_{\Omega \times \Omega} W(x - y) \rho(x) \rho(y) dx dy,$$

with $W(x) = \frac{|x|^2}{2} - \ln|x|$. We show that taking variational of $E(\rho(x))$ with respect to x leads to the following equations in Eulerian coordinate:

$$\frac{\delta E}{\delta x} = \rho \nabla_x F'(\rho) = \rho \nabla_x \left(\int_{\Omega} W(x - y) \rho(y) dy \right) = \rho \int_{\Omega} W'(x - y) \rho(y) dy,$$

and in Lagrangian coordinate:

$$\frac{\delta E}{\delta x} = \rho(X, 0) \int_{\Omega} W'(x - y) \rho(y) dy.$$

Let's set x to be implicit and y to be explicit, details can be reached in Appendix. Taking the initial value (4.10) with $C_g = \sigma = 1$, we apply scheme (3.3)-(3.4), incorporating the regularization term $\epsilon \Delta_X x^{k+1}$, and define the last term of (3.3) as provided in (A.6), to simulate the numerical experiments. The density plot at $t = 10$ and energy plot with different regularization parameter ϵ are shown in Fig. 11. It can be observed that the density achieves the equilibrium state [11]

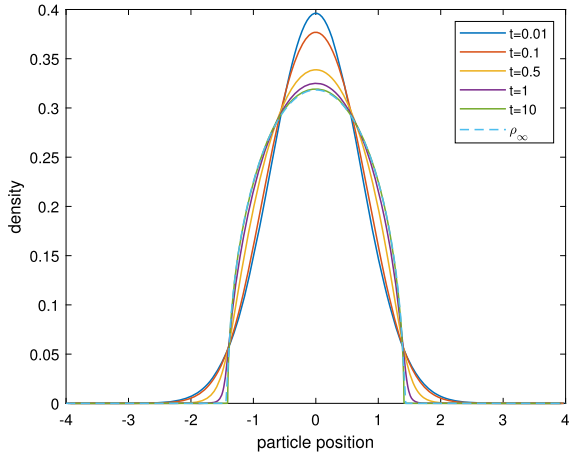
$$\rho_{\infty} = \frac{C_{ag}}{\pi} \sqrt{(2 - x^2)_+}, \tag{4.11}$$

as ϵ decreases, where $C_{ag} = 1/\sqrt{2}$ is determined by the property of mass conservation.

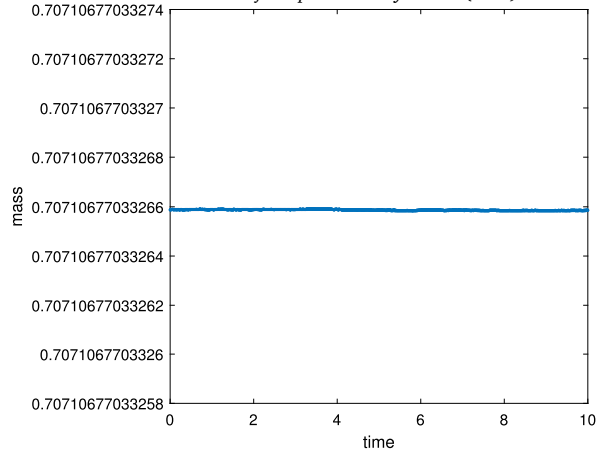
Now we use scheme (3.3)-(3.4) with the regularization term $\epsilon \Delta_X x^{k+1}$, $\epsilon = 10^{-4} \delta t$ to make numerical experiments by choosing the initial value (4.10) with $\sigma = C_g = 1$. As shown in Fig. 12, the solution will converge to the equilibrium state. If we take the initial value (4.10) with $\sigma = 0.1$, $C_g = 1$, it will converge to ρ_{∞} (4.11) with $C_{ag} = \sqrt{0.1/2}$ where the numerical results are displayed in Fig. 13. Both results indicate that the numerical solution will converge to a stationary state which is consistent with the theoretical result, and the proposed scheme is mass conserving and energy dissipating. As shown in diagram (d) in Fig. 12 and Fig. 13, the scaling law of the relative energy is also verified with theoretical results.

For the fully explicit numerical scheme, the corresponding modified discrete energy can be taken by $\hat{E}_h^{k+1} = \sum_{j=0}^{N-1} \frac{\delta E_h}{\delta x_j}(\mathbf{x}^k)(x_j^{k+1} - x_j^k) + E_h(\mathbf{x}^k)$, then the last term in the numerical scheme (3.3) will be taken as $\frac{\delta E_h}{\delta x_j}(\mathbf{x}^k)$. Now we make the numerical experiments by using (3.3)-(3.4) with the regularization term $\epsilon \Delta_X x^{k+1}$, $\epsilon = 10^{-2} \delta t$ where numerical results are shown in Fig. 14. It can be observed that the numerical solution also converges to stationary state, and the total mass is preserved well.

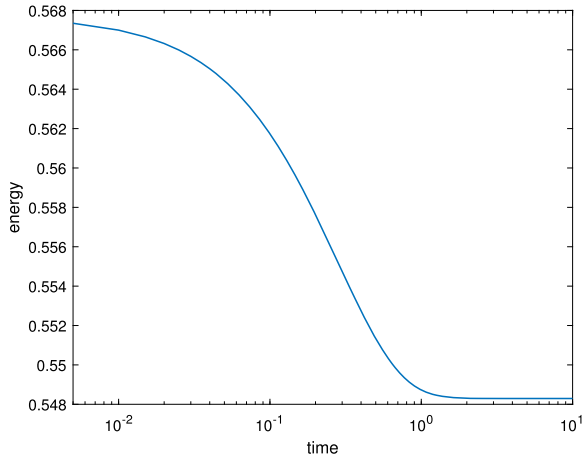
If we set x to be explicit and y to be implicit in the numerical scheme, details can be found in Appendix. We use scheme (3.3)-(3.4), in which the last term is adjusted according to (A.7), and the regularization term $\epsilon \Delta_X x^{k+1}$, $\epsilon = 10^{-4} \delta t$ to conduct numerical exper-



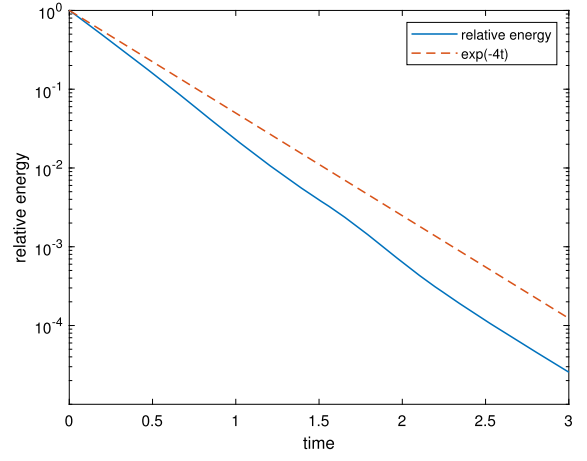
(a) Density



(b) Mass conservation



(c) Energy dissipation



(d) Relative energy

Fig. 12. Aggregation equation solved by (3.3)-(3.4) with the last term defined by (A.6), the regularization term $\epsilon \Delta_x x^{k+1}$, $\epsilon = 10^{-2} \delta t$. The initial value (4.10), $C_g = \sigma = 1$, $N = 200$, $\delta t = 1/200$.

iments, the numerical results can be found in Fig. 15 which show that the scheme preserves total mass, and the numerical solution will converge to its stationary state. The energy is also dissipative with $E_h(x^{k+1})$ defined by (A.5) in Appendix.

We set x and y both implicit in numerical scheme (3.3)-(3.4), and implement numerical experiments by using scheme (3.3)-(3.4) with the last term defined by (A.8), and the regularization term $\epsilon \Delta_x x^{k+1}$, $\epsilon = 10^{-2} \delta t$, the numerical results are displayed in Fig. 16 which implies that the proposed numerical scheme is also stable with $E_h(x^{k+1})$ defined by (A.5) in Appendix.

4.1.4. Keller-Segel model

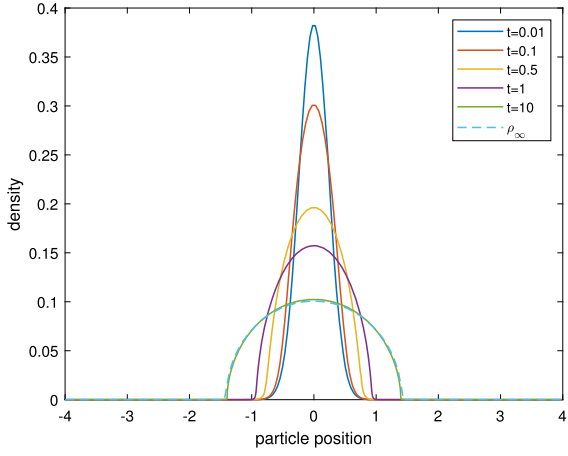
Consider the Keller-Segel model [24] with the following energy:

$$E(\rho) = \int_{\Omega} U(\rho(x)) + \rho V(x) dx + \int_{\Omega \times \Omega} W(x-y) \rho(x) \rho(y) dx dy,$$

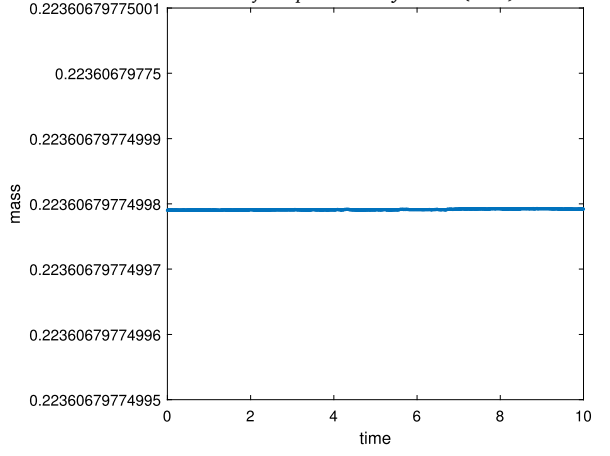
where $U = \rho \log \rho$, $V(x) = 0$ and $W(x) = \frac{1}{2\pi} \ln |x|$. Taking variational derivative with respect to x , we have

$$\frac{\delta E}{\delta x} = \rho \nabla_x U'(\rho(x)) + \rho \int_{\Omega} W'(x-y) \rho(y) dy. \tag{4.12}$$

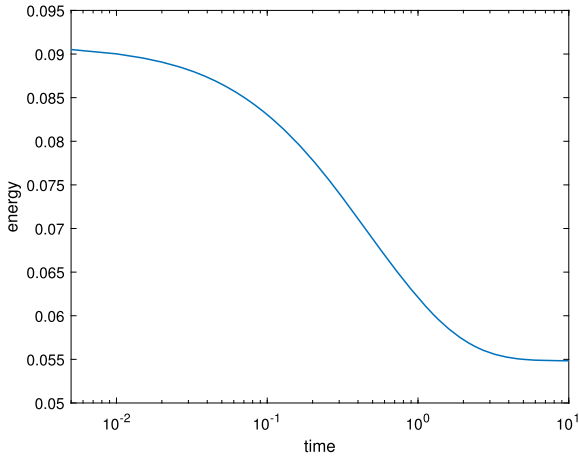
Rewriting (4.12) into Lagrangian coordinate:



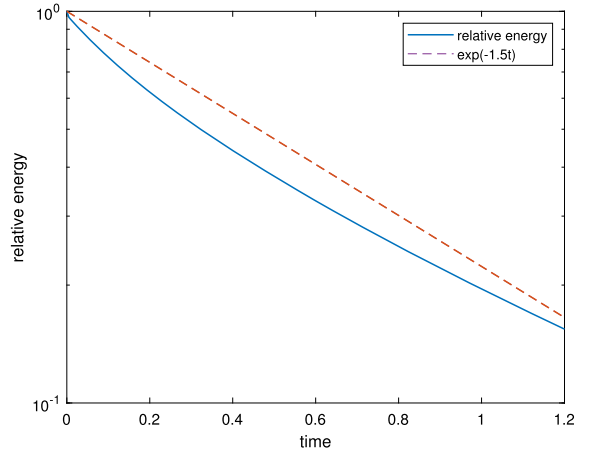
(a) Density



(b) Mass conservation

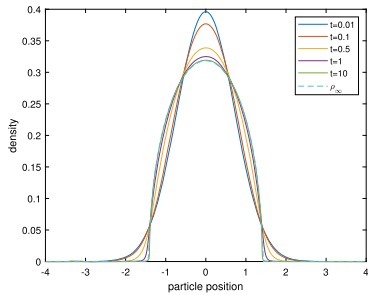


(c) Energy dissipation

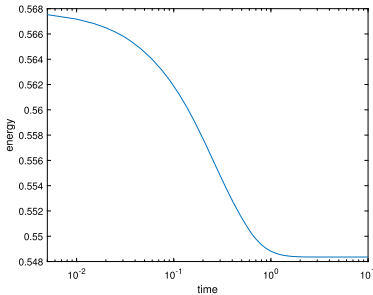


(d) Relative energy

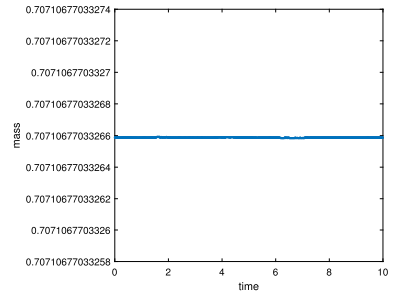
Fig. 13. Aggregation equation solved by (3.3)-(3.4) with the last term defined by (A.6), the regularization term $\epsilon \Delta_X x^{k+1}$, $\epsilon = 10^{-4} \delta t$. The initial value (4.10), $C_g = 1$, $\sigma = 0.1$, $N = 200$, $\delta t = 1/200$.



(a) Density



(b) Energy dissipation



(c) Mass conservation

Fig. 14. Aggregation equation solved by fully explicit scheme with the regularization term $\epsilon \Delta_X x^{k+1}$, $\epsilon = 10^{-2} \delta t$, the initial value is taken as (4.10) with $C_g = \sigma = 1$, $M = 200$, $\delta t = 1/200$.

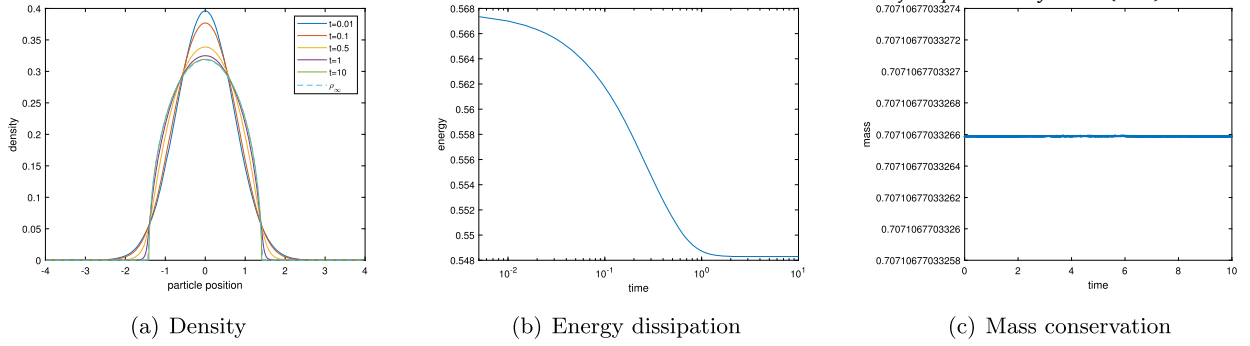


Fig. 15. Aggregation equation solved by (3.3)-(3.4) with the last term modified by (A.7), the regularization term $\epsilon \Delta_x x^{k+1}$, $\epsilon = 10^{-4} \delta t$. The initial value (4.10), $C_g = \sigma = 1$, $N = 200$, $\delta t = 1/200$.

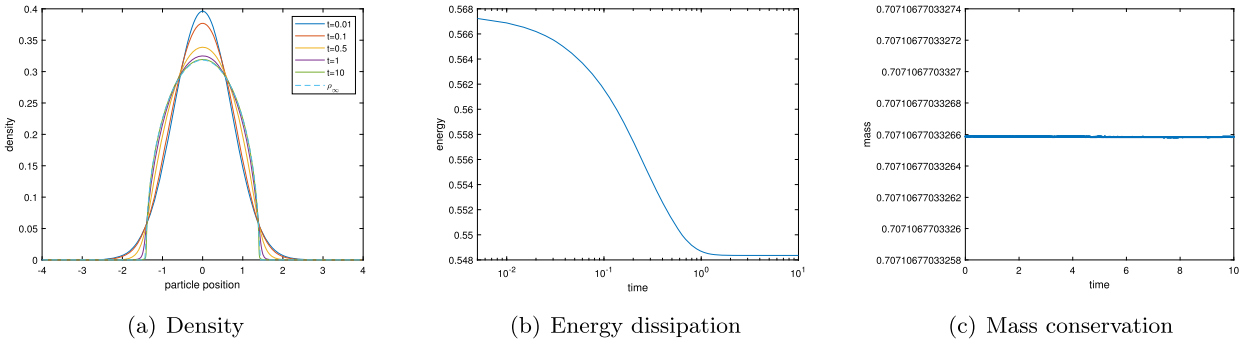


Fig. 16. Aggregation equation solved by (3.3)-(3.4) with the last term defined by (A.8), the regularization term $\epsilon \Delta_x x^{k+1}$, $\epsilon = 10^{-2} \delta t$. The initial value (4.10), $C_g = \sigma = 1$, $M = 200$, $\delta t = 1/200$.

$$\frac{\delta E}{\delta x} = \rho(X, 0) \left(\frac{\partial_X U'(\frac{\rho(X, 0)}{\partial_X x})}{\partial_X x} + \int_{\Omega} W'(x - y) \rho(Y, 0) dY \right). \tag{4.13}$$

Consider the following initial value with one well:

$$\rho_0(x) = \frac{C_{ks}}{\sqrt{2\pi}} e^{-x^2/2} + 10^{-8}, \quad x \in [-15, 15], \tag{4.14}$$

and the initial condition with double well:

$$\rho_0(x) = \frac{C_{ks}}{\sqrt{\pi}} (e^{-4(x+2)^2} + e^{-4(x-2)^2}) + 10^{-8}, \quad x \in [-15, 15], \tag{4.15}$$

combined with the Dirichlet boundary condition $x|_{\partial\Omega} = X|_{\partial\Omega}$. We simulate numerical experiments by using scheme (3.3)-(3.4) without regularization term, and the last term of (3.3) defined by (A.9).

Taking $C_{ks} = 1$ in (4.14) and (4.15) to implement numerical experiments, respectively. As shown in Fig. 17 and Fig. 18, it can be observed that numerical solutions remain to be positivity and bounded for all time. If we choose $C_{ks} = 5\pi$ to make numerical simulations, solutions also remain to be positivity. Finally, we observe that numerical solutions blow up in finite time shown in Fig. 17 and Fig. 18.

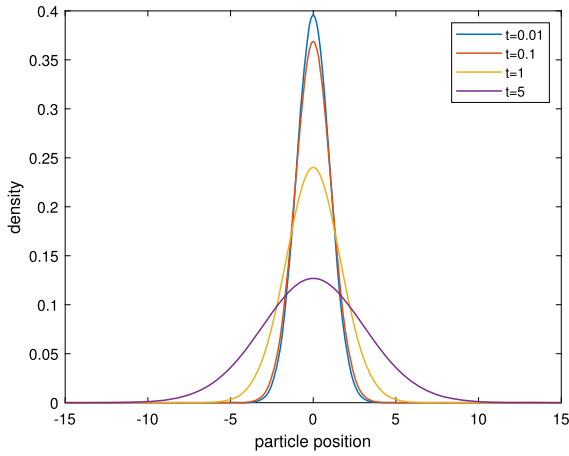
4.2. Two dimension

In this subsection, we focus on numerical simulations in 2D. For simplicity, to avoid solving nonlinear equations, we only validate the accuracy and efficiency for explicit numerical schemes (3.26)-(3.27) proposed in Section 3.2. We also take the Porous-Medium equation, Keller-Segel equation and Aggregation equation as examples.

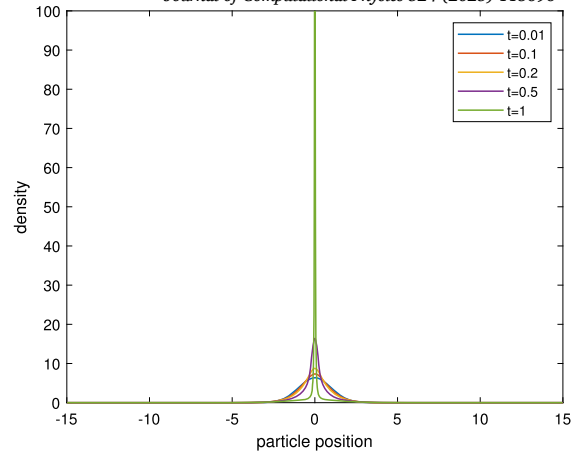
4.2.1. Porous-medium equation

The 2-D Barenblatt solution takes on the following form:

$$B_{m,2}(\mathbf{x}, t) = \left(C_{B2} - \frac{\kappa(m-1)}{4m} \frac{|\mathbf{x}|^2}{(t+1)^\kappa} \right)_+^{1/(m-1)}, \tag{4.16}$$

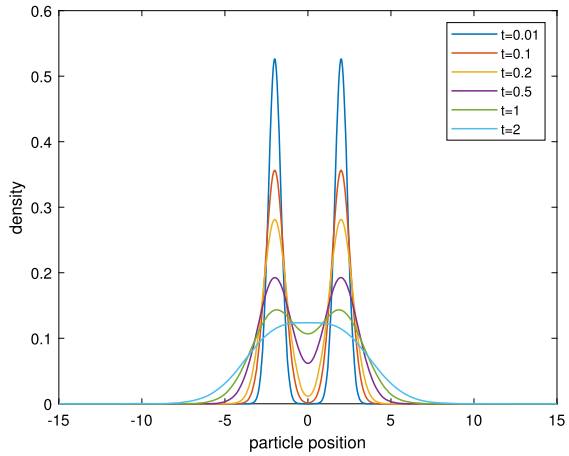


(a) Density with $C_{ks} = 1$

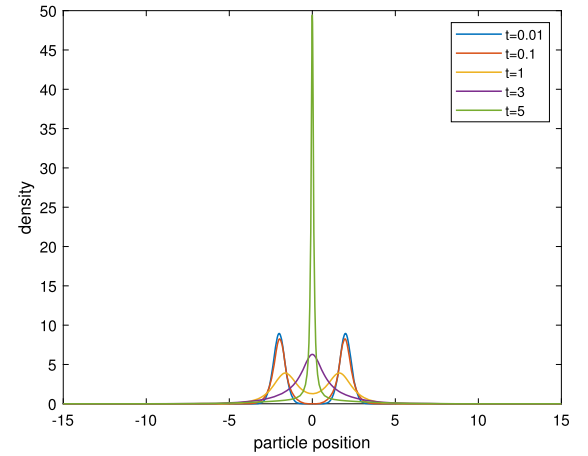


(b) Density with $C_{ks} = 5\pi$

Fig. 17. Keller-Segel model solved by (3.3)-(3.4) without regularization term, the last term of (3.3) is defined by (A.9). The initial value (4.14) with $C_{ks} = 1$ and 5π , $M = 800$, $\delta t = 1/800$.



(a) Density with $C_{ks} = 1$



(b) Density with $C_{ks} = 5\pi$

Fig. 18. Keller-Segel model solved by (3.3)-(3.4) without regularization term, the last term of (3.3) is defined by (A.9). The double-well initial value (4.15), $C_{ks} = 1$ and 5π , $M = 800$, $\delta t = 1/800$.

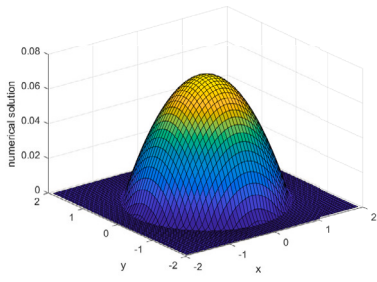
where $\kappa = 1/m$, and C_{B2} is a positive constant. The solution has a compact support $|\mathbf{x}| \leq \xi_m(t)$ for any finite time with

$$\xi_m(t) = \sqrt{\frac{4mC_{B2}}{\kappa(m-1)}}(t+1)^{\kappa/2}. \tag{4.17}$$

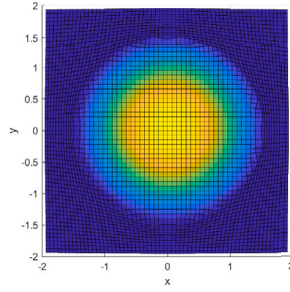
Now, we take the Barenblatt solution with $C_{B2} = 0.1$ as initial condition to make numerical experiments by using scheme (3.26)-(3.27) with the regularization term $\epsilon \Delta_{\mathbf{x}} \mathbf{x}^{k+1}$, $\epsilon = 10^{-3} \delta t$ for $m = 2$, $\epsilon = 10^{-1} \delta t$ for $m = 5$. The evolution of the numerical solution is shown in Fig. 19 and Fig. 21 for $m = 2$, $m = 5$, respectively, it can be found that the profile of density changes as the trajectory moves outward, and the free boundaries move at a finite speed. The plots of the absolute error between the numerical solution and the exact solution are also displayed, it can be observed that the main part of the error is around the free boundaries.

The trajectories at various times are shown in Fig. 20 and Fig. 22 for $m = 2$ and $m = 5$, respectively, which implies that the tendency of the numerical interface is consistent with the exact one calculated by (4.17).

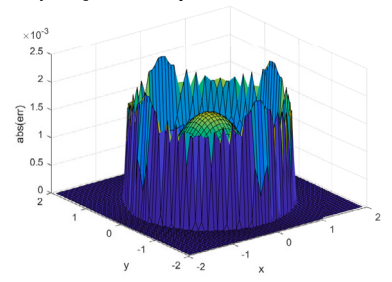
The energy curves are shown in Fig. 23 which indicates that the energy dissipation law holds in both cases where $m = 2$ and $m = 5$. Fig. 24 illustrates the minimum and maximum determinant values for both $m = 2$ and $m = 5$ with various regularization terms, respectively. It is evident from the plots that the determinant value maintains its positivity. Further, a positive distance can be observed between the minimum value and zero. The convergence order of the numerical solution with the exact solution $B_{m,2}(\mathbf{x}, 0, 1)$, $m = 2$ and $m = 2.5$ are shown in Table 6.



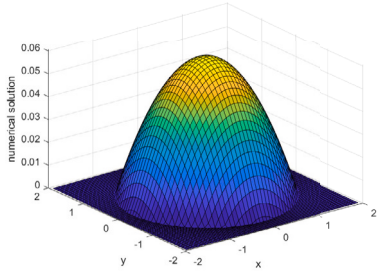
(a) Numerical solution at $t = 1$



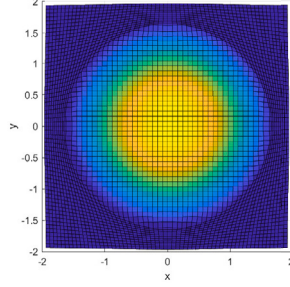
(b) Numerical solution at $t = 1$



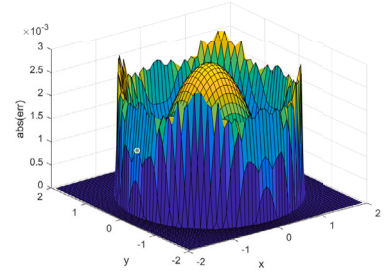
(c) $|B_{2,2}(\mathbf{x}, t) - \rho_h|$ at $t = 1$



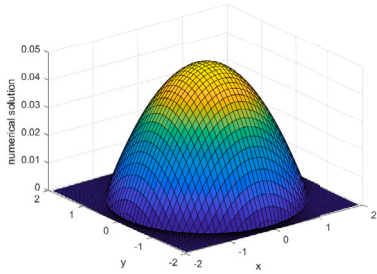
(d) Numerical solution at $t = 2$



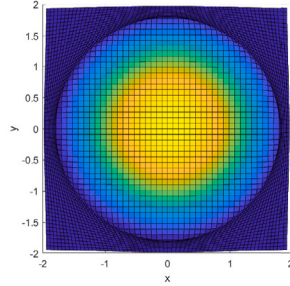
(e) Numerical solution at $t = 2$



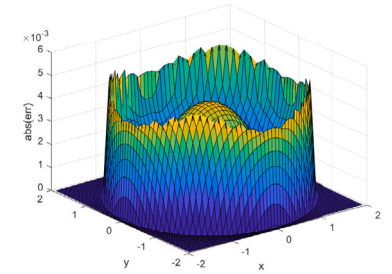
(f) $|B_{2,2}(\mathbf{x}, t) - \rho_h|$ at $t = 2$



(g) Numerical solution at $t = 4$

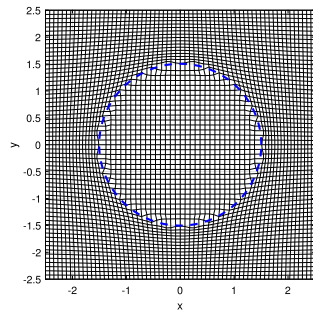


(h) Numerical solution at $t = 4$

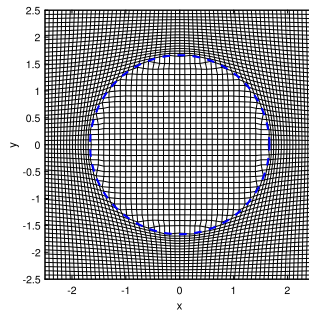


(i) $|B_{2,2}(\mathbf{x}, t) - \rho_h|$ at $t = 4$

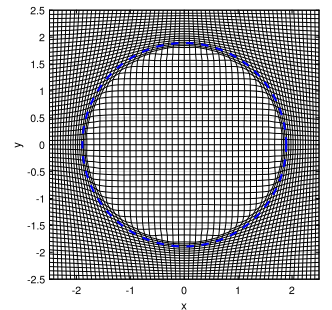
Fig. 19. Numerical solution solved by (3.26)-(3.27) with the regularization term $\epsilon \Delta_{\mathbf{x}} \mathbf{x}^{k+1}$, $\epsilon = 10^{-3} \delta t$, the initial value is Barenblatt solution with $C_{B2} = 0.1$, $m = 2$, $M_x = M_y = 64$, $\delta t = 0.01$.



(a) Trajectory at $t = 1$

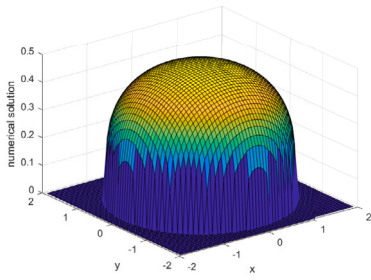


(b) Trajectory at $t = 2$

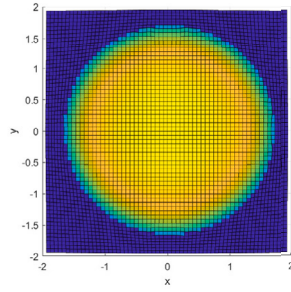


(c) Trajectory at $t = 4$

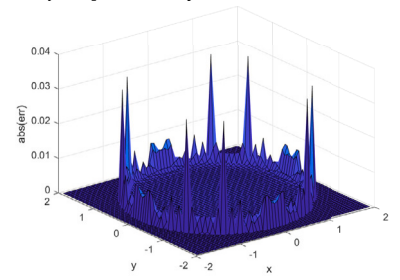
Fig. 20. Trajectories solved by (3.26)-(3.27) with the regularization term $\epsilon \Delta_{\mathbf{x}} \mathbf{x}^{k+1}$, $\epsilon = 10^{-3} \delta t$, the initial value is Barenblatt solution with $C_{B2} = 0.1$, $m = 2$, $M_x = M_y = 64$, $\delta t = 0.01$. The blue line represents the exact interface of the support set calculated by (4.17).



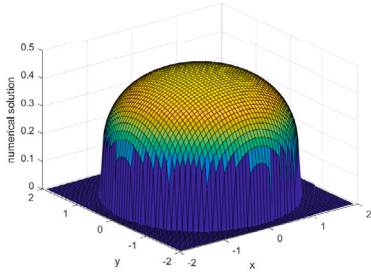
(a) Numerical solution at $t = 1$



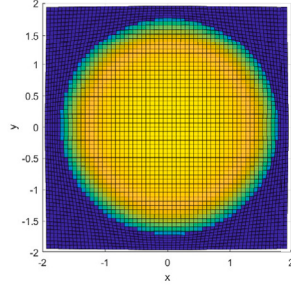
(b) Numerical solution at $t = 1$



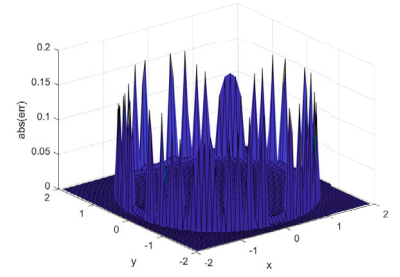
(c) $|B_{5,2}(\mathbf{x}, t) - \rho_h|$ at $t = 1$



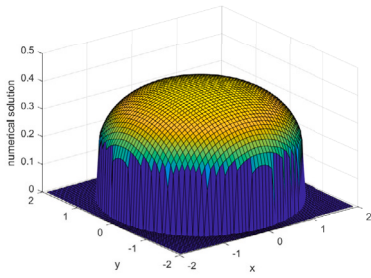
(d) Numerical solution at $t = 2$



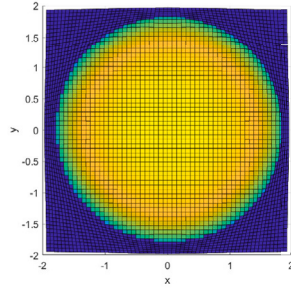
(e) Numerical solution at $t = 2$



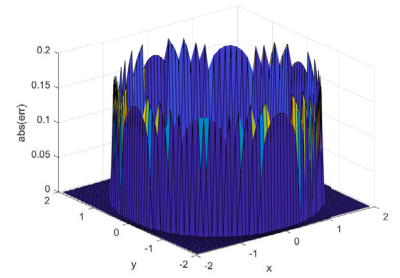
(f) $|B_{5,2}(\mathbf{x}, t) - \rho_h|$ at $t = 2$



(g) Numerical solution at $t = 4$

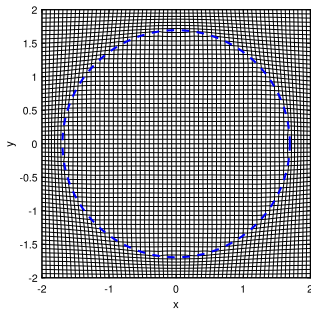


(h) Numerical solution at $t = 4$

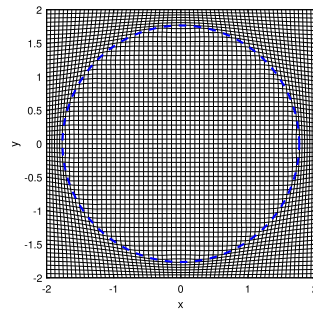


(i) $|B_{5,2}(\mathbf{x}, t) - \rho_h|$ at $t = 4$

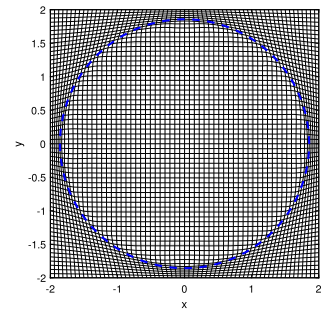
Fig. 21. Numerical solution solved by (3.26)-(3.27) with the regularization term $\epsilon \Delta_x \mathbf{x}^{k+1}$, $\epsilon = 10^{-1} \delta t$, the initial value is Barenblatt solution with $C_{B_2} = 0.1$, $m = 5$, $M_x = M_y = 64$, $\delta t = 0.01$.



(a) Trajectory at $t = 1$

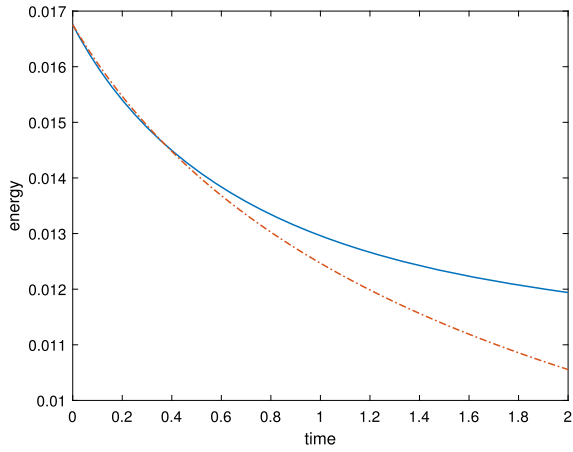


(b) Trajectory at $t = 2$

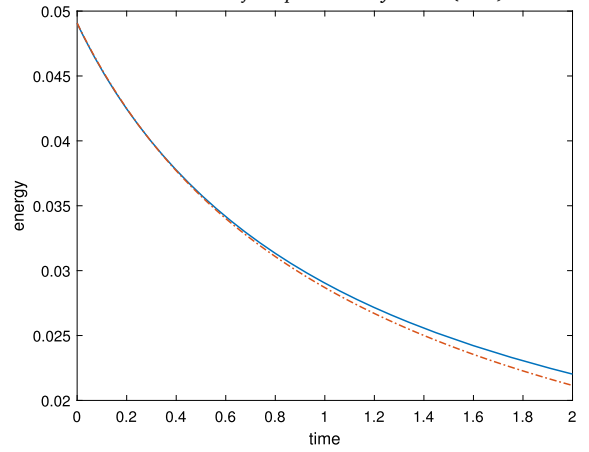


(c) Trajectory at $t = 4$

Fig. 22. Trajectories solved by (3.26)-(3.27) with the regularization term $\epsilon \Delta_x \mathbf{x}^{k+1}$, $\epsilon = 10^{-1} \delta t$, the initial value is Barenblatt solution with $C_{B_2} = 0.1$, $m = 5$, $M_x = M_y = 64$, $\delta t = 0.01$. The blue line represents the exact interface of the support set calculated by (4.17).

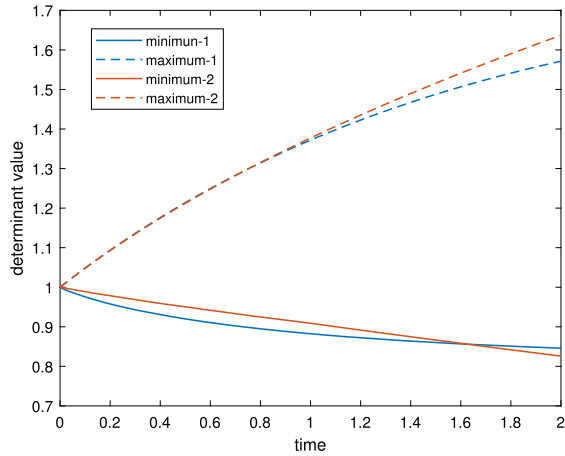


(a) $m = 2$

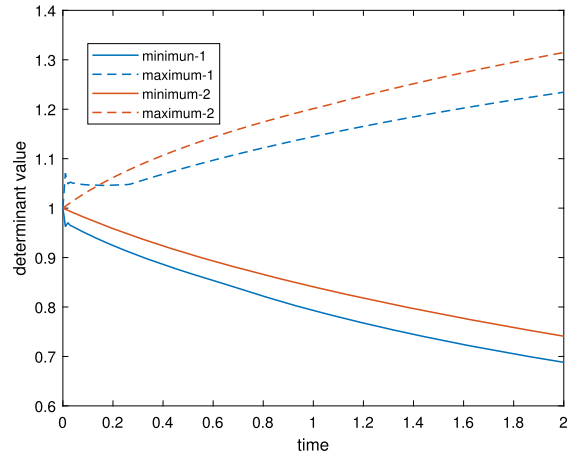


(b) $m = 5$

Fig. 23. Energy solved by (3.26)-(3.27) with different regularization terms. Set $M_x = M_y = 64$, $\delta t = 0.01$, the initial value is Barenblatt solution with $C_{B2} = 0.1$, $m = 2$, $m = 5$. The blue solid lines: $\epsilon \Delta_X \mathbf{x}^{k+1}$, $\epsilon = h_x^2$. The red dashed lines: $\epsilon_k \Delta_X (\mathbf{x}^{k+1} - \mathbf{x}^k)$, $\epsilon_k = 0.1$.



(a) $m = 2$



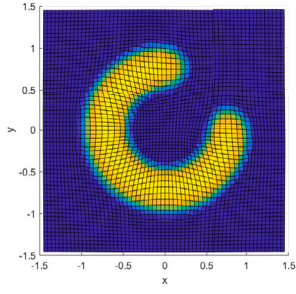
(b) $m = 5$

Fig. 24. Determinant values solved by (3.26)-(3.27) with different regularization terms. Set $M_x = M_y = 64$, $\delta t = 0.01$, the initial value is Barenblatt solution with $C_{B2} = 0.1$, $m = 2$, $m = 5$. The blue lines: $\epsilon \Delta_X \mathbf{x}^{k+1}$, $\epsilon = h_x^2$. The red lines: $\epsilon_k \Delta_X (\mathbf{x}^{k+1} - \mathbf{x}^k)$, $\epsilon_k = 0.1$.

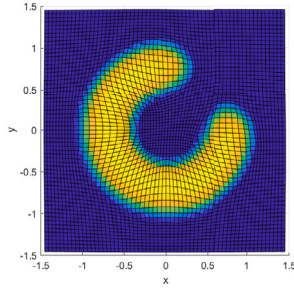
Table 6

Convergence order with $B_{m,2}(x, 0.1)$, $C_{B2} = 0.1$, $m = 2$ and $m = 2.5$ in $[-2, 2] \times [-2, 2]$. Numerical solutions are solved by (3.26)-(3.27) with regularization term $\epsilon \Delta_X \mathbf{x}^{k+1}$, $\epsilon = h_x^2$.

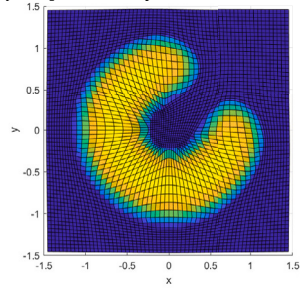
$M_x \times M_y$	N_t	$m = 2$		$m = 2.5$	
		L_h^2 error (ρ)	order	L_h^2 error (ρ)	order
16x16	16	0.0029		0.0054	
32x32	32	0.0014	1.0506	0.0026	1.0544
64x64	64	7.5117e-04	0.8982	0.0014	0.8931
128x128	128	3.6211e-04	1.0527	6.5371e-04	1.0987
256x256	256	1.7947e-04	1.0127	3.0605e-04	1.0949



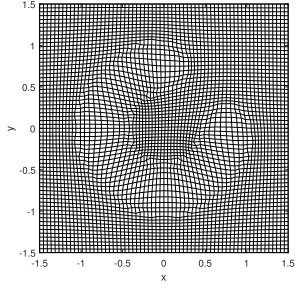
(a) Numerical solution at $t = 0.1$



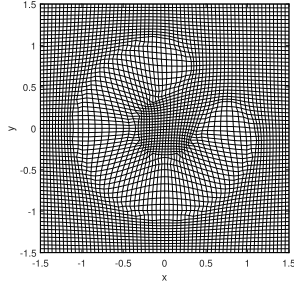
(b) Numerical solution at $t = 0.2$



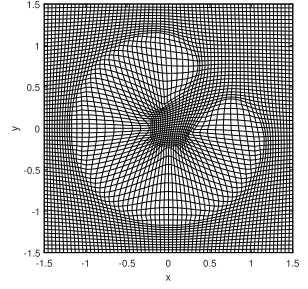
(c) Numerical solution at $t = 0.5$



(d) Trajectory at $t = 0.1$



(e) Trajectory at $t = 0.2$



(f) Trajectory at $t = 0.5$

Fig. 25. Numerical solution solved by (3.26)-(3.27) with the regularization term $\epsilon \Delta_{\mathbf{x}} \mathbf{x}^{k+1}$, $\epsilon = 0.1\delta t$, $m = 3$, the initial value (4.18) in $[-1.5, 1.5] \times [-1.5, 1.5]$, $M_x = M_y = 64$, $\delta t = 0.001$.

Non-radial problem. Consider the following initial value:

$$\rho_0(x, y) = \begin{cases} 25(0.25^2 - (\sqrt{x^2 + y^2} - 0.75)^2)^{\frac{3}{2}}, & \sqrt{x^2 + y^2} \in [0.5, 1] \text{ and } (x < 0 \text{ or } y < 0), \\ 25(0.25^2 - x^2 - (y - 0.75)^2)^{\frac{3}{2}}, & x^2 + (y - 0.75)^2 \leq 0.25^2 \text{ and } x \geq 0, \\ 25(0.25^2 - (x - 0.75)^2 - y^2)^{\frac{3}{2}}, & (x - 0.75)^2 + y^2 \leq 0.25^2 \text{ and } y \geq 0, \\ 0, & \text{otherwise,} \end{cases} \quad (4.18)$$

which has a partial donut-shaped support [29]. Let's set $m = 3$, $M_x = M_y = 64$, $\delta t = 0.001$, and use scheme (3.26)-(3.27) with the regularization term $\epsilon \Delta_{\mathbf{x}} \mathbf{x}^{k+1}$, $\epsilon = 0.1\delta t$ to implement the numerical experiments, numerical results are shown in Fig. 25, where the evolution of the trajectories can be found. We can observe that the scheme (3.26)-(3.27) handles this situation well. However, it should be noted that this approach cannot handle topological changes automatically, which serves as a limitation of our method.

Now we take the initial value as

$$\rho_0(x, y) = e^{-20((x-0.5)^2 + (y-0.5)^2)}, \quad x \in [-2, 2] \times [-2, 2]. \quad (4.19)$$

Let's set $m = 2$, $M_x = M_y = 64$, $\delta t = 0.01$, and use scheme (3.26)-(3.27) with the regularization term $\epsilon \Delta_{\mathbf{x}} \mathbf{x}^{k+1}$, $\epsilon = 0.1\delta t$ to simulate the numerical experiments, results are shown in Fig. 26. It can be found that the proposed scheme (3.26)-(3.27) can handle the nonradial case well.

4.2.2. Aggregation equation

Consider the following aggregation equation:

$$\partial_t \rho = \nabla \cdot (\rho \nabla W * \rho), \quad W : \mathbb{R}^2 \rightarrow \mathbb{R}. \quad (4.20)$$

We simulate the evolution of solutions to (4.20) with

$$W(\mathbf{x}) = \frac{|\mathbf{x}|^2}{2} - \ln |\mathbf{x}|,$$

and the initial value

$$\rho_0(x, y) = C_{2d} e^{-x^2 - y^2}, \quad (4.21)$$

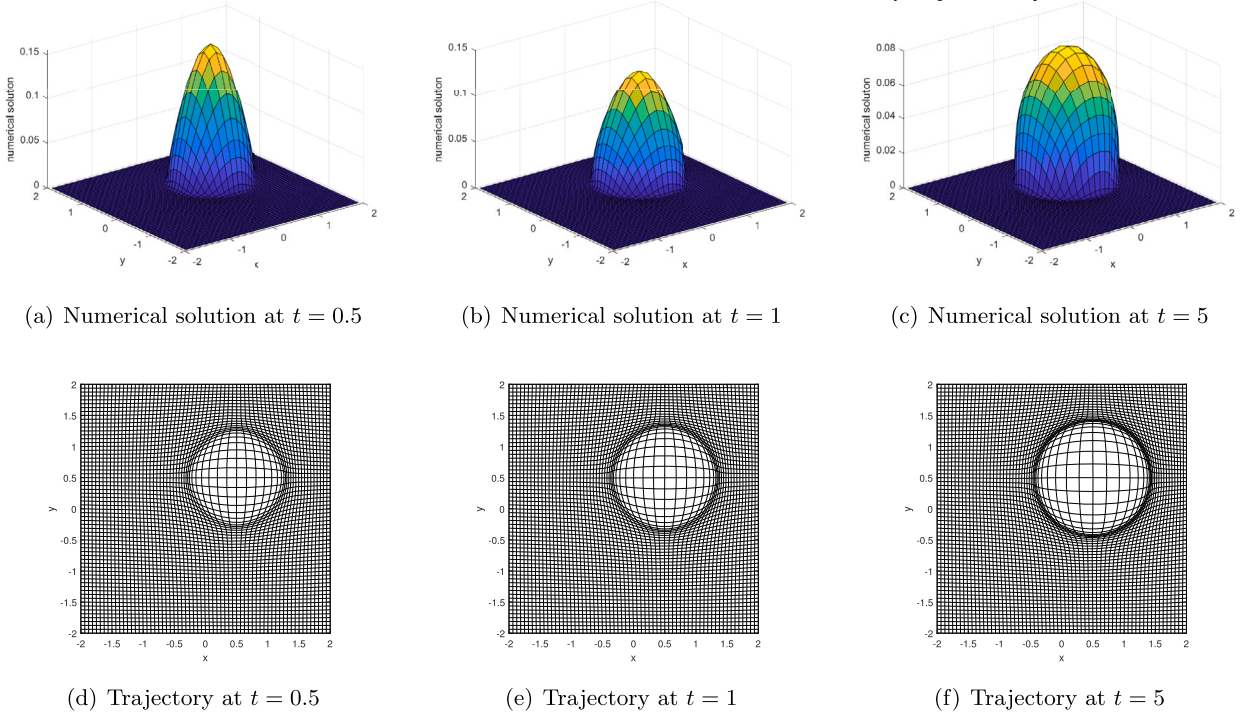


Fig. 26. Numerical solution solved by (3.26)-(3.27) with the regularization term $\epsilon \Delta_{\mathbf{x}} \mathbf{x}^{k+1}$, $\epsilon = 0.1\delta t$, $m = 2$, the initial value (4.19) in $[-2, 2] \times [-2, 2]$, $M_x = M_y = 64$, $\delta t = 0.01$.

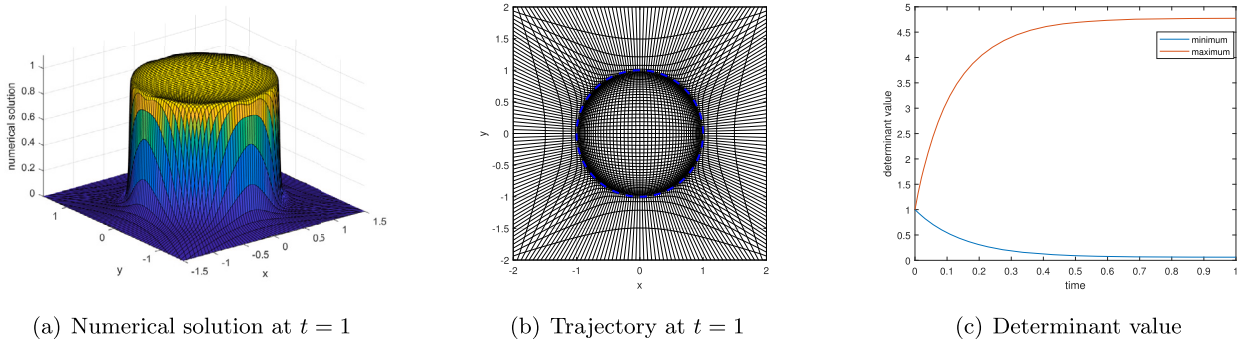


Fig. 27. Aggregation equation solved by (3.26)-(3.27) with the regularization term $\epsilon \Delta_{\mathbf{x}} \mathbf{x}^{k+1}$, $\epsilon = 0.1\delta t$, the initial value (4.21) in $[-2, 2] \times [-2, 2]$, $M_x = M_y = 64$, $\delta t = 0.01$.

in $[-2, 2] \times [-2, 2]$, $C_{2d} = 1$, $M_x = M_y = 64$, $\delta t = 0.01$. Using scheme (3.26)-(3.27) with the regularization term $\epsilon \Delta_{\mathbf{x}} \mathbf{x}^{k+1}$, $\epsilon = 0.1\delta t$ to simulate the numerical experiments, the numerical solution and trajectory plots at $t = 1$ are shown in Fig. 27. The blue line in the trajectory plot represents the unit circle. As can be observed the solution converges to a characteristic function on the disk of radius 1, centered at $(0, 0)$, recovering analytic results on solutions of the aggregation equation with Newtonian repulsion [9,22,28]. Moreover, the determinant value plot is also presented in Fig. 27, we find that despite the minimum value diminishing over time, the distance between the minimum and zero remains positive as the density tends to a steady state.

4.2.3. Aggregation diffusion equation

Now we simulate several examples of aggregation-diffusion equation:

$$\partial_t \rho = \nabla \cdot (\rho \nabla W * \rho) + \nu \Delta \rho^m, \quad W : \mathbb{R}^2 \rightarrow \mathbb{R}, \quad m \geq 1. \tag{4.22}$$

For the aggregation diffusion equation (4.22), we take $W(\mathbf{x}) = -\frac{1}{\pi} e^{-|\mathbf{x}|^2}$, $m = 3$ and $\nu = 0.1$. The initial value is taken as

$$\rho_0(x, y) = \frac{1}{2} \chi_{\{|x| \leq 2.5, |y| \leq 2.5\}}(x, y). \tag{4.23}$$

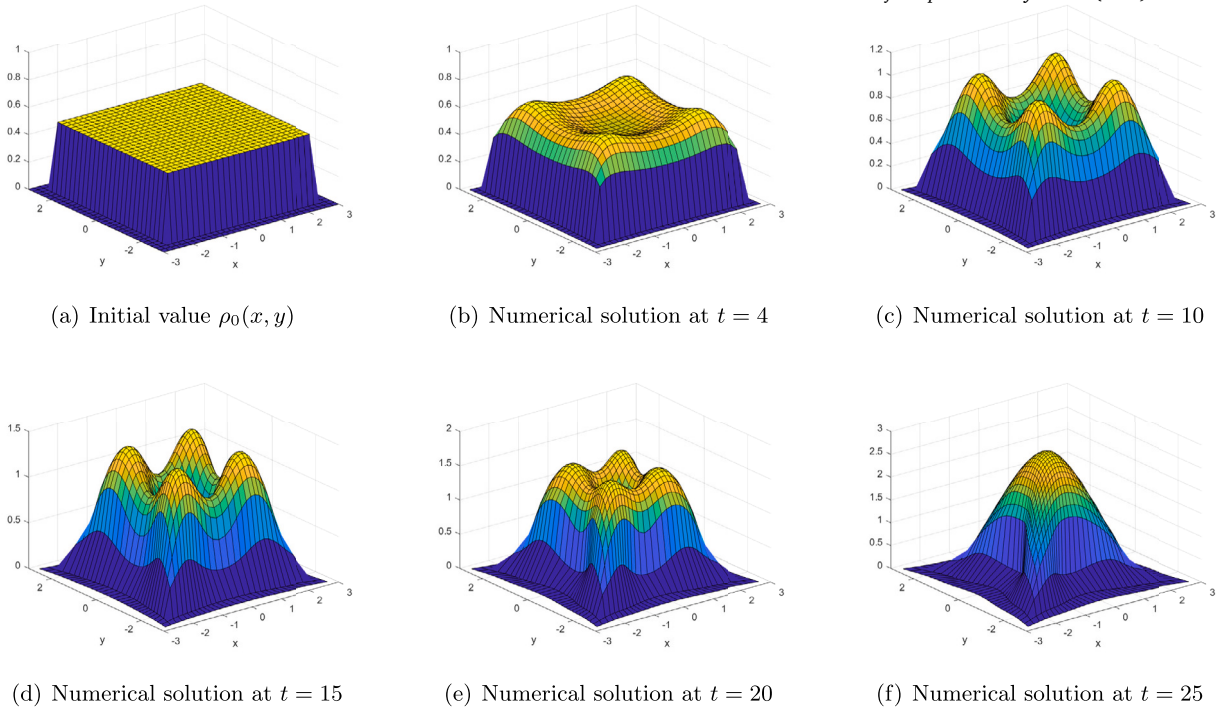


Fig. 28. Evolution of the numerical solution for the aggregation diffusion equation solved by (3.26)-(3.27) with the regularization term $\epsilon \Delta_{\mathbf{x}} \mathbf{x}^{k+1}$, $\epsilon = 0.1\delta t$, initial value (4.23) in $[-3, 3] \times [-3, 3]$, $m = 3$, $\nu = 0.1$, $M_x = M_y = 32$, $\delta t = 0.01$.

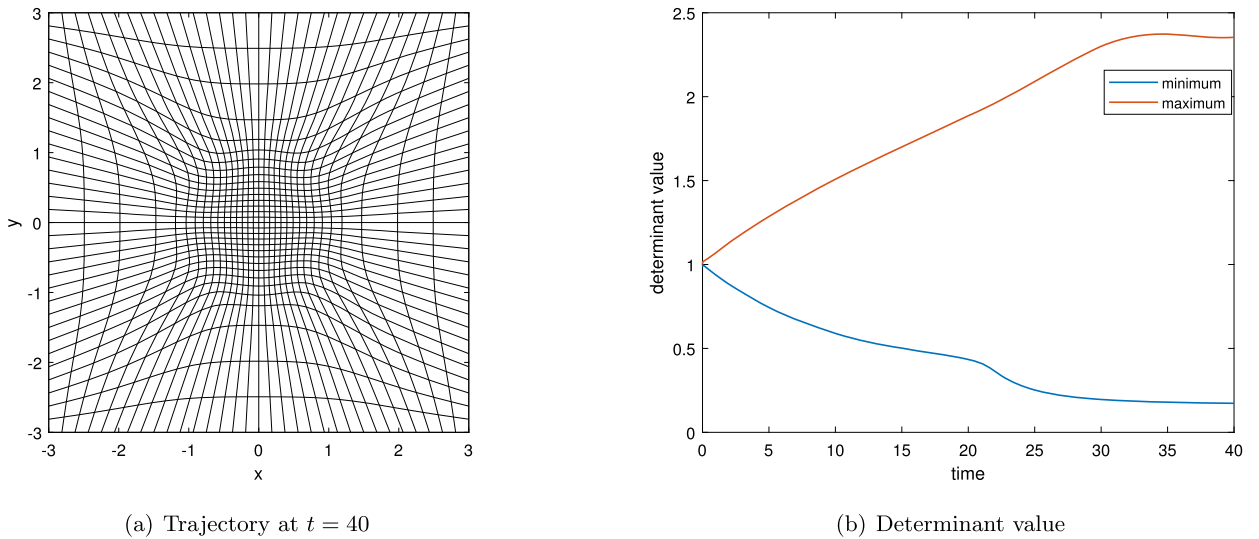
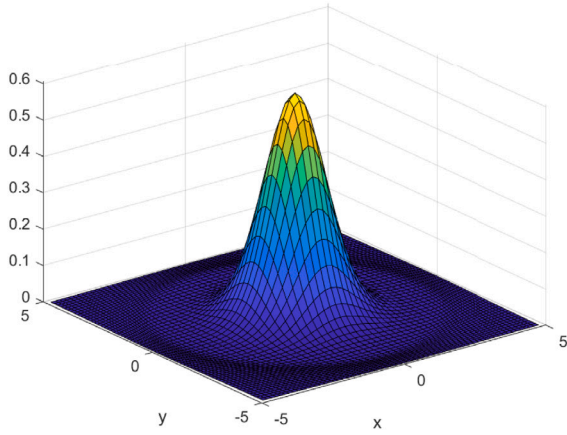


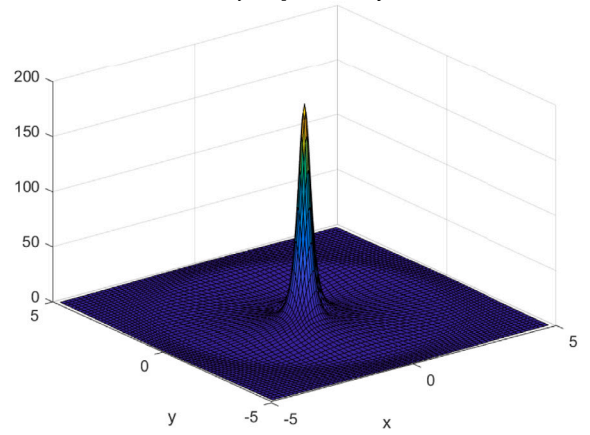
Fig. 29. Trajectory and determinant value for the aggregation diffusion equation solved by (3.26)-(3.27) with the regularization term $\epsilon \Delta_{\mathbf{x}} \mathbf{x}^{k+1}$, $\epsilon = \delta t$, initial value (4.23) in $[-3, 3] \times [-3, 3]$, $m = 3$, $\nu = 0.1$, $M_x = M_y = 32$, $\delta t = 0.01$.

Using scheme (3.26)-(3.27) with the regularization term $\epsilon \Delta_{\mathbf{x}} \mathbf{x}^{k+1}$, $\epsilon = 0.1\delta t$ to carry out numerical experiments, the evolution of density can be found in Fig. 28, the solution tends to form four bumps at the four angles at the beginning, and finally approaches a single bump equilibrium [8,9]. The trajectory and determinant value plots are depicted in Fig. 29, which implies that there is no distortion or swap during the evolution of the solution, and that the minimum value of the determinant is lower bounded away from zero.

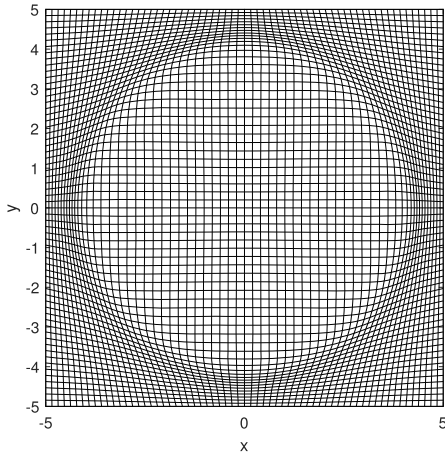
We also simulate the evolution of the solution for the Keller-Segel equation, which is the aggregation-diffusion equation (4.22) with the kernel $W(\mathbf{x}) = \frac{1}{2\pi} \ln(|\mathbf{x}|)$ for $\nu = 1$, $m = 1$ and $m = 2$, the global existence and blow-up of solutions are displayed. Taking the



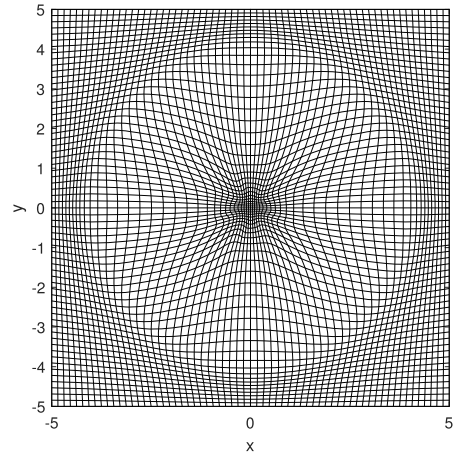
(a) Density with $C_{2d} = 1$ at $t = 0.25$



(b) Density with $C_{2d} = 20$ at $t = 0.25$



(c) Trajectory with $C_{2d} = 1$ at $t = 0.25$



(d) Trajectory with $C_{2d} = 20$ at $t = 0.25$

Fig. 30. Keller-Segel model solved by (3.26)-(3.27) with the regularization term $\epsilon \Delta_x \mathbf{x}^{k+1}$, $\epsilon = 0.1\delta t$, initial value (4.21), $m = 1$, $M_x = M_y = 64$, $\delta t = 0.001$.

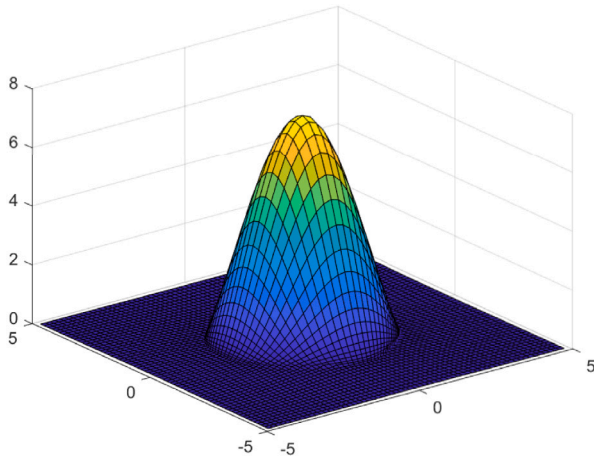
initial value (4.21), and the constant C_{2d} will be chosen as 1 and 20 in the following numerical experiments. The numerical solution is solved by scheme (3.26)-(3.27) with regularization term $\epsilon \Delta_x \mathbf{x}^{k+1}$, $\epsilon = 0.1\delta t$.

For the case when $m = 1$, the numerical solution can be found in Fig. 30. The solution decays to zero as time increases, given $C_{2d} = 1$. Conversely, when $C_{2d} = 20$, the solution becomes sharply peaked at the origin, which can be regarded as the blow-up phenomenon. As for the case when $m = 2$, we can observe from Fig. 31 that the solution converges to a stable state denoted by a single bump, provided $C_{2d} = 20$. Fig. 32 illustrates the determinant value plots for $m = 1$ and $m = 2$. It can be noticed that the determinant values remain positive for the given time. However, since the particles are clustered at the center for $m = 1$ and at the circumference for $m = 2$, the particle trajectories will actually be distorted or exchanged as time increases, and the positive value of the determinant will not always be maintained.

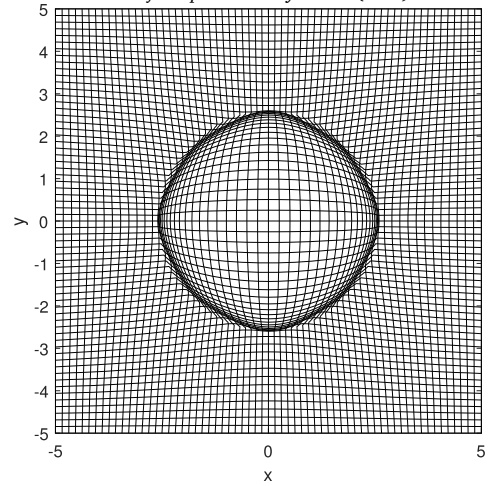
5. Concluding remarks

We constructed in this paper new numerical schemes for the Wasserstein gradient flows using a flow dynamic approach based on the Benamou-Bernier formula. We showed that the new schemes preserve essential structures of the Wasserstein gradient flows. More precisely, the fully discrete schemes are shown to be positivity-preserving, mass conservative and energy dissipative. Moreover, it is shown that the schemes are uniquely solvable in the one dimensional case.

We presented ample numerical experiments to show that the proposed schemes are indeed positivity preserving, mass conservative and energy stable. Our numerical results also indicate that the new schemes can capture accurately the movement of the trajectory and the finite propagation speed for the Porous-Medium equation, and can simulate blow-up phenomenon of the Keller-Segel equation.

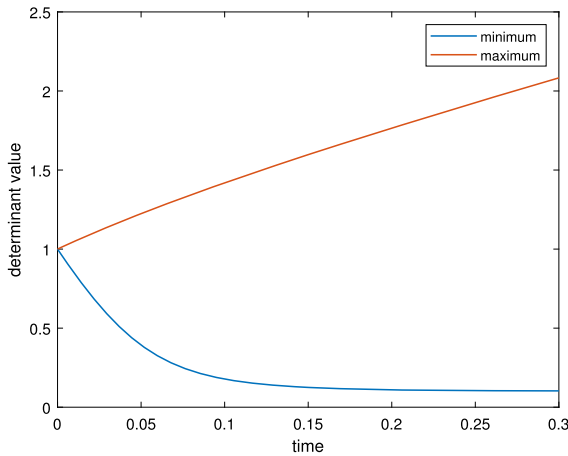


(a) Density with $C_{2d} = 20$ at $t = 0.12$

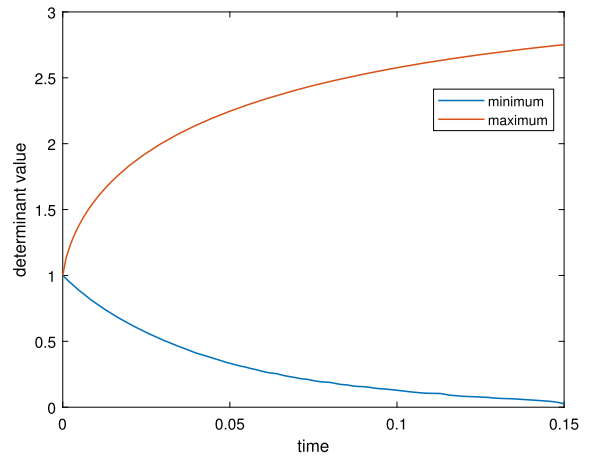


(b) Trajectory with $C_{2d} = 20$ at $t = 0.12$

Fig. 31. Keller-Segel model solved by (3.26)-(3.27) with the regularization term $\epsilon \Delta_x x^{k+1}$, $\epsilon = 0.1\delta t$, initial value (4.21) at $t = 0.12$, $m = 2$, $M_x = M_y = 64$, $\delta t = 0.001$.



(a) $m = 1$ with $C_{2d} = 20$



(b) $m = 2$ with $C_{2d} = 20$

Fig. 32. Determinant value for the Keller-Segel model with $m = 1, 2$, solved by (3.26)-(3.27) with the regularization term $\epsilon \Delta_x x^{k+1}$, $\epsilon = 0.1\delta t$, initial value (4.21), $M_x = M_y = 64$, $\delta t = 0.001$.

CRedit authorship contribution statement

Qing Cheng: Writing – review & editing, Writing – original draft, Visualization, Supervision, Methodology, Conceptualization. **Qianqian Liu:** Writing – review & editing, Visualization, Software, Conceptualization. **Wenbin Chen:** Writing – review & editing, Methodology, Funding acquisition, Conceptualization. **Jie Shen:** Writing – review & editing, Writing – original draft, Methodology, Funding acquisition, Conceptualization.

Declaration of competing interest

The authors declare that they have no known competing financial interests or personal relationships that could have appeared to influence the work reported in this paper.

Acknowledgements

Cheng is supported by NSFC 12301522 and the Fundamental Research Funds for the Central Universities, Liu is supported by NSFC 123B2015, Chen is supported by the NSFC 12071090 and NSFC 12241101, and Shen is supported by NSFC 12371409.

Appendix A

In this section, some details about the numerical experiments are presented.

A.1. Porous-medium and Fokker-Planck equations in 1D

For the Porous-Medium problem with free boundaries, the following boundary condition can be obtained by using the fact that $\rho|_{\partial\Omega} = 0$ as discussed in [19]:

$$(\partial_X x)^{m-1} \partial_t x = -\frac{m}{m-1} \frac{\partial_X(\rho(X, 0))^{m-1}}{\partial_X x}. \tag{A.1}$$

The numerical free boundary conditions are proposed as follows:

$$\left(\frac{x_1^k - x_0^k}{\delta X}\right)^{m-1} \frac{x_0^{k+1} - x_0^k}{\delta t} = -\frac{m}{m-1} \frac{\frac{(\rho(X_1, 0))^{m-1} - (\rho(X_0, 0))^{m-1}}{\delta X}}{\frac{x_1^{k+1} - x_0^{k+1}}{\delta X}}, \tag{A.2}$$

$$\left(\frac{x_N^k - x_{N-1}^k}{\delta X}\right)^{m-1} \frac{x_N^{k+1} - x_N^k}{\delta t} = -\frac{m}{m-1} \frac{\frac{(\rho(X_N, 0))^{m-1} - (\rho(X_{N-1}, 0))^{m-1}}{\delta X}}{\frac{x_N^{k+1} - x_{N-1}^{k+1}}{\delta X}}. \tag{A.3}$$

The free boundaries problem for the Porous-Medium equation in the numerical experiments is solved with above free boundary conditions.

Similarly, for the Fokker-Planck equation with free boundaries, the following boundary condition can be obtained by using the fact that $\rho|_{\partial\Omega} = 0$:

$$\partial_t x = -\frac{m}{m-1} \frac{\partial_X(\rho(X, 0))^{m-1}}{(\partial_X x)^m} - V'(x), \tag{A.4}$$

which can be solved by equations analogous to (A.2)-(A.3).

A.2. Aggregation equation in 1D

In the subsection, we give details about the numerical experiments for the aggregation equation in 1D.

Implicit-explicit. Let us set x to be implicit and y to be explicit in scheme (3.3)-(3.4), define the following discrete energy:

$$\begin{aligned} E_h(\mathbf{x}^{k+1}) &= \delta X \sum_{i=0}^{N-1} \rho(X_{i+\frac{1}{2}}, 0) \sum_{j=0}^{N-1} \rho_{j+\frac{1}{2}}^k \int_{x_j^k}^{x_{j+1}^k} \left(\frac{|x_{i+\frac{1}{2}}^{k+1} - y|^2}{2} - \ln(|x_{i+\frac{1}{2}}^{k+1} - y|) \right) dy, \\ &= \delta X \sum_{i=0}^{N-1} \rho(X_{i+\frac{1}{2}}, 0) \sum_{j=0}^{N-1} \rho_{j+\frac{1}{2}}^k \left(-\frac{1}{6} (x_{i+\frac{1}{2}}^{k+1} - y)^3 + (x_{i+\frac{1}{2}}^{k+1} - y) \ln(|x_{i+\frac{1}{2}}^{k+1} - y|) - (x_{i+\frac{1}{2}}^{k+1} - y) \right) \Big|_{x_j^k}^{x_{j+1}^k} \\ &= \delta X \sum_{i=0}^{N-1} \rho(X_{i+\frac{1}{2}}, 0) \sum_{j=0}^{N-1} \rho_{j+\frac{1}{2}}^k \left(-\frac{1}{6} (x_{i+\frac{1}{2}}^{k+1} - x_{j+1}^k)^3 + \frac{1}{6} (x_{i+\frac{1}{2}}^{k+1} - x_j^k)^3 + x_{j+1}^k - x_j^k \right) \\ &\quad + \delta X \sum_{i=0}^{N-1} \rho(X_{i+\frac{1}{2}}, 0) \sum_{j=0}^{N-1} \rho_{j+\frac{1}{2}}^k \left((x_{i+\frac{1}{2}}^{k+1} - x_{j+1}^k) \ln(|x_{i+\frac{1}{2}}^{k+1} - x_{j+1}^k|) - (x_{i+\frac{1}{2}}^{k+1} - x_j^k) \ln(|x_{i+\frac{1}{2}}^{k+1} - x_j^k|) \right), \end{aligned} \tag{A.5}$$

and the following result can be obtained by simple calculations:

$$\begin{aligned} \frac{\delta E_h^{k+1}}{\delta x_i^{k+1}} &= \delta X \rho(X_{i+\frac{1}{2}}, 0) \sum_{j=0}^{N-1} \rho_{j+\frac{1}{2}}^k \left(-\frac{1}{4} (x_{i+\frac{1}{2}}^{k+1} - x_{j+1}^k)^2 + \frac{1}{4} (x_{i+\frac{1}{2}}^{k+1} - x_j^k)^2 \right) \\ &\quad + \delta X \rho(X_{i-\frac{1}{2}}, 0) \sum_{j=0}^{N-1} \rho_{j+\frac{1}{2}}^k \left(-\frac{1}{4} (x_{i-\frac{1}{2}}^{k+1} - x_{j+1}^k)^2 + \frac{1}{4} (x_{i-\frac{1}{2}}^{k+1} - x_j^k)^2 \right) \\ &\quad + \delta X \rho(X_{i+\frac{1}{2}}, 0) \sum_{j=0}^{N-1} \rho_{j+\frac{1}{2}}^k \left(\frac{1}{2} \ln(|x_{i+\frac{1}{2}}^{k+1} - x_{j+1}^k|) - \frac{1}{2} \ln(|x_{i+\frac{1}{2}}^{k+1} - x_j^k|) \right) \\ &\quad + \delta X \rho(X_{i-\frac{1}{2}}, 0) \sum_{j=0}^{N-1} \rho_{j+\frac{1}{2}}^k \left(\frac{1}{2} \ln(|x_{i-\frac{1}{2}}^{k+1} - x_{j+1}^k|) - \frac{1}{2} \ln(|x_{i-\frac{1}{2}}^{k+1} - x_j^k|) \right). \end{aligned} \tag{A.6}$$

One can also find that

$$\begin{aligned} \frac{\delta^2 E_h^{k+1}}{\delta(x_i^{k+1})^2} &= \delta X(\rho(X_{i+\frac{1}{2}}, 0) + \rho(X_{i-\frac{1}{2}}, 0)) \sum_{j=0}^{N-1} \frac{\rho_{j+\frac{1}{2}}^k}{4} (x_{j+1}^k - x_j^k) \\ &+ \delta X \rho(X_{i+\frac{1}{2}}, 0) \sum_{j=0}^{N-1} \frac{\rho_{j+\frac{1}{2}}^k}{4} \left(\frac{1}{x_{i+\frac{1}{2}}^{k+1} - x_{j+1}^k} - \frac{1}{x_{i+\frac{1}{2}}^{k+1} - x_j^k} \right) \\ &+ \delta X \rho(X_{i-\frac{1}{2}}, 0) \sum_{j=0}^{N-1} \frac{\rho_{j+\frac{1}{2}}^k}{4} \left(\frac{1}{x_{i-\frac{1}{2}}^{k+1} - x_{j+1}^k} - \frac{1}{x_{i-\frac{1}{2}}^{k+1} - x_j^k} \right) > 0, \end{aligned}$$

where the fact that $\frac{1}{x-y}|_a^b = \int_a^b \frac{1}{(x-y)^2} dy > 0$ for $a < b$ has been utilized in the last inequality. Then the discrete energy is convex since the Hessian matrix $\nabla^2 E_h$ is positive definite.

Explicit-implicit. If we set x to be explicit and y to be implicit in scheme (3.3)-(3.4), i.e.

$$\begin{aligned} \frac{\delta E_h^{k+1}}{\delta x_i^{k+1}} &= \delta X \rho(X_{i+\frac{1}{2}}, 0) \sum_{j=0}^{N-1} \rho_{j+\frac{1}{2}}^k \left(-\frac{1}{4}(x_{i+\frac{1}{2}}^k - x_{j+1}^{k+1})^2 + \frac{1}{4}(x_{i+\frac{1}{2}}^k - x_j^{k+1})^2 \right) \\ &+ \delta X \rho(X_{i-\frac{1}{2}}, 0) \sum_{j=0}^{N-1} \rho_{j+\frac{1}{2}}^k \left(-\frac{1}{4}(x_{i-\frac{1}{2}}^k - x_{j+1}^{k+1})^2 + \frac{1}{4}(x_{i-\frac{1}{2}}^k - x_j^{k+1})^2 \right) \\ &+ \delta X \rho(X_{i+\frac{1}{2}}, 0) \sum_{j=0}^{N-1} \rho_{j+\frac{1}{2}}^k \left(\frac{1}{2} \ln(|x_{i+\frac{1}{2}}^k - x_{j+1}^{k+1}|) - \frac{1}{2} \ln(|x_{i+\frac{1}{2}}^k - x_j^{k+1}|) \right) \\ &+ \delta X \rho(X_{i-\frac{1}{2}}, 0) \sum_{j=0}^{N-1} \rho_{j+\frac{1}{2}}^k \left(\frac{1}{2} \ln(|x_{i-\frac{1}{2}}^k - x_{j+1}^{k+1}|) - \frac{1}{2} \ln(|x_{i-\frac{1}{2}}^k - x_j^{k+1}|) \right). \end{aligned} \tag{A.7}$$

Implicit-implicit. If we take both x and y implicit in scheme (3.3)-(3.4), set $\frac{\delta E_h^{k+1}}{\delta x_i^{k+1}}$ as follows:

$$\begin{aligned} \frac{\delta E_h^{k+1}}{\delta x_i^{k+1}} &= \delta X \rho(X_{i+\frac{1}{2}}, 0) \sum_{j=0}^{N-1} \rho_{j+\frac{1}{2}}^k \left(-\frac{1}{4}(x_{i+\frac{1}{2}}^{k+1} - x_{j+1}^{k+1})^2 + \frac{1}{4}(x_{i+\frac{1}{2}}^{k+1} - x_j^{k+1})^2 \right) \\ &+ \delta X \rho(X_{i-\frac{1}{2}}, 0) \sum_{j=0}^{N-1} \rho_{j+\frac{1}{2}}^k \left(-\frac{1}{4}(x_{i-\frac{1}{2}}^{k+1} - x_{j+1}^{k+1})^2 + \frac{1}{4}(x_{i-\frac{1}{2}}^{k+1} - x_j^{k+1})^2 \right) \\ &+ \delta X \rho(X_{i+\frac{1}{2}}, 0) \sum_{j=0}^{N-1} \rho_{j+\frac{1}{2}}^k \left(\frac{1}{2} \ln(|x_{i+\frac{1}{2}}^{k+1} - x_{j+1}^{k+1}|) - \frac{1}{2} \ln(|x_{i+\frac{1}{2}}^{k+1} - x_j^{k+1}|) \right) \\ &+ \delta X \rho(X_{i-\frac{1}{2}}, 0) \sum_{j=0}^{N-1} \rho_{j+\frac{1}{2}}^k \left(\frac{1}{2} \ln(|x_{i-\frac{1}{2}}^{k+1} - x_{j+1}^{k+1}|) - \frac{1}{2} \ln(|x_{i-\frac{1}{2}}^{k+1} - x_j^{k+1}|) \right). \end{aligned} \tag{A.8}$$

A.3. Keller-Segel model in 1D

The discrete energy for the Keller-Segel model in 1D is defined as follows:

$$\begin{aligned} E_h(x^{k+1}) &= \sum_{i=0}^{N-1} \delta X \rho(X_{i+\frac{1}{2}}, 0) \log \left(\frac{\rho(X_{i+\frac{1}{2}}, 0)}{\frac{x_{i+1}^{k+1} - x_i^{k+1}}{\delta X}} \right) - \frac{\delta X}{2\pi} \sum_{i=0}^{N-1} \rho(X_{i+\frac{1}{2}}, 0) \\ &\times \sum_{j=0}^{N-1} \rho_{j+\frac{1}{2}}^k \left((x_{i+\frac{1}{2}}^{k+1} - x_{j+1}^k) \ln(|x_{i+\frac{1}{2}}^{k+1} - x_{j+1}^k|) - (x_{i+\frac{1}{2}}^{k+1} - x_j^k) \ln(|x_{i+\frac{1}{2}}^{k+1} - x_j^k|) \right), \end{aligned}$$

it can be calculated that

$$\frac{\delta E_h^{k+1}}{\delta x_i^{k+1}} = -\frac{\delta X}{2\pi} \rho(X_{i+\frac{1}{2}}, 0) \sum_{j=0}^{N-1} \rho_{j+\frac{1}{2}}^k \left(\frac{1}{2} \ln(|x_{i+\frac{1}{2}}^{k+1} - x_{j+1}^k|) - \frac{1}{2} \ln(|x_{i+\frac{1}{2}}^{k+1} - x_j^k|) \right)$$

$$\begin{aligned}
 & -\frac{\delta X}{2\pi} \rho(X_{i-\frac{1}{2}}, 0) \sum_{j=0}^{N-1} \rho_{j+\frac{1}{2}}^k \left(\frac{1}{2} \ln(|x_{i-\frac{1}{2}}^{k+1} - x_{j+1}^k|) - \frac{1}{2} \ln(|x_{i-\frac{1}{2}}^{k+1} - x_j^k|) \right) \\
 & + \frac{\delta X \rho(X_{i+\frac{1}{2}}, 0)}{x_{i+1}^{k+1} - x_i^{k+1}} - \frac{\delta X \rho(X_{i-\frac{1}{2}}, 0)}{x_i^{k+1} - x_{i-1}^{k+1}},
 \end{aligned} \tag{A.9}$$

and we have

$$\begin{aligned}
 \frac{\delta^2 E_h}{\delta(x_i^{k+1})^2} &= -\frac{\delta X}{2\pi} \rho(X_{i+\frac{1}{2}}, 0) \sum_{j=0}^{N-1} \frac{\rho_{j+\frac{1}{2}}^k}{4} \left(\frac{1}{x_{i+\frac{1}{2}}^{k+1} - x_{j+1}^k} - \frac{1}{x_{i+\frac{1}{2}}^{k+1} - x_j^k} \right) \\
 & - \frac{\delta X}{2\pi} \rho(X_{i-\frac{1}{2}}, 0) \sum_{j=0}^{N-1} \frac{\rho_{j+\frac{1}{2}}^k}{4} \left(\frac{1}{x_{i-\frac{1}{2}}^{k+1} - x_{j+1}^k} - \frac{1}{x_{i-\frac{1}{2}}^{k+1} - x_j^k} \right) \\
 & + \frac{\delta X \rho(X_{i+\frac{1}{2}}, 0)}{(x_{i+1}^{k+1} - x_i^{k+1})^2} + \frac{\delta X \rho(X_{i-\frac{1}{2}}, 0)}{(x_i^{k+1} - x_{i-1}^{k+1})^2}.
 \end{aligned} \tag{A.10}$$

Notice that

$$-\sum_{j=0}^{N-1} \rho_{j+\frac{1}{2}}^k \left(\frac{1}{x_{i+\frac{1}{2}}^{k+1} - x_{j+1}^k} - \frac{1}{x_{i+\frac{1}{2}}^{k+1} - x_j^k} \right) = \sum_{j=0}^{N-1} \rho_{j+\frac{1}{2}}^k \int_{x_j^k}^{x_{j+1}^k} \frac{-1}{(x_{i+\frac{1}{2}}^{k+1} - y)^2} dy < 0, \tag{A.11}$$

$$-\sum_{j=0}^{N-1} \rho_{j+\frac{1}{2}}^k \left(\frac{1}{x_{i-\frac{1}{2}}^{k+1} - x_{j+1}^k} - \frac{1}{x_{i-\frac{1}{2}}^{k+1} - x_j^k} \right) = \sum_{j=0}^{N-1} \rho_{j+\frac{1}{2}}^k \int_{x_j^k}^{x_{j+1}^k} \frac{-1}{(x_{i-\frac{1}{2}}^{k+1} - y)^2} dy < 0. \tag{A.12}$$

However, the positivity or negativity of $\frac{\delta^2 E_h}{\delta(x_i^{k+1})^2}$ is not determined. Whether the discrete energy is convex or not is uncertain, since the positivity or negativity of the Hessian matrix $\nabla^2 E_h$ is not clear.

Data availability

No data was used for the research described in the article.

References

- [1] Luigi Ambrosio, Nicola Gigli, Giuseppe Savaré, Gradient Flows: in Metric Spaces and in the Space of Probability Measures, Springer Science & Business Media, 2005.
- [2] Donald G. Aronson, The porous medium equation, in: Nonlinear Diffusion Problems: Lectures given at the 2nd 1985 Session of the Centro Internazionale Matematico Estivo (CIME) held at Montecatini Terme, Italy, June 10–June 18, 1985, 2006, pp. 1–46.
- [3] Donald G. Aronson, Luis A. Caffarelli, Shoshana Kamin, How an initially stationary interface begins to move in porous medium flow, *SIAM J. Math. Anal.* 14 (4) (1983) 639–658.
- [4] Jean-David Benamou, Yann Brenier, A computational fluid mechanics solution to the Monge-Kantorovich mass transfer problem, *Numer. Math.* 84 (3) (2000) 375–393.
- [5] Jean-David Benamou, Guillaume Carlier, Maxime Laborde, An augmented Lagrangian approach to Wasserstein gradient flows and applications, *ESAIM Proc. Surv.* 54 (2016) 1–17.
- [6] Clément Bonet, Nicolas Courty, François Septier, Lucas Drumetz, Efficient gradient flows in sliced-Wasserstein space, *Trans. Mach. Learn. Res.* (2022).
- [7] Clément Cancès, Thomas O. Gallouët, Gabriele Todeschi, A variational finite volume scheme for Wasserstein gradient flows, *Numer. Math.* 146 (2020) 437–480.
- [8] José A. Carrillo, Alina Chertock, Yanghong Huang, A finite-volume method for nonlinear nonlocal equations with a gradient flow structure, *Commun. Comput. Phys.* 17 (1) (2015) 233–258.
- [9] José A. Carrillo, Katy Craig, Li Wang, Chaozhen Wei, Primal dual methods for Wasserstein gradient flows, *Found. Comput. Math.* 22 (2022) 1–55.
- [10] José A. Carrillo, Bertram Düring, Daniel Matthes, David S. McCormick, A Lagrangian scheme for the solution of nonlinear diffusion equations using moving simplex meshes, *J. Sci. Comput.* 75 (2018) 1463–1499.
- [11] José A. Carrillo, Lucas C.F. Ferreira, Juliana C. Precioso, A mass-transportation approach to a one dimensional fluid mechanics model with nonlocal velocity, *Adv. Math.* 231 (1) (2012) 306–327.
- [12] José A. Carrillo, Ansgar Jüngel, Peter A. Markowich, Giuseppe Toscani, Andreas Unterreiter, Entropy dissipation methods for degenerate parabolic problems and generalized Sobolev inequalities, *Monatshefte Math.* 133 (2001) 1–82.
- [13] Jose A. Carrillo, Daniel Matthes, Marie-Therese Wolfram, Lagrangian schemes for Wasserstein gradient flows, *Handb. Numer. Anal.* 22 (2021) 271–311.
- [14] José A. Carrillo, Robert J. McCann, Cédric Villani, Kinetic equilibration rates for granular media and related equations: entropy dissipation and mass transportation estimates, *Rev. Mat. Iberoam.* 19 (3) (2003) 971–1018.
- [15] José A. Carrillo, Giuseppe Toscani, Asymptotic L^1 -decay of solutions of the porous medium equation to self-similarity, *Indiana Univ. Math. J.* 49 (2000) 113–142.
- [16] Wenbin Chen, Qianqian Liu, Jie Shen, Error estimates and blow-up analysis of a finite-element approximation for the parabolic-elliptic Keller-Segel system, *Int. J. Numer. Anal. Model.* 19 (2022) 275–298.

- [17] Qing Cheng, Chun Liu, Jie Shen, A new interface capturing method for Allen-Cahn type equations based on a flow dynamic approach in Lagrangian coordinates, I. One-dimensional case, *J. Comput. Phys.* 419 (2020) 109509.
- [18] Chenghua Duan, Wenbin Chen, Chun Liu, Xingye Yue, Shenggao Zhou, Structure-preserving numerical methods for nonlinear Fokker–Planck equations with nonlocal interactions by an energetic variational approach, *SIAM J. Sci. Comput.* 43 (1) (2021) B82–B107.
- [19] Chenghua Duan, Chun Liu, Cheng Wang, Xingye Yue, Numerical methods for porous medium equation by an energetic variational approach, *J. Comput. Phys.* 385 (2019) 13–32.
- [20] Bob Eisenberg, Computing the field in proteins and channels, *J. Membr. Biol.* 150 (1) (1996) 1–25.
- [21] Bob Eisenberg, Yunkyong Hyon, Chun Liu, Energy variational analysis of ions in water and channels: field theory for primitive models of complex ionic fluids, *J. Chem. Phys.* 133 (10) (2010).
- [22] Razvan C. Fetecau, Yanghong Huang, Theodore Kolokolnikov, Swarm dynamics and equilibria for a nonlocal aggregation model, *Nonlinearity* 24 (10) (2011) 2681.
- [23] Francis Filbet, A finite volume scheme for the Patlak–Keller–Segel Chemotaxis model, *Numer. Math.* 104 (2006) 457–488.
- [24] Dirk Horstmann, From 1970 until present: the Keller–Segel model in Chemotaxis and its consequences I, *Jahresber. Dtsch. Math.-Ver.* 105 (3) (2003) 103–165.
- [25] Richard Jordan, David Kinderlehrer, Felix Otto, The variational formulation of the Fokker–Planck equation, *SIAM J. Math. Anal.* 29 (1) (1998) 1–17.
- [26] Evelyn F. Keller, Lee A. Segel, Initiation of slime mold aggregation viewed as an instability, *J. Theor. Biol.* 26 (3) (1970) 399–415.
- [27] David Kinderlehrer, Léonard Monsaingeon, Xiang Xu, A Wasserstein gradient flow approach to Poisson–Nernst–Planck equations, *ESAIM Control Optim. Calc. Var.* 23 (1) (2017) 137–164.
- [28] Wuchen Li, Jianfeng Lu, Li Wang, Fisher information regularization schemes for Wasserstein gradient flows, *J. Comput. Phys.* 416 (2020) 109449.
- [29] Chun Liu, Yiwei Wang, On Lagrangian schemes for porous medium type generalized diffusion equations: a discrete energetic variational approach, *J. Comput. Phys.* 417 (2020) 109566.
- [30] Chun Liu, Yiwei Wang, A variational Lagrangian scheme for a phase-field model: a discrete energetic variational approach, *SIAM J. Sci. Comput.* 42 (6) (2020) B1541–B1569.
- [31] Chun Liu, Hao Wu, An energetic variational approach for the Cahn–Hilliard equation with dynamic boundary condition: model derivation and mathematical analysis, *Arch. Ration. Mech. Anal.* 233 (1) (2019) 167–247.
- [32] Fawang Liu, Vo Anh, Ian Turner, Numerical solution of the space fractional Fokker–Planck equation, *J. Comput. Appl. Math.* 166 (1) (2004) 209–219.
- [33] Hailiang Liu, Wumaier Maimaitiyiming, A dynamic mass transport method for Poisson–Nernst–Planck equations, *J. Comput. Phys.* 473 (2023) 111699.
- [34] Hailiang Liu, Zhongming Wang, An entropy satisfying discontinuous Galerkin method for nonlinear Fokker–Planck equations, *J. Sci. Comput.* 68 (2016) 1217–1240.
- [35] Jianguo Liu, Li Wang, Zhennan Zhou, Positivity-preserving and asymptotic preserving method for 2D Keller–Segel equations, *Math. Comput.* 87 (311) (2018) 1165–1189.
- [36] Qianqian Liu, Chenghua Duan, Wenbin Chen, EnVarA-FEM for the flux-limited porous medium equation, *J. Comput. Phys.* 493 (2023) 112432.
- [37] Cuong Ngo, Weizhang Huang, A study on moving mesh finite element solution of the porous medium equation, *J. Comput. Phys.* 331 (2017) 357–380.
- [38] Lars Onsager, Reciprocal relations in irreversible processes. I, *Phys. Rev.* 37 (4) (1931) 405.
- [39] Lars Onsager, Reciprocal relations in irreversible processes. II, *Phys. Rev.* 38 (12) (1931) 2265.
- [40] Lorenzo Pareschi, Mattia Zanella, Structure preserving schemes for nonlinear Fokker–Planck equations and applications, *J. Sci. Comput.* 74 (2018) 1575–1600.
- [41] Jie Shen, Jie Xu, Unconditionally bound preserving and energy dissipative schemes for a class of Keller–Segel equations, *SIAM J. Numer. Anal.* 58 (3) (2020) 1674–1695.
- [42] John William Strutt, Some general theorems relating to vibrations, *Proc. Lond. Math. Soc.* 1 (1) (1871) 357–368.
- [43] Juan Luis Vázquez, *The Porous Medium Equation: Mathematical Theory*, Oxford University Press on Demand, 2007.
- [44] Shufen Wang, Simin Zhou, Shuxun Shi, Wenbin Chen, Fully decoupled and energy stable BDF schemes for a class of Keller–Segel equations, *J. Comput. Phys.* 449 (2022) 110799.
- [45] Yiwei Wang, Chun Liu, Some recent advances in energetic variational approaches, *Entropy* 24 (5) (2022) 721.
- [46] Yiwei Wang, Tengfei Zhang, Chun Liu, A two species micro–macro model of wormlike micellar solutions and its maximum entropy closure approximations: an energetic variational approach, *J. Non-Newton. Fluid Mech.* 293 (2021) 104559.
- [47] Michael Winkler, Aggregation vs. Global diffusive behavior in the higher-dimensional Keller–Segel model, *J. Differ. Equ.* 248 (12) (2010) 2889–2905.
- [48] Qiang Zhang, Zilong Wu, Numerical simulation for porous medium equation by local discontinuous Galerkin finite element method, *J. Sci. Comput.* 38 (2009) 127–148.